AD-A051 833 SRI INTERNATIONAL MENLO PARK CA F/G 11/6
A STUDY TO DETERMINE THE MECHANISMS OF CORROSION OF COPPER-NICK--ETC(U)
FEB 78 D D MACDONALD, B C SYRETT, S S WING N00014-77-C-0046

UNCLASSIFIED NL

1 OF 2
AD
A051833

A STUDY TO DETERMINE THE MECHANISMS OF CORROSION OF COPPER-NICKEL ALLOYS IN SULFIDE-POLLUTED SEAWATER

Annual Report Covering the Period
February 2, 1977 through February 1, 1978

February 1, 1978

By: D. D. Macdonald, B. C. Syrett, and S. S. Wing

Prepared for:

Office of Naval Research
800 North Quincy Street
Arlington, Virginia 22217

Attn: Dr. Philip A. Clarkin, Code 471
Director, Metallurgy Program
Materials Sciences Division

ONR Contract No. N00014-77-C-0046, NR 036-116
SRI Project No. PYU 6077

SRI International
333 Ravenswood Avenue
Menlo Park, California 94025
(415) 326-6200
Cable: SRI INTL MPK
TWX: 910-373-1246

SRI International

(6)

A STUDY TO DETERMINE THE MECHANISMS OF CORROSION OF COPPER-NICKEL ALLOYS IN SULFIDE-POLLUTED SEAWATER.

(9) Annual rept. 2 Feb 77 - 1 Feb 78,

Annual Report Covering the Period
February 2, 1977 through February 1, 1978

February 1, 1978 (11) 1 Feb 78

(10) By: D. D. Macdonald, B. C. Syrett, S. S. Wing

Prepared for:

(12) 175 p.

Office of Naval Research
800 North Quincy Street
Arlington, Virginia 22217

Attn: Dr. Philip A. Clarkin, Code 471
Director, Metallurgy Program
Materials Sciences Division

(15) ONR Contract No. N00014-77-C-0046 NR 036-116
SRI Project No. PYU 6077

Approved:

R. W. Bartlett

R. W. Bartlett, Director
Materials Research Center

P. J. Jorgensen
Vice President
Life and Physical Sciences

SRI International

410 281

TABLE OF CONTENTS

APPENDICES (Concluded)

INTRODUCTION AND OBJECTIVES

Accelerated corrosion of marine components manufactured from copper-nickel alloys in polluted seawater has been recognized for some time. Although a considerable amount of work has been reported on this topic, no completely acceptable mechanism for the accelerated attack has been formulated. This is partly due to the difficulties inherent in analyzing experimental data for a complex system like this, but it is also due to failure in previous studies to use experimental techniques that are capable of yielding detailed mechanistic information.

This report describes the first year's results of a multiyear program of the study of the corrosion of 90:10 Cu:Ni and 70:30 Cu:Ni alloys in sulfide-polluted seawater. The specific goals of the present work were grouped into the following six tasks:

(1) Build the specialized test system required to conduct the research program.

(2) Investigate the effect of dissolved oxygen in sulfide-free water on the corrosion rate, rate controlling step, and character of the corrosion product at several immersion times.

(3) Investigate the effect of dissolved sulfide in oxygen-free water on the corrosion rate, rate controlling step, and character of the corrosion product at several immersion times.

(4) Begin investigating the synergistic effect of oxygen and sulfide on the corrosion rate, rate controlling step, and character of the corrosion product at several immersion times.

(5) In seawater containing selected levels of oxygen and sulfide, begin investigating the effect of seawater velocity on the corrosion rate, rate controlling step, and character of the corrosion product.

(6) Determine which of the semicontinuous methods of measuring corrosion rate are most applicable under the environmental conditions studied in this research program.

SUMMARY OF TECHNICAL ACCOMPLISHMENTS

The principal findings of this study are discussed in detail in six appendices attached to this report. Three of these appendices have been submitted to journals for publication in the open literature. The authors and titles of these papers, and the journals to which they have been submitted, are as follows:

(1) "Methods for Measuring Corrosion Rates of Copper-Nickel Alloys in Flowing Seawater," by D. D. Macdonald, B. C. Syrett, and S. S. Wing. Submitted to Corrosion, 1977. This paper will also be presented by D. D. Macdonald to the Symposium on Effects of Pollution and Velocity on Seawater Corrosion, Corrosion 78, Houston, Texas, March 1978 (Appendix I).

(2) "An Impedance Interpretation of Small Amplitude Cyclic Voltammetry--I: Theoretical Analysis for a Resistive-Capacitive System," by D. D. Macdonald. Submitted to the Journal of the Electrochemical Society, 1977 (Appendix II).

(3) "The Effect of Dissolved Sulfide on the Corrosion of copper-Nickel Alloys in Flowing Seawater," by D. D. Macdonald, B. C. Syrett, and S. S. Wing. Submitted to Corrosion, 1978 (Appendix IV).

The principal findings of the first year's program are summarized below.

Experimental Test System (Task 1)

Construction details of the experimental test system and flow channel configuration are given in Appendix I. Briefly, a recirculating loop constructed mainly from 3/4-inch PVC pipe was used. Two test channels, one for each alloy, were mounted in tandem. Each test section was

preceded by a 30-inch length of the appropriate alloy tubing with an internal diameter equal to that of the test specimens. This served to equilibrate both the velocity boundary layer and the concentration boundary layer thicknesses before the fluid contacted the specimens.

Tubular test specimens (one inch in length) of each alloy were cut from a stock of heat exchanger tubing. Five specimens of each alloy were mounted axially in each of the test sections and were electrically insulated from each other by Delrin spacers. The spacers were machined so that the gaps between the specimens did not exceed 0.025 inches. We believe that this configuration permitted nearly continuous concentration boundary layer profiles to be established down the lengths of the test sections. Delrin was chosen as the spacer material because of its insulating properties and its excellent resistance to creep.

The recirculating loop contained facilities for full-flow filtration, precise velocity control, and measurement of the pressure drops across the test sections. This latter information was used to estimate fluid shear stresses at the specimen surfaces (see Appendix I for details).

Experimental Techniques (Task 6)

Task 6 of the work plan required an assessment to be made of various semicontinuous methods for measuring the corrosion rate under the environmental conditions used in this work. Accordingly, we examined three electrochemical relaxation methods for determining the polarization resistance (R_p): the linear polarization (or small-amplitude cyclic voltammetry, SACV), ac impedance, and potential step techniques. The extensive data obtained in this assessment demonstrate that the corroding interface can exhibit very long relaxation times; hence, use of the SACV and ac impedance techniques for estimating R_p require very low voltage sweep-rates and frequencies, respectively. For instance, we were able

to obtain impedance data at frequencies as low as 0.0005 Hz. Few studies on fundamental electrochemical work have been reported in this frequency domain, and to our knowledge no previous attempts have been made to use the impedance technique at such low frequency for the estimation of polarization resistance in corrosion research. However, it was found that even at the very low frequencies used in our study, the magnitude of the impedance, and the real component of the complex impedance vector, were frequently much less than the true dc polarization resistance as determined by SACV and by extrapolation of the ac impedance data to zero frequency.

As well as providing an estimate for R_p, the frequency dependence of the complex impedance yielded valuable information on the number of relaxation processes that occur at the interface. For instance, it was generally found that at least two relaxation processes occur on each alloy, and we suggest that the low frequency relaxation arises from charge transport across a surface film. Thus, an increase in the diameter of the low frequency semicircle in the complex plane with time, as observed for both alloys in oxygenated seawater (see Appendix I), is consistent with the existence of a growing surface film. Furthermore, addition of sulfide to the seawater was found to greatly decrease the diameter of the low frequency semicircle, thereby demonstrating sulfide-induced loss of passivity.

Very early in this study it was observed that the linear polarization (or SACV) technique commonly used for estimating polarization resistance in corrosion research gave rise to current/voltage curves that exhibited hysteresis between the forward and reverse sweeps (see Figure 7, Appendix II). This type of response is characteristic of systems that have very high interfacial capacitances. A theoretical study of this phenomenon was undertaken (Appendix II) by using transform analysis to

derive transient and steady-state responses of an electrical equivalent circuit for the interface. This work established criteria for the extraction of reliable data for the dc polarization resistance from the observed SACV response, and also demonstrated that valuable information on the capacitance of the interface can be obtained from the variation of the hysteresis current with voltage sweep-rate. Interfacial capacitance data yield useful mechanistic information about the corrosion processes.

The potential step technique was used only sparingly in this work, since it does not yield any information that cannot be obtained by use of the SACV and ac impedance techniques. Nevertheless, the potential step method yielded polarization resistance data that agree with those given by the SACV and ac impedance techniques, provided that sufficient time was allowed for decay of the transient contribution to the current.

The polarization resistance data for both alloys in flowing oxygenated seawater were converted to weight loss by use of the Stern-Geary relationship (see Appendix I). Excellent agreement with direct weight loss measurements was obtained in contrast to previous reports for copper-nickel alloys in flowing seawater. We believe that our success was due to monitoring the polarization resistance at short times, and to ensuring that the measured interfacial impedance was a good approximation of the dc polarization resistance.

Classical cyclic voltammetry, in which the potential is swept linearly between the kinetic limits of stability of the solvent (seawater), was used to provide back-up electrochemical information for the interpretation of the corrosion data.

Behavior of Copper-Nickel Alloys in Oxygenated Flowing Seawater (Task 2)

Details of our work on the corrosion of 90:10 Cu:Ni and 70:30 Cu:Ni alloys in flowing seawater (fluid velocity = 1.62 m/s) at four oxygen concentrations over the range 0.045 mg/liter to 26.3 mg/liter are given in Appendices I and III. The findings of this study are summarized as follows:

(1) The 70:30 Cu:Ni alloy exhibits superior corrosion resistance to the 90:10 Cu:Ni alloy over the exposure times used (up to 330 hours), provided that the oxygen concentration is maintained at or beneath the air-saturated value of 6.60 mg/liter. At higher oxygen concentration, a sharp breakdown in the corrosion resistance of the high nickel alloy is observed, to the extent that in the oxygen saturated system ($[O_2]$ = 26.3 mg/liter) no difference between the high and low nickel alloys is apparent. The loss in corrosion resistance of the 70:30 Cu:Ni alloy is believed to be due to a positive shift in the corrosion potential to a range in which the surface oxide film is no longer as protective. This is reflected in the cyclic voltammograms by large anodic currents at these potentials.

(2) The variation of corrosion potential with oxygen concentration, and some potential step data, indicate that for the short exposure times considered here, the corrosion reaction is cathodically controlled at low oxygen concentrations, but is anodically controlled at high concentrations.

(3) Impedance spectra indicate the existence of at least two clearly separated relaxation processes during corrosion of the alloys in oxygenated seawater, one of which is consistent with ion or electron transport through a surface film having a distribution in thickness (Appendix I).

(4) Energy dispersive X-ray (EDX) analysis and Auger electron spectrometry (AES) indicate that the surface films formed on both alloys after exposure to oxygenated seawater consist essentially of copper and nickel oxides and minor amounts of copper hydroxychlorides (Appendix III). Small amounts of potassium, calcium, and sulfur (probably

sulfate) were also detected, and it is believed that these components are coprecipitated onto the surface during growth of the films.

Behavior of Copper-Nickel Alloys in Sulfide-Polluted Seawater (Task 3)

The corrosion behavior of 90:10 Cu:Ni alloy and 70:30 Cu:Ni alloy in flowing seawater (fluid velocity = 1.62 m/s) containing varying amounts of sulfide ($H_2S + HS^- + S^{2-}$) is discussed in Appendix IV. The experimental techniques used for investigating the corrosion and related electrochemical phenomena are the same as those described in Appendix I. However, the corrosion experiments were performed with simultaneous control of the pH and total sulfide concentration in the system.

The principal findings of this work are summarized as follows:

(1) The smallest concentration of sulfide used (0.85 mg/liter total sulfide) is sufficient to induce breakdown of passivity and hence corrosion resistance of 90:10 Cu:Ni and 70:30 Cu:Ni alloys in flowing seawater. In the presence of this total sulfide concentration, the polarization resistance for the high and low nickel alloys was reduced by a factor of 70 and 8, respectively, compared with the low-oxygen sulfide-free systems. Higher sulfide concentrations had little additional effect on the polarization resistance.

(2) Energy dispersive X-ray (EDX) analysis, Auger electron spectrometry (AES), and X-ray diffraction studies indicate that the principal corrosion product is orthorhomic cuprous sulfide (Cu_2S), although minor amounts of cubic Cu_2S and copper-defficient cuprous sulfide (Cu_xS where $x < 2$) were also observed in the corrosion film on the 90:10 Cu:Ni alloy. The scale on the high nickel alloy was not sufficiently crystalline to permit phase identification by X-ray diffraction analysis, but both the EDX analyses and the AES results are consistent with the formation of cuprous sulfide on the 70:30 Cu:Ni alloy also.

(3) Analysis of the corrosion potential behavior of the alloys in sulfide-containing systems indicates that the presence of as little as 0.85 mg/liter of sulfide causes a distinct change in mechanism of the corrosion process. Thus, in the sulfide-free systems, reduction of oxygen appears to be the only viable cathodic partial process, and the alloys therefore behave as noble materials in oxygen-free seawater. In the presence of sulfide, however, the corrosion potential behavior shows that hydrogen evolution is a viable cathodic reaction, and in these systems acid attack on the alloys is possible. We believe that this change in mechanism, and the activating influence of dissolved sulfide, is responsible for the accelerated corrosion of 90:10 Cu:Ni alloy and 70:30 Cu:Ni alloy in sulfide-polluted seawater.

Effect of Oxygen and Sulfide on the Corrosion of Copper-Nickel Alloys in Seawater (Task 4)

A survey of the literature has shown that dissolved sulfide is oxidized rapidly in aerated seawater to form elemental (colloidal) sulfur, as well as various sulfur oxyanions. Previous work has also shown that elemental sulfur is highly corrosive towards carbon steel, and it was reasoned that severe corrosion of copper-nickel alloys could also occur upon exposure to this element in aqueous systems. Accordingly, we decided that any preliminary study of the effect of the copresence of oxygen and sulfide on the corrosion of copper-nickel alloys in seawater should include an investigation of the corrosive properties of colloidal sulfur.

Preliminary experiments (Appendix V) have confirmed that elemental sulfur in colloidal form in seawater is highly corrosive towards the copper-nickel alloys of interest in this work. In particular, the corrosion rate of 90:10 Cu:Ni alloy was found to be more than eighty times greater than that for a control experiment in the absence of colloidal sulfur. In the case of the 70:30 Cu:Ni alloy, the increase was less dramatic, but the corrosion rate in the presence of colloidal sulfur was still greater than that in the control experiment by a factor of 4.

Effect of Fluid Velocity on the Corrosion of Copper-Nickel Alloys in Seawater (Task 5)

The preliminary experiments described in Appendix VI indicate that both the 90:10 Cu:Ni alloy and 70:30 Cu:Ni alloy suffer a breakdown in corrosion resistance in aerated seawater when the fluid flow velocity is increased from 1.62 m/s to 3.67 m/s. This finding is contrary to previous studies, which indicate that this phenomenon occurs only for the high nickel alloy. The increase in fluid velocity resulted in reductions in the polarization resistance of 90:10 Cu:Ni and 70:30 Cu:Ni alloys by factors of at least 80 and 500, respectively.

ACKNOWLEDGMENTS

The authors wish to thank B. Wood for the AES analyses, J. Terry for the SEM-EDX analyses, and E. Farley for the X-ray diffraction analyses of corrosion product films. Also, the help of A. Bayce and G. Craig in some aspects of this study is greatly appreciated.

Appendix I

METHODS FOR MEASURING CORROSION RATES OF COPPER-NICKEL ALLOYS IN FLOWING SEAWATER

D. D. Macdonald, B. C. Syrett, and S. S. Wing

Materials Research Center
SRI International
Menlo Park, California 94025

ABSTRACT

The corrosion of 90:10 Cu:Ni and 70:30 Cu:Ni alloys in flowing seawater (1.62 m/s) has been studied as a function of oxygen concentration using the linear polarization, ac impedance, and potential step methods for measuring the polarization resistance. Satisfactory agreement is obtained between these three semicontinuous techniques and measurements of weight loss, thereby demonstrating the suitability of electrochemical methods for monitoring the corrosion rate of cupronickel alloys in seawater. The high-nickel alloy is found to be more corrosion-resistant than the 90:10 Cu:Ni alloy under the conditions employed, provided that $[O_2] \leq 6.60$ mg/l. In oxygen-saturated seawater, the superior behavior of the 70:30 Cu:Ni alloy is no longer observed. The loss in corrosion resistance of the 70:30 Cu:Ni alloy is correlated with a shift in the corrosion potential, to a value more noble than the "break-away potential" (defined here as the potential at which a sudden increase in anodic current occurs on sweeping the potential in the active to noble direction).

INTRODUCTION

The application of electrochemical techniques for measuring corrosion rates of metals in condensed media is now well established.[1,2] The most frequently used technique is linear polarization, which makes use of a linearized Butler-Volmer type expression for the current within a few millivolts of the corrosion potential (E_{corr}). Experimentally, this technique requires estimation of the polarization resistance $R_p = (\partial E/\partial i)_{E = E_{corr}}$, which is then substituted into the Stern-Geary relationship to yield the corrosion current.

Two fundamental problems exist with this technique. First, linear polarization is nonspecific for the corrosion reaction. Thus, any electrochemical reaction, irrespective of whether or not it leads to corrosion of the metal, will contribute to the current flowing across the interface, and therefore will partly determine the magnitude of the polarization resistance. For example, the oxidation of molecular hydrogen gives rise to an anodic current that, under some circumstances, cannot be distinguished from a metal oxidation (i.e., corrosion) current on the basis of linear polarization alone. Second, the polarization resistance is frequently determined by use of a small-amplitude, time-dependent excitation function, usually in the form of a saw-tooth voltage applied

between the sample and the reference electrode by use of a potentiostat. However, the quantity measured by use of a time-dependent signal is strictly the impedance of the interface, which in general contains capacitive and inductive components in addition to the expected resistive component. Because the impedance becomes equal to the resistance only in the limit of infinitely low frequency (i.e., in the steady state), it is necessary to develop methods for delineating the resistive, capacitive, and inductive contributions to the total impedance when using time-dependent excitation signals.[2]

In this paper, we explore the application of three electrochemical techniques for the measurement of the corrosion rates of copper-nickel alloys 706 (90:10 Cu:Ni) and 715 (70:30 Cu:Ni) in flowing seawater. The experiments have been carried out over a range of oxygen concentrations (0.045, 0.85, 6.6, and 26.3 mg/l), and for exposure periods of up to 330 hours. Emphasis is placed upon comparing the corrosion rates as determined by use of the linear polarization, ac impedance, and potential step electrochemical methods with those evaluated directly from measurements of weight loss.

EXPERIMENTAL

Flow Loop

A schematic diagram of the flow loop used in this work is shown in Figure 1. The circuit was constructed from 3/4-inch PVC pipe (schedule 40), and contains facilities for full-flow filtration, liquid sampling, gas sparging, and precise flow-velocity control by use of bypass lines. Flow velocities of 0 to 3.7 m/s are available, although the present work was carried out at a constant velocity of 1.2 m/s. The flow velocity through the tandem flow channels was measured with a conventional rotameter.

Filtered seawater was obtained from the Steinhart Aquarium, San Francisco, and had the properties listed in Table 1. The seawater was collected in polyethylene lined 55 gallon drums, and was continuously purged with air to inhibit growth of anaerobic organisns during storage. These drums were used as the reservoirs during the experiments, and were purged continuously with the appropriate mixture of nitrogen and oxygen to establish the desired concentration of oxygen in the system. The oxygen concentration was monitored with a commercial Teflon membrane probe (oxygen meter) contained in a bypass around the rotameter. The probe served only to indicate the constancy of the oxygen concentration

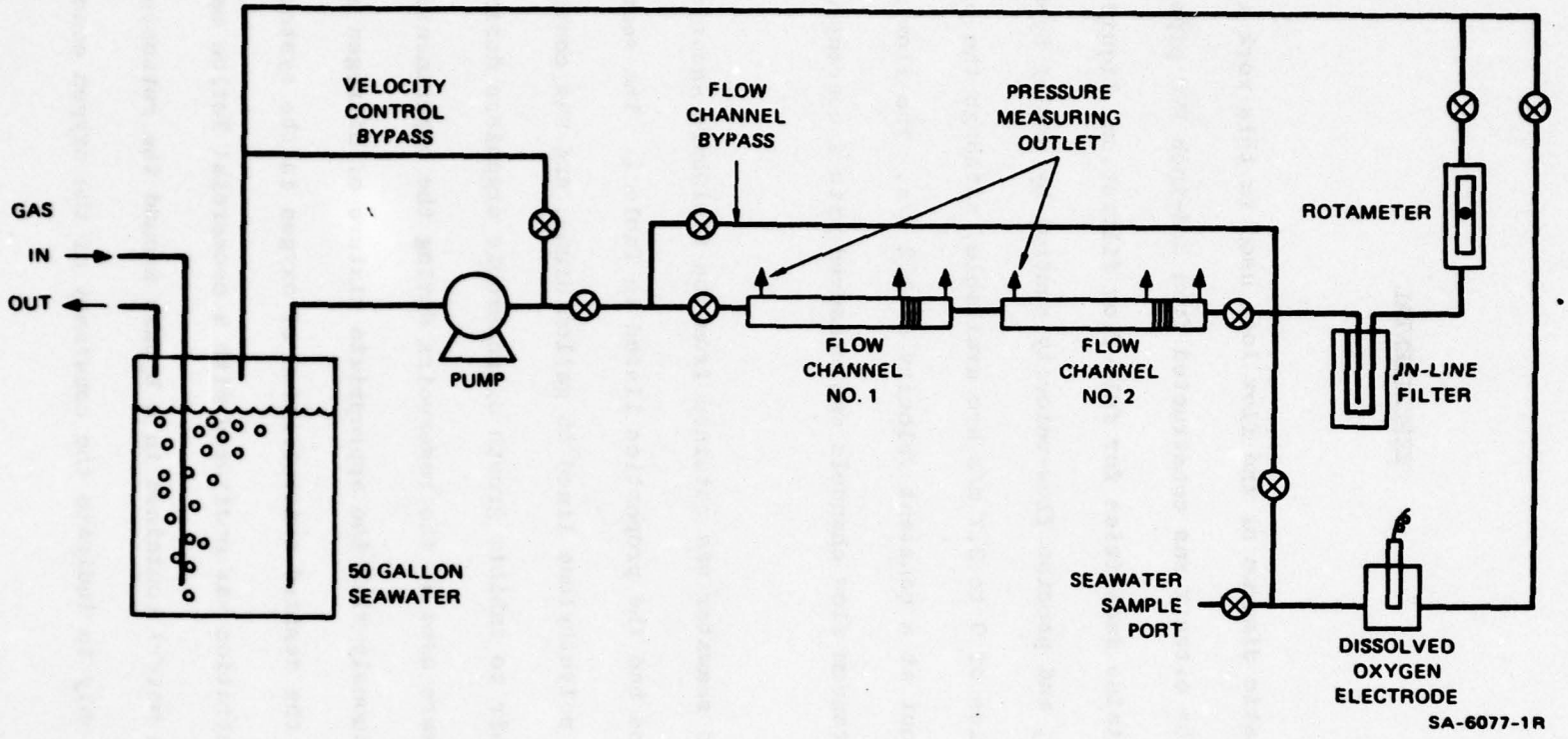

Figure 1 Schematic Diagram of the Flow Loop

Table 1

CHEMICAL AND PHYSICAL PROPERTIES OF THE SEAWATER

Property		Comments
Salinity	29 parts per thousand	Data supplied by Steinhart Aquarium for seawater collected at the same time as that use in this work
Density	1.0214 gm/cm^3	
Turbidity	0.2 Jackson	
pH	7.9 ± 0.1	
	8.1 ± 0.02	Measured at SRI International Normal range 8.1 to 8.3

during a run. The actual concentrations quoted in this paper were determined by Winkler titration.[3]

Specimen Flow Channel

The specimen flow channel used in this work is shown in Figure 2. The specimens consisted of 2.54 cm lengths of condenser tubing (1.384 cm I.D., 1.715 cm O.D.) separated by Delrin spacers. Chemical compositions and physical properties of the two alloys are listed in Table 2. The ends of the specimens were given 2 degree outside cambers, so that compression of the assembly by the four support bolts would generate an outward radial stress in the Delrin spacers and suppress extrusion of the spacer material into the fluid stream. Delrin was chosen as the spacer material because of its chemical inertness and excellent creep resistance. The mechanical properties of this material permitted use of thin spacer sections (< 0.064 cm between samples) to minimize disturbance of the concentration boundary layer established in the approach sections.

The internal surfaces of the specimens were used in their as-received mechanical condition. Close inspection revealed that the surface was smooth and free of striations, and we believed that applying an abraded finish would provide no advantage. Furthermore, use of the samples in their as-received condition should permit a more valid comparison of the experimental corrosion rate with that observed in the field.

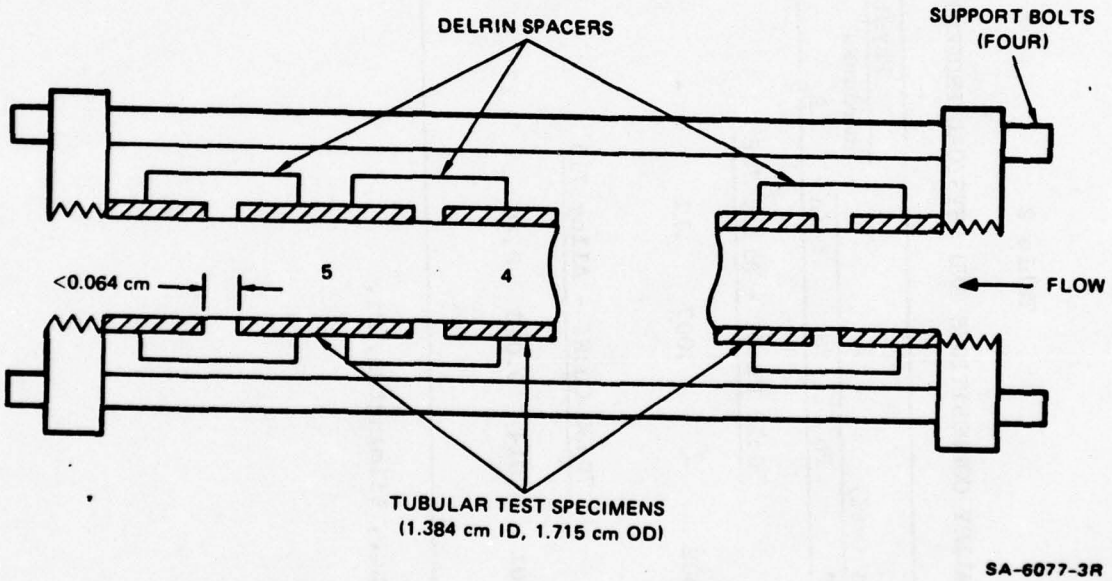

Figure 2 Design of the Specimen Flow Channel

Table 2

ALLOY COMPOSITIONS AND PHYSICAL PROPERTIES*

Composition (wt%)								Physical Properties		
								Hardness	Y.S.	T.S.
Cu	Ni	Mn	Fe	P	Pb	S	Zn	R_B	X 1000 psi	X 1000 psi
90:10 Cu:Ni - Alloy 706										
88.16	10.04	0.3	1.43	.002	-	.007	.12	-	21	45
70:30 Cu:Ni - Alloy 715										
69.3	29.0	0.52	0.70	0.001	0.014	0.016	0.40	27	29	66

*As supplied by Stanley Supply Inc., Wilmington, Ca.

Before an experiment, the five specimens of each alloy were descaled in HCl/H_2SO_4 (ASTM Recommended Practice G1-72 for copper alloys), rinsed with distilled water, and weighed after air-drying. Because of possible interference between the measuring technique and the free corrosion rate, a strict schedule of specimen versus experiment was adopted in this work. Thus, corrosion potential and weight loss measurements were restricted to the first and fifth specimens only. These specimens were not subjected to any polarization experiments. Likewise, linear polarization, ac impedance, and potential step experiments were restricted exclusively to the second, third, and fourth specimens, respectively. The cyclic voltammograms obtained at the end of each run were measured on the fourth specimen only. The corrosion potentials of neighboring specimens were not disturbed significantly during aquisition of polarization data, thereby indicating minimal interaction between adjacent specimens.

Each flow channel was preceded by a 67 cm length (approxiamtely) of copper-nickel tube of identical composition and internal diameter as the specimens. The purpose of this approach section was to equilibrate the velocity and concentration boundary layers before fluid contanct with the specimens. A 15 cm length of the same tubing was placed immediately downstream from the flow channel to serve as the counter electrode for the electrochemical work. The calomel reference electrode was placed in a side arm off the exit to the differential monometer (Figure 3).

The shear stress experienced at the surface can be calculated from the measured pressure drop per unit length of specimen. Because the specimen length was small (2.54 cm), the direct measurement of the pressure drop across a single specimen was impractical. Accordingly, the pressure drop was measured over the much larger length, X, of the approach section, and it was assumed that the pressure drop per unit length was the same for both the approach section and the flow channel.

A pressure measurement involved first adjusting the height of reservoir A or B until the fluid levels in the side arms, were identical (see Figure 3). The differential pressure measurement was then taken directly from the manometer as ΔH, in units of centimeters of water (density 1,000 g/cm^3). The differential pressure, ΔP, in pascals is, therefore, given as 98.06 x ΔH. For the flow velocity used in this work (1.62 m/s), the pressure drop per unit length of channel, $\Delta P/X$, was found to be 3068 Pa/m for the Alloy 706 (upstream) channel and 2935 Pa/m for the Alloy 715 (downstream) channel, with an estimated precision of ±1%. The pressure drop across a single 2.54-cm-long specimen is calculated to be only about 75 Pa, so it would have been impractical to make an accurate pressure drop measurement across a single specimen using the differential manometer shown in Figure 3.

The surface shear stress at the wall of a specimen (or the approach section) was calculated using the equation[4]

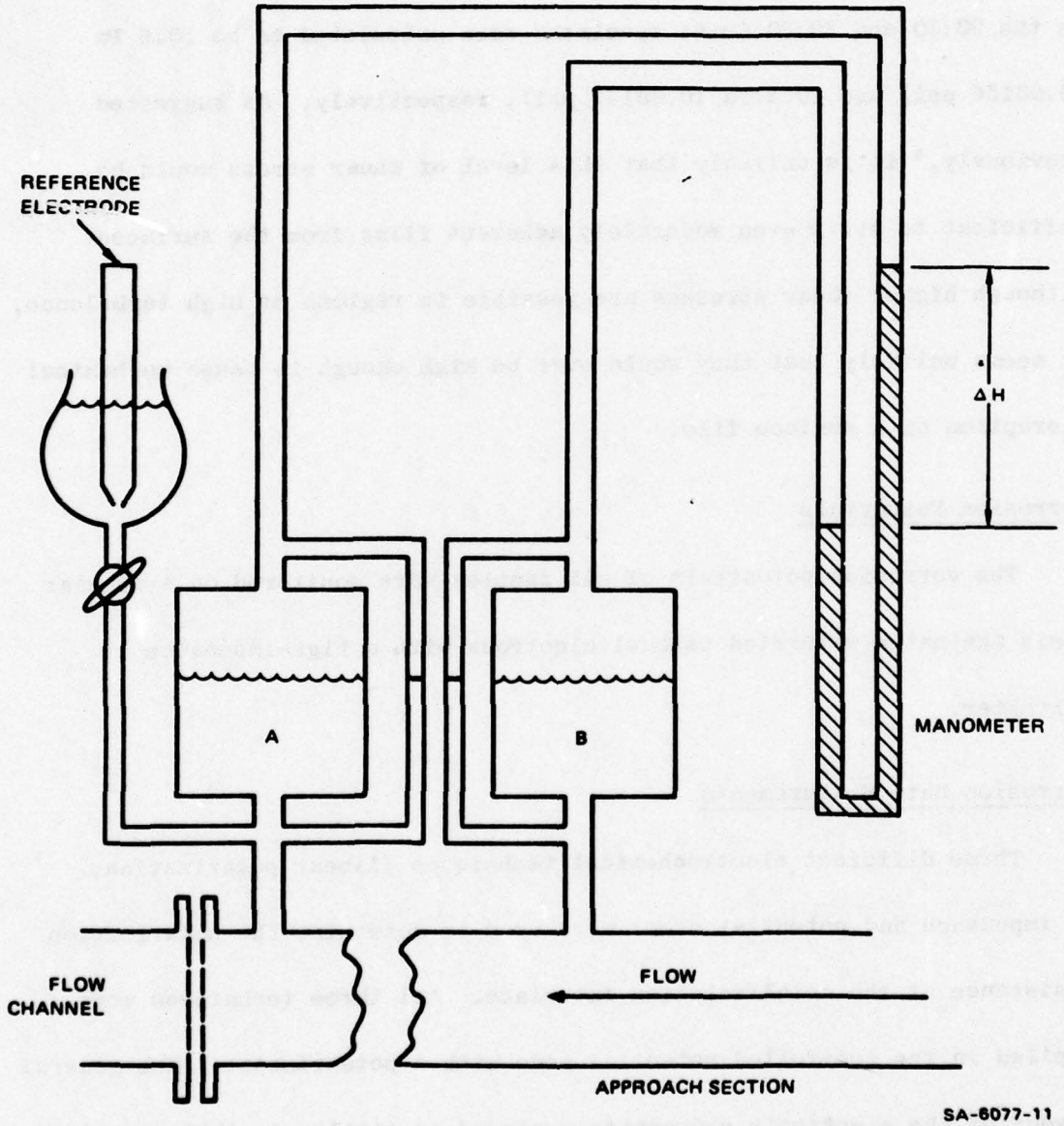

Figure 3 Differential Manometer and Reference Electrode System

$$\tau_w = \Delta P/4(X/L) \quad (1)$$

Where L is the specimen diameter (1.384 cm). The surface shear stresses on the 90:10 and 70:30 Cu:Ni specimens were calculated to be 10.6 Pa (0.00154 psi) and 10.2 Pa (0.00147 psi), respectively. As suggested previously,[4] it is unlikely that this level of shear stress would be sufficient to strip even moderately adherent films from the surfaces. Although higher shear stresses are possible in regions of high turbulence, it seems unlikely that they would ever be high enough to cause mechanical disruption of a surface film.

Corrosion Potentials

The corrosion potentials of all samples were monitored on a regular basis against a saturated calomel electrode with a high-impedance voltmeter.

Corrosion Rate Measurements

Three different electrochemical techniques (linear polarization, ac impedance and potential step) were used to determine the polarization resistance at the metal/solution interface. All three techniques were applied in the controlled potential mode with a potentiostat. The general layout of the electronic components employed is similar to that described in the literature.[2] Particular care was taken to ensure that the system response to a time-dependent excitation did not result from instrumental

artifacts. For instance, in ac impedance work, a phase shift may occur at the current follower output because of the characteristics of the operational amplifier employed, or because of external capacitances associated with leads and contacts.[2] In the present work the performance of the circuit was monitored by regular checks against a number of dummy cells containing both resistive and capacitive components. The dummy cells used were characterized by a wide range of relaxation times.

Linear polarization data were generated by imposing a small-amplitude (20 mV peak-to-peak) saw-tooth potential across the interface. Voltage sweep rates over the range 0.1 mV/s to 50 mV/s were employed, and the current/voltage curves were recorded with an X-Y recorder.

Surface impedance data were generated as a function of frequency (1×10^{-3} Hz to 4×10^{3} Hz) by imposing a 11 mV peak-to-peak sinusoidal signal across the interface. The components of the impedance were calculated from the dimensions of the steady-state Lissajous figures[5] generated by simultaneously imposing the sinusoidal response current and voltage excitation across the Y and X axes, respectively, of an oscilloscope (1 Hz to 4×10^{3} Hz) or fast response X-Y recorder (1×10^{-3} Hz to 1 Hz).

The decay of current with time under potentiostatic conditions was investigated by imposing a small-amplitude potential step ($\Delta E = \pm$ 10 mV) across the interface at zero time. The current was then recorded for

approximately five minutes or until an apparently constant value was obtained.

Cyclic Voltammetry

At the end of each run, cyclic voltammograms were determined for a specimen of each alloy. The voltammograms were measured between the potential limits of -1.5 V and 1.0 V (vs a saturated calomel reference electrode), and at a voltage sweep rate of 0.05 V/s.

RESULTS

Corrosion Potential

The variation of the average corrosion potential with time for two specimens each of copper-nickel alloys 706 (90:10 Cu:Ni) and 715 (70:30 Cu:Ni) is shown as a function of oxygen concentration in Figures 4 and 5, respectively. In general, the high-nickel alloy exhibited very unsteady corrosion potential behavior, particularly at short times. Conversely, E_{corr} for the low-nickel alloy showed little tendency for random fluctuation, and was highly reproducible between the two samples located at either end of the flow channel.

The variation of E_{corr} with oxygen concentration for both alloys after 200 hours exposure is shown in Figure 6. These plots show that, for all oxygen concentrations except 26.3 mg/l, the low-nickel alloy has the most active corrosion potential. However, the difference in corrosion potential between the two alloys decreases with increasing oxygen concentration, such that in oxygen-saturated seawater the two alloys are indistinguishable as far as the open-circuit corrosion potentials is concerned for this time of exposure.

The most interesting features of the data plotted in Figure 6 are the minima observed in the curves showing E_{corr} as a function of

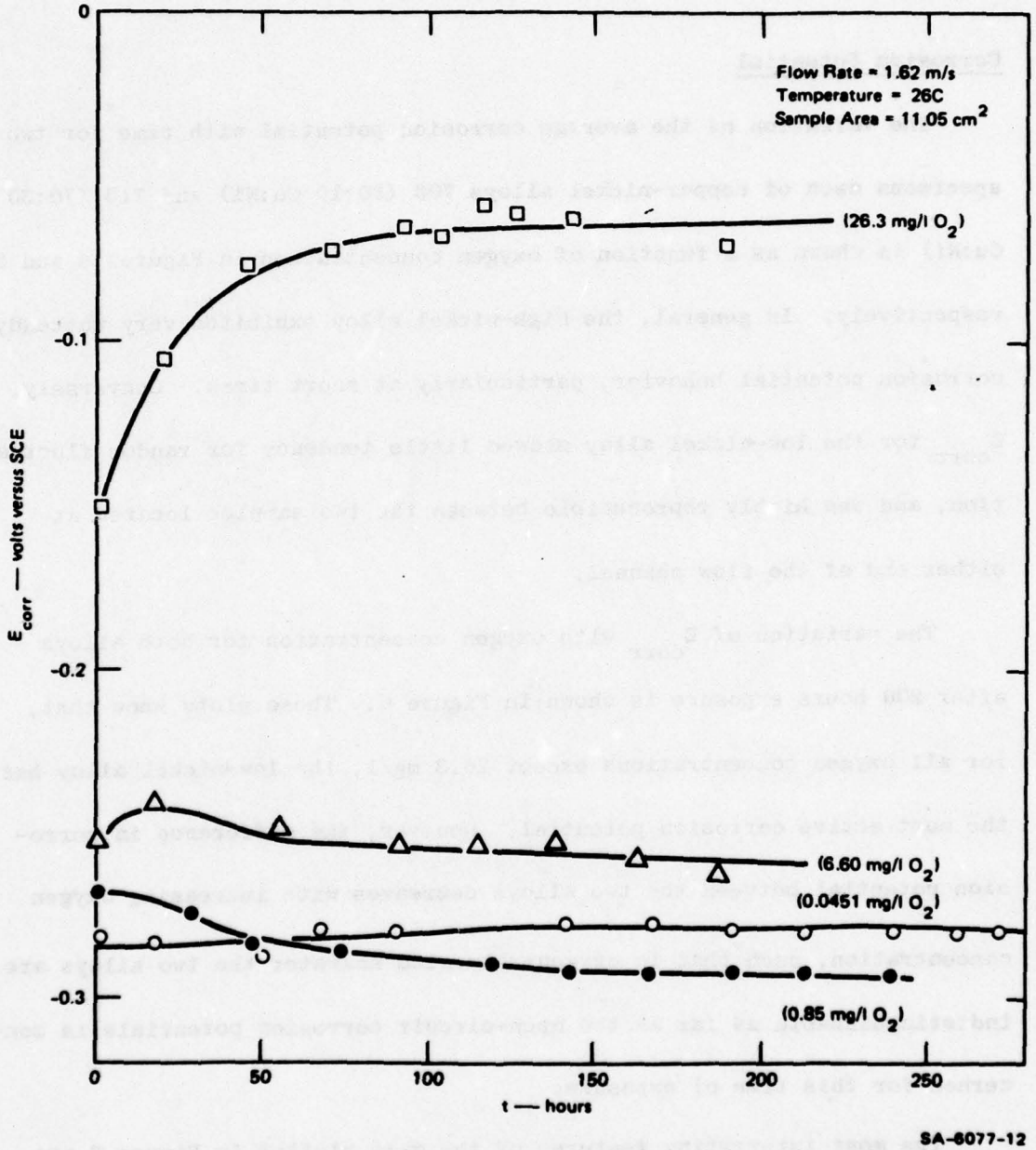

Figure 4 Corrosion Potential (E_{corr}) Versus Time for 90:10 Cu:Ni Alloy in Flowing Seawater as a Function of Oxygen Concentration

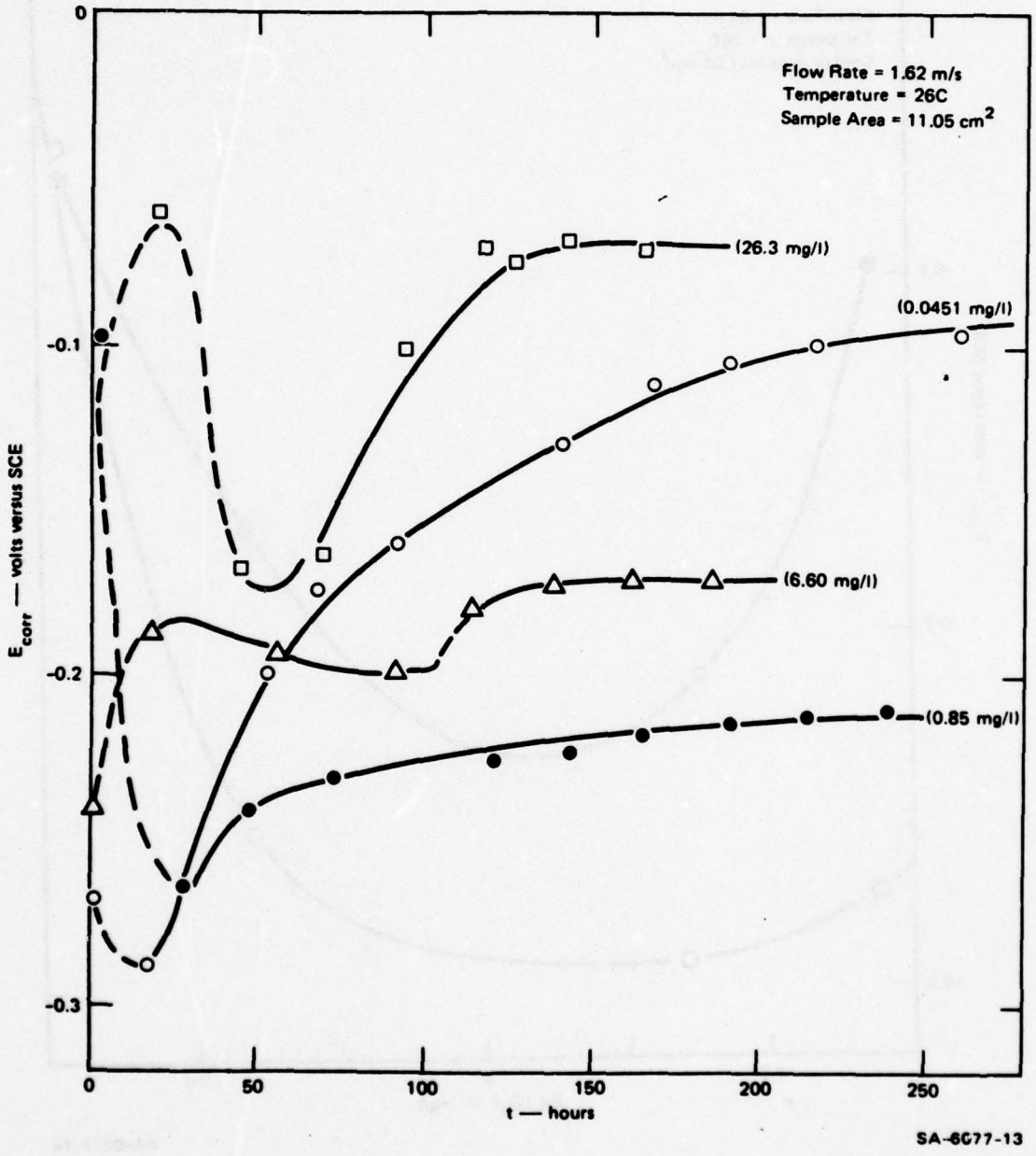

Figure 5 Corrosion Potential (E_{corr}) Versus Time for 70:30 Cu:Ni Alloy in Flowing Seawater as a Function of Oxygen Concentration

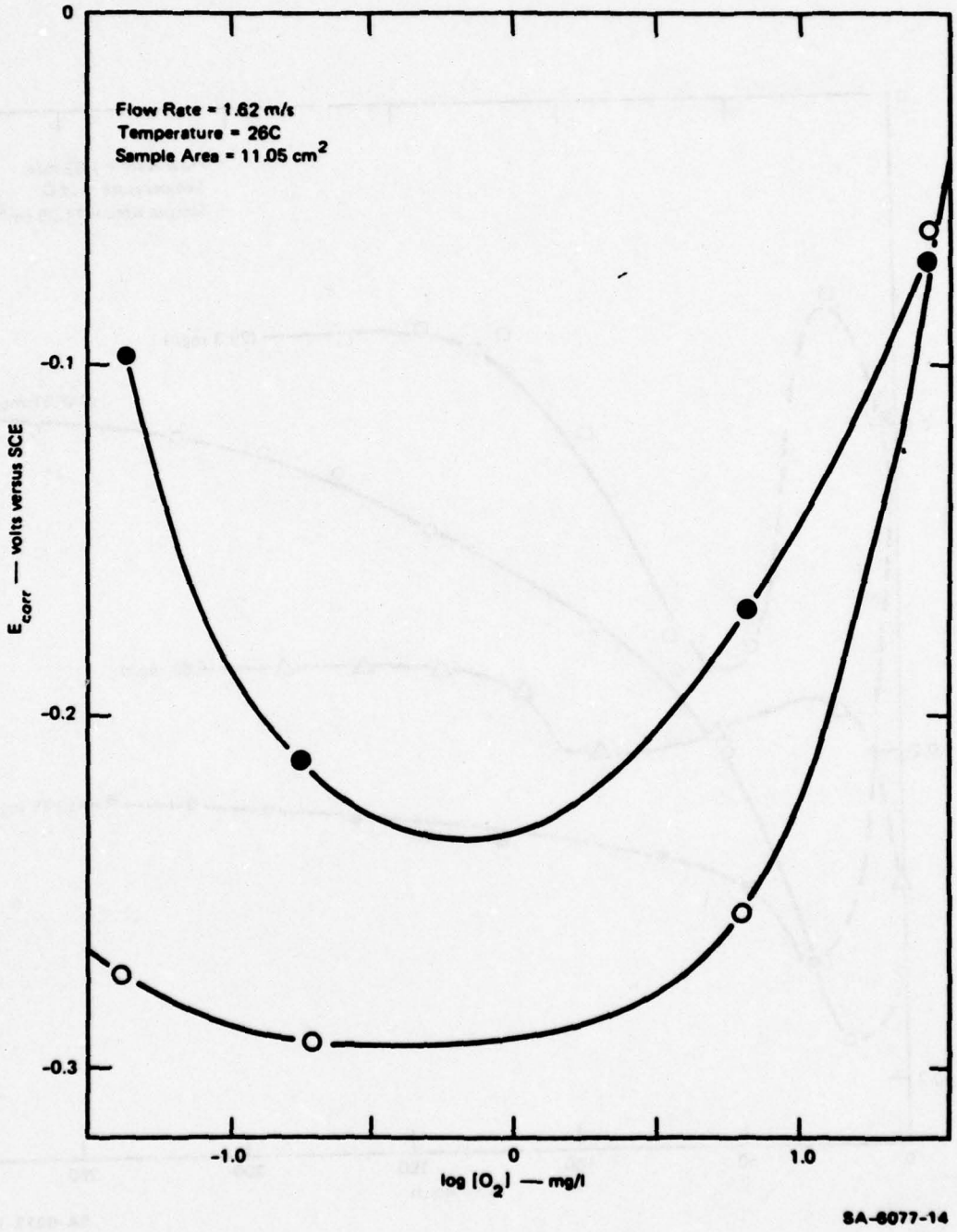

Figure 6 Variation of the Corrosion Potential (E_{corr}) With Oxygen Concentration (mg/l) for 90:10 Cu:Ni (O) and 70:30 Cu:Ni (●) After 200 Hours Exposure to Flowing Seawater

$[O_2]$ for both alloys at 0.5 ~ 1.5 mg/l of dissolved oxygen. Extrema of this type could reflect a change in rate control from the anodic partial reaction at high concentrations of oxygen to the cathodic partial reaction at low concentrations.

Corrosion Rate Measurements

Typical responses of the current to sawtooth (linear polarization technique), sinusoidal (ac impedance technique), and step potential excitations are shown schematically in Figure 7. With all these techniques, the magnitude of the corrosion impedance vector, $\tilde{Z}_c$, at a given frequency (ac impedance and linear polarization) or time (potential step polarization) is given by

$$\left|\tilde{Z}_c\right| = \Delta E/\Delta i \qquad (2)$$

where ΔE and Δi are the amplitudes of the potential excitation and current response functions, respectively. In the limit of zero frequency (linear polarization and ac impedance), or infinite time (potential step), $\left|Z_c\right|$ is equal to the polarization resistance. In this case, the current-voltage curves for the sawtooth and sinusoidal potential exciations collapse into single lines, whereas the current becomes independent of time for potential step polarization.

In this paper, we report data for the linear polarization method at only a single scan-rate (or frequency) for each experiment. The scan

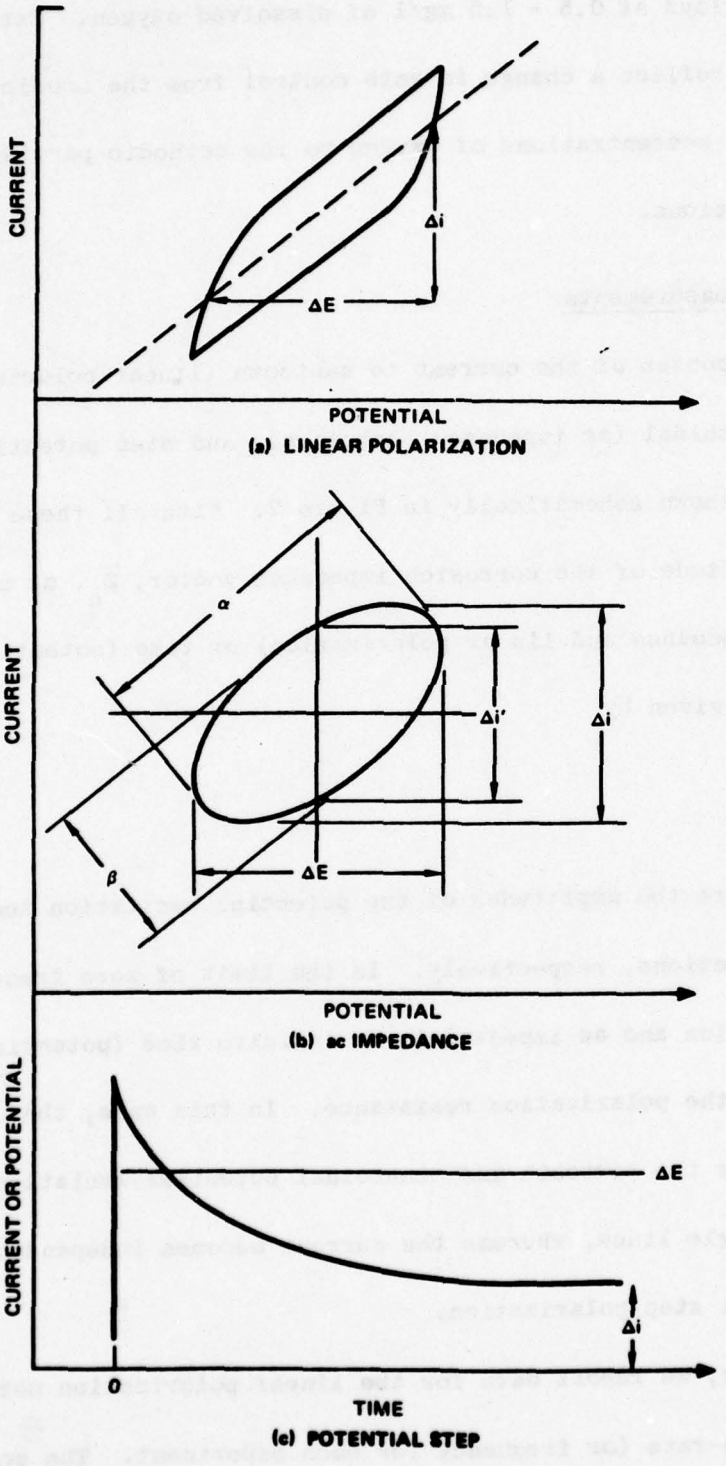

Figure 7 Schematic Current-Voltage Responses for Linear Polarization ac Impedance, and Potential Step Experiments

rates chosen were sufficiently low (0.1 to 0.5 mV/s) that minimal hysteresis was observed on the forward and reverse sweeps. Accordingly, the measured impedance is most likely very close to the polarization resistance. A theoretical analysis of the complete current-voltage curve for this technique will be published shortly.[6]

AC impedance data have been obtained in the present study over the frequency range 4×10^3 Hz to 1×10^{-3} Hz. Following conventional methods[2,7] for the analysis of electrode impedance data, we calculate the equivalent series resistance, R_s, and capacitance C_s, (Figure 8a) from the dimensions of the ellipse, using the expressions[5]

$$R_s = \left|\tilde{Z}_c\right| \cos \varphi \tag{3}$$

$$1/\omega C_s = \left|\tilde{Z}_c\right| \sin \varphi \tag{4}$$

where ω is the angular frequency in radians/s, and the phase angle, φ, is given by one of the two following relationships

$$\sin \varphi = \Delta i'/\Delta i \tag{5}$$

or

$$\sin \varphi = \alpha\beta/\Delta i\, \Delta E \tag{6}$$

The quantities $\Delta i'$, α and β are defined in Figure 7. We have found Equation 5 to be convenient for the high frequency studies (1 Hz to 4×10^3 Hz), where a permanent record of the ellipse from the oscilloscope

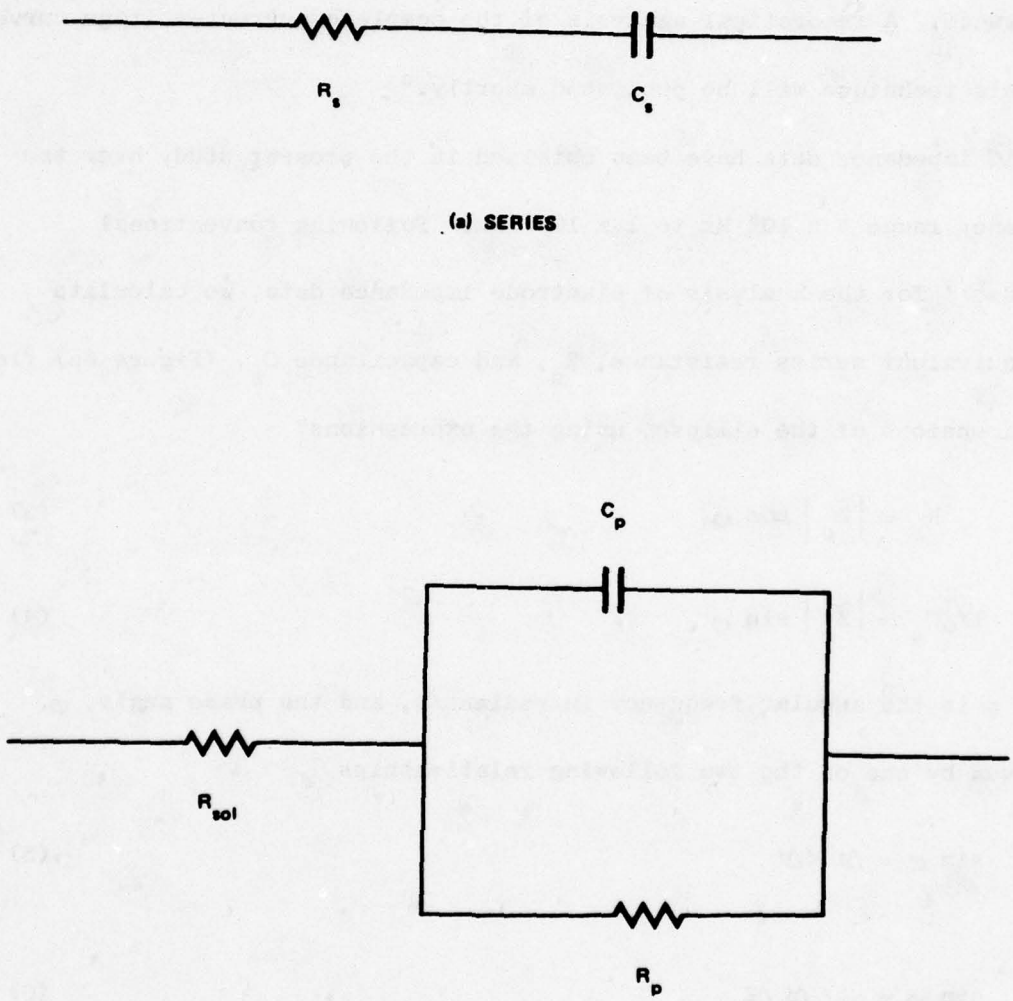

Figure 8 **Series and Parallel Equivalent Circuits for A Corroding Interface**

was not available. On the other hand, both equations 5 and 6 were used to calculate the phase angle from the permanent X-Y recorder traces.

The most convenient method for displaying electrode impedance data is in the form of the complex plane, in which the resistive and capacitive components of the complex impedance vector for the series of RC equivalent circuit[2]

$$\tilde{Z}_c = R_s - j/\omega C_s \qquad (7)$$

where $j = \sqrt{-1}$, are plotted along the abscissa and ordinate, respectively.

Typical impedance diagrams for the 90:10 and 70:30 Cu:Ni alloys are shown in Figures 9 and 10, respectively. Because of the large frequency range employed, it is generally necessary to plot parts of the diagrams separately to illustrate pertinent features. At low frequencies, the impedance plots for both alloys are semicircular, as predicted[2] for parallel RC circuits of the type shown in Figure 8b.

In the limit of zero frequency, the impedance of the parallel capacitance shown in Figure 8b is infinite. Accordingly, the impedance of the equivalent circuit under dc conditions is equal to $R_p + R_{sol}$ (point Y, Figure 9), where R_{sol} is commonly identified with the resistance of the solution between the sample and the reference electrode, and R_p is the polarization resistance. At very high frequencies the capacitor is highly conductive so that the impedance of the circuit is equal to

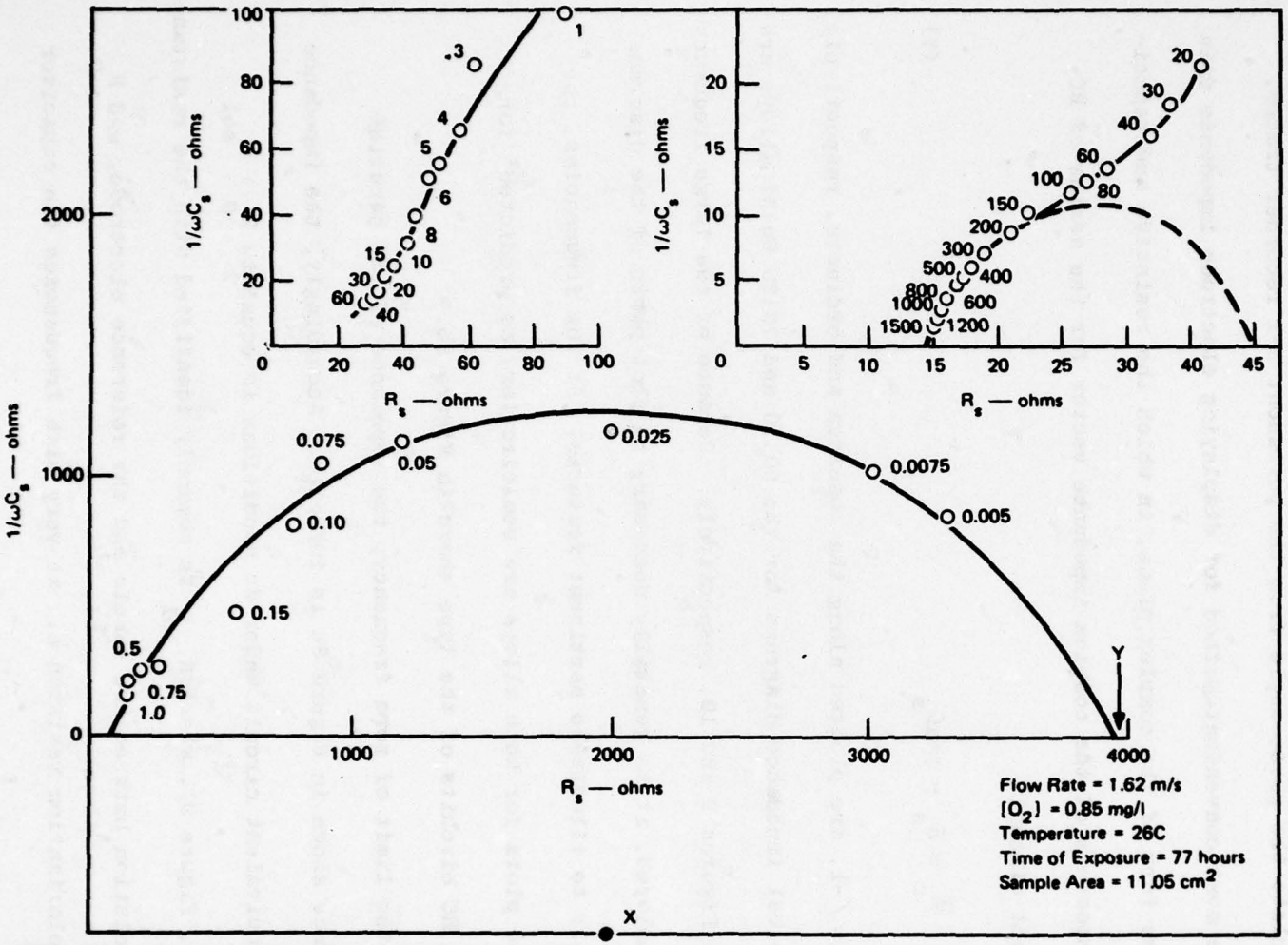

NOTE: The number next to each point designates frequency in Hz.

SA-6077-18

Figure 9 Complex Impedance Plane Plot for 90:10 Cu:Ni in Flowing Seawater

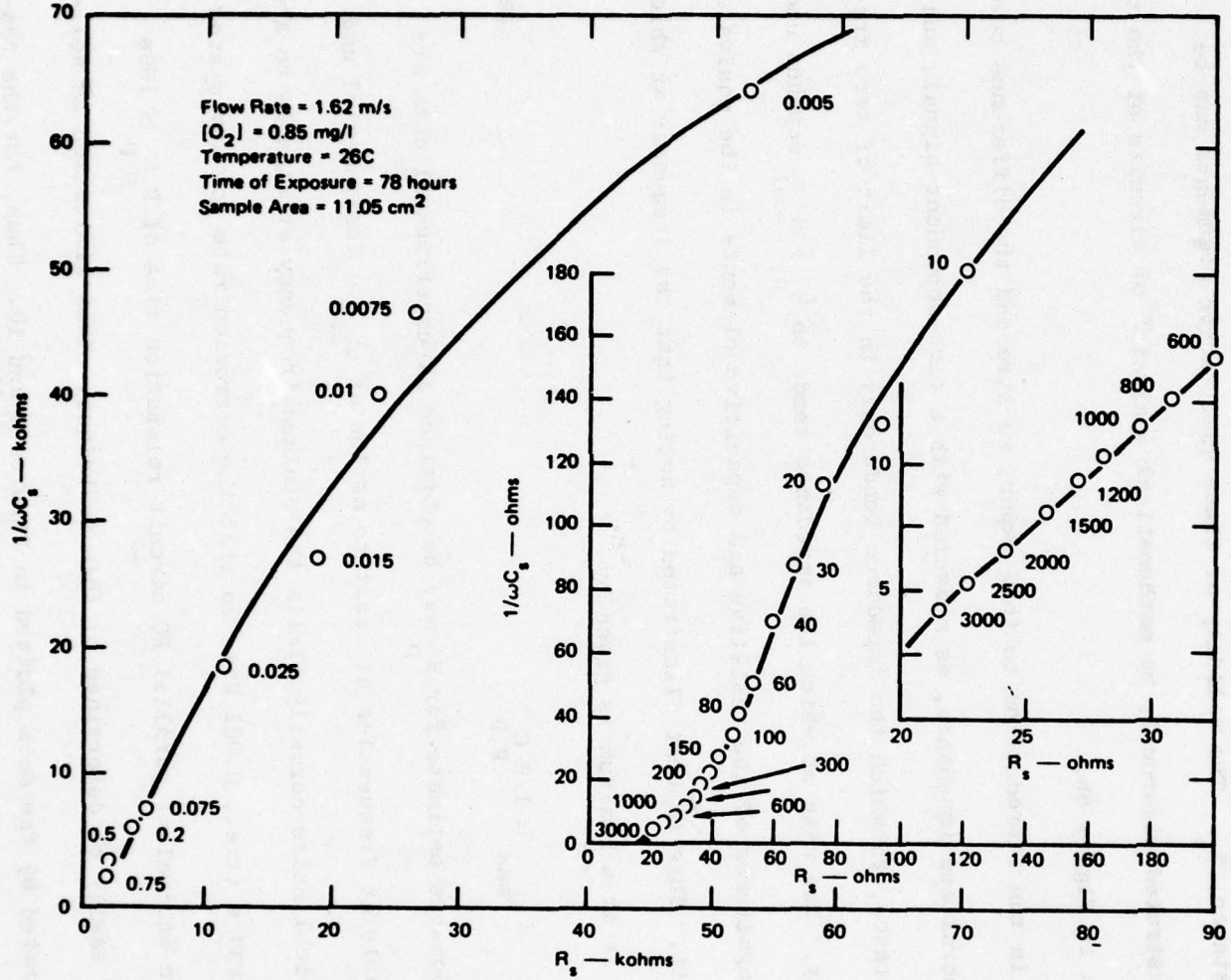

NOTE: The number next to each point designates frequency in Hz.

SA-6077-19

Figure 10 Complex Impedance Plane Plot for 70:30 Cu:Ni in Flowing Seawater

R_{sol}. Thus, the difference between the low frequency and high frequency intercepts on the real axis of the complex plane gives the corrosion resistance, R_p. The validity of these qualitative arguments can be demonstrated rigorously by mathematical analysis[2] of circuits of the type shown in Figure 8b.

In the introduction to this paper, we stressed the difference between a generalized impedance, as measured with a time-dependent signal, and a resistance, to which the impedance tends only in the limit of zero frequency. The rate at which the impedance tends to $R_p + R_{sol}$ depends upon the magnitudes of the resistive and capacitive elements in the equivalent circuit. This is best illustrated by noting that the frequency at which $1/\omega C_s$ is at a maximum is given by

$$\omega_{max} = 1/R_p C_p \quad . \tag{9}$$

A reasonable estimate for R_p may be obtained if experimental data are available at frequencies at least to as low as ω_{max}. Instrumental and electrical noise normally limits the minimum frequency attainable to about 0.006 rad/s (i.e., 0.001 Hz), so that the corrosion rate for any system with an equivalent parallel RC circuit relaxation time of $R_p C_p > 160$s cannot easily be determined by this technique. This limitation is well-illustrated by the data plotted in Figures 9 and 10. Thus, for the conditions chosen, a clearly defined, low-frequency semicircle is exhibited

by the 90:10 Cu:Ni alloy but not by the 70:30 alloy. The difference may be partially attributed to the much larger value for R_p for the high-nickel alloy. Thus, at a frequency of 5×10^{-3} Hz, the polarization resistance for 90:10 Cu:Ni is 3300 ohms, whereas that for the 70:30 Cu:Ni alloy in the same system is 53,000 ohms.

Polarization resistances for the two alloys as a function of time and oxygen concentration, as determined using the linear polarization, ac impedance, and potential step techniques, are plotted in Figure 11 and 12 In those cases that make comparison possible, the linear polarization and impedance techniques show good agreement. A less satisfactory correlation exists between the linear polarization and the potential step methods. The good agreement between the first two techniques is expected because the magnitude of the impedance for linear components in the limit of low frequency should be independent of the technique employed for its measurement. That is so because the conductances of the time- and frequency-dependent capacitive elements become vanishingly small. In the potential step-polarization case, some deviation from the other two techniques is expected for systems that do not exhibit symmetrical polarization curves about the corrosion potential. Recent theoretical work[8] suggests that comparison of the responses to small (e.g., 10 mV) anodic and cathodic potential steps can be used to indicate which of the two partial processes controls the rate of the overall corrosion reaction. For instance, the

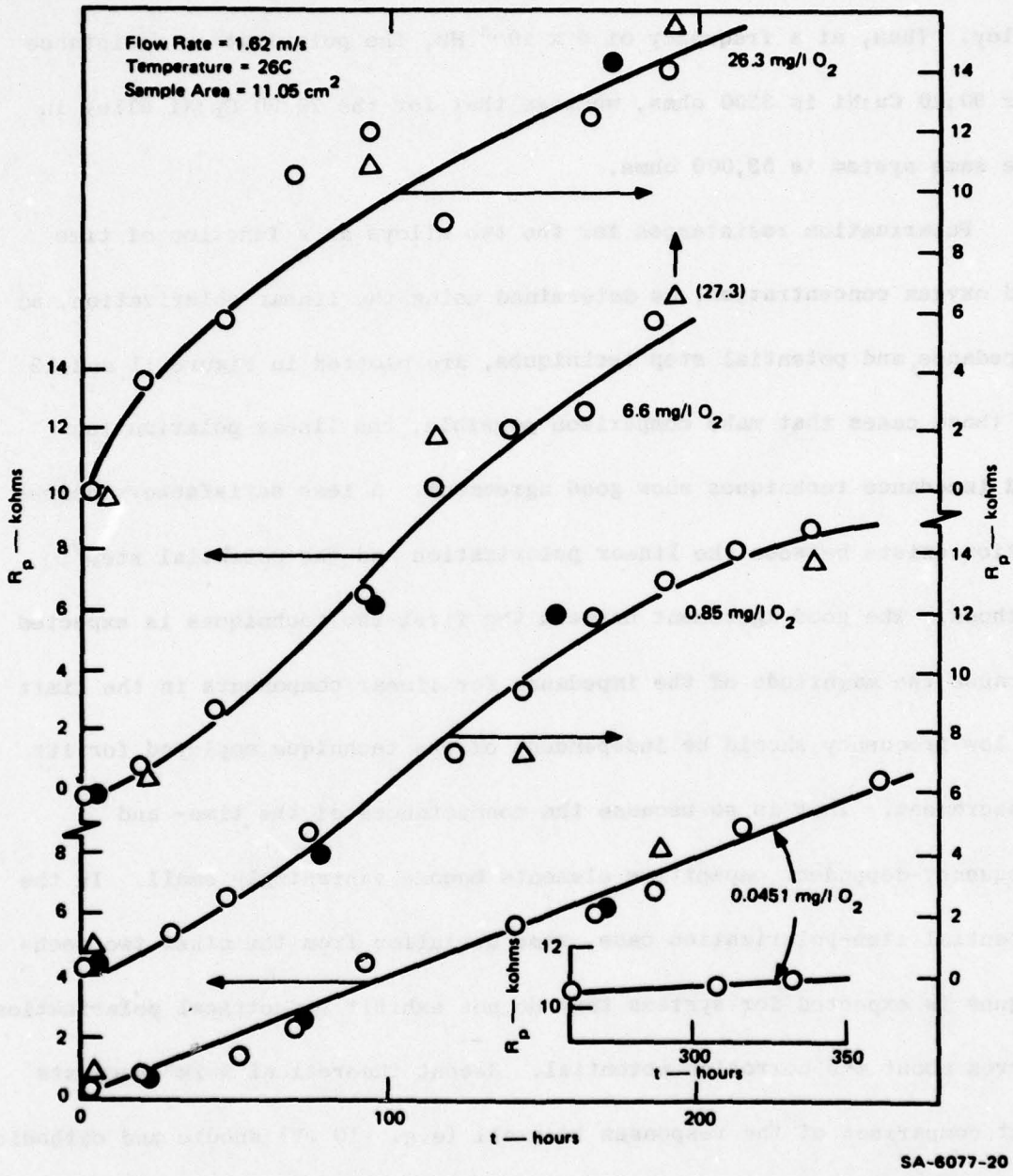

Figure 11 Polarization Resistance (R_p) as a Function of Time and Oxygen Concentration for 90:10 Cu:Ni Alloy in Flowing Seawater
O-linear polarization, e-ac impedance, Δ-potential step

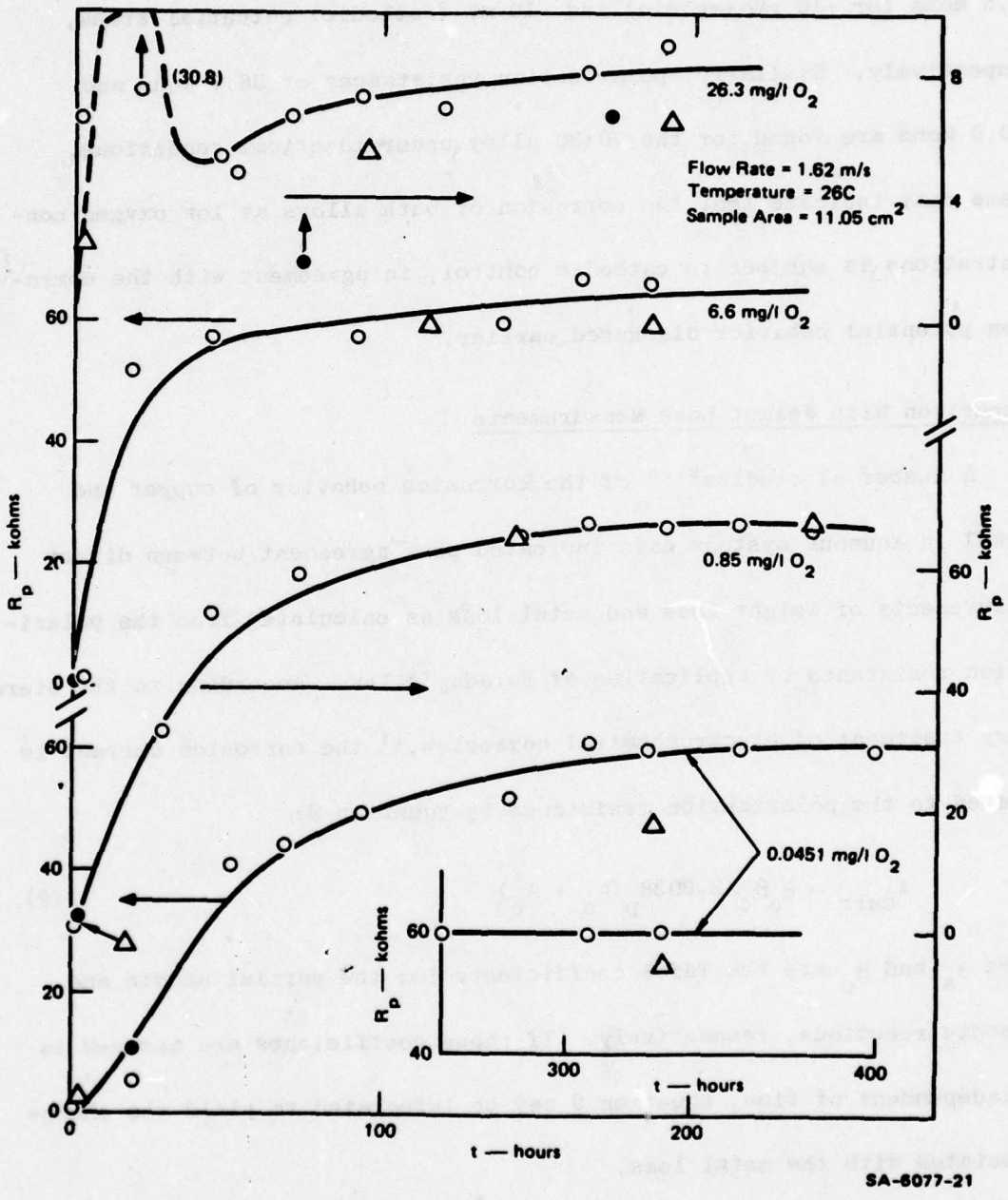

Figure 12 Polarization Resistance (R_p) as a Function of Time and Oxygen Concentration for 70:30 Cu:Ni Alloy in Flowing Seawater O-linear polarization, •-ac impedance, Δ-potential step

the corrosion resistance of 90:10 Cu:Ni alloy in flowing seawater with $[O_2]$ = 0.0451 mg/l at 26 C after 308 hours of exposure is 10.4 kohm and 37.5 kohm for +10 mV (anodic) and -10 mV (cathodic) potential steps, respectively. Similarly, polarization resistances of 38.7 kohm and 100.0 kohm are found for the 70:30 alloy under identical conditions. These data indicate that the corrosion of both alloys at low oxygen concentrations is subject to cathodic control, in agreement with the corrosion potential behavior discussed earlier.

Comparison With Weight Loss Measurements

A number of studies[9,10] of the corrosion behavior of copper and nickel in aqueous systems have indicated poor agreement between direct measurements of weight loss and metal loss as calculated from the polarization resistance by application of Faraday's law. According to the Stern-Geary treatment of electrochemical corrosion,[11] the corrosion current is related to the polarization resistance by Equation 9:

$$i_{corr} = \beta_a \beta_c / 2.303 R_p (\beta_a + \beta_c) \qquad (9)$$

where β_a and β_c are the Tafel coefficients for the partial anodic and cathodic reactions, respectively. If these coefficients are assumed to be independent of time, Equation 9 may be integrated to yield the charge associated with the metal loss,

$$Q_{corr} = \left[\beta_a \beta_c / 2.303(\beta_a + \beta_c)\right] \int_0^t R_p^{-1} \, dt \qquad (10)$$

provided that no parasitic charge transfer reactions occur. Application of Faraday's law therefore yields the weight loss as

$$\Delta W = -\bar{M} Q_{corr} / \bar{n} F \qquad (11)$$

where the composition-averaged atomic weight ($\bar{M}$) and change in oxidation state ($\bar{n}$) are given by

$$\bar{M} = X_{Cu} M_{Cu} + X_{Ni} M_{Ni} \qquad (12)$$

and

$$\bar{n} = X_{Cu} + 2X_{Ni} \quad . \qquad (13)$$

In Equations 12 and 13, X_{cu} and X_{Ni} are the mole fractions of copper and nickel in the alloy. Furthermore, it is assumed that these components are oxidized to the +1 (cuprous) and +2 (nickelous) states, respectively.

The integral contained in Equation 10 was evaluated numerically for each of the curves for R_p as a function of time plotted in Figures 11 and 12. No direct evaluation of β_a and β_c has been attempted in this work.* Instead, the theoretical weight loss has been calculated for the limiting case of either pure anodic control ($\beta_a = \infty$, $\beta_c = 0.06$ V) or pure cathodic control ($\beta_a = 0.06$ V, $\beta_c = \infty$). The calculated and experimental weight

---

*The direct measurement of β_a and β_c involves large deviations of the potential from E_{corr}, and hence, significant changes in the morphology and nature of the specimen surface. Accordingly, direct evaluation of these coefficients was not considered practical in this work.

losses for the two alloys at the four oxygen concentrations of interest are listed in Table 3.

Recognizing that the Tafel coefficients were not measured directly, and that the true values for β_a and β_c could easily differ by ± 50% from those assumed, excellent agreement is obtained between the directly measured weight loss and that calculated using Equation 12, with the exception of the 70:30 Cu:Ni alloy in the oxygen saturated system ($[O_2]$ = 26.3 mg/1). In that case, both the corrosion potential and the polarization resistance exhibited large fluctuations at short times. Observed fluctuations of R_p to low values could result in large, but undetected, corrosion currents. Accordingly, the difference between the measured and calculated weight losses listed in Table 3 for this system is not considered serious. Also, for 70:30 Cu:Ni alloy in seawater containing 0.85 mg/1 and 6.60 mg/1 oxygen, the calculated weight loss is probably on the high side because a linear, rather than parabolic, decrease in $1/R_p$ (see Equation 11) was assumed between adjacent points. Consequently, an overestimation of both Q_{corr} and ΔW is expected. This linear approximation did not lead to significant error in the case of 90:10 Cu:Ni alloy because the $1/R_p$ values for this material did not change as rapidly during the critical first thirty hours.

Previous work has suggested that the linear polarization technique tends to underestimate the weight loss for the corrosion of both copper[9]

Table 3

COMPARISON BETWEEN EXPERIMENTAL AND CALCULATED WEIGHT LOSS

$[O_2]$ (mg/l)	Exposure Period (hours)	Weight Loss (mg) Experimental	Calculated
	90:10 Cu:Ni		
0.045	336.5	5.92 ± 0.3	6.60
0.85	246.5	6.00 ± 0.1	5.45
6.60	189	7.78 ± 0.1	6.63
26.3	196	3.18 ± 0.1	2.69
	70:30 Cu:Ni		
0.045	336.5	1.65 ± 0.35	2.49[a]
0.85	246.5	2.10 ± 0.1	3.12[a]
6.60	189	4.45 ± 1.5	4.94[a]
26.3	196	9.33 ± 0.03	1.20[b]

[a]These calculated values are probably too high (see text).
[b]This calculated value is probably too low (see text).

and nickel[10] in aqueous systems under ambient conditions. We now believe that this probably results from very high (but undetected) corrosion rates at short times. We therefore stress the need for semicontinuous monitoring of the corrosion rate from the time that the metal first contacts the corrosive environment. The generally excellent agreement between the calculated and directly measured weight losses obtained in the present study shows that, provided sufficient care is taken to obtain data at very short times, the linear polarization technique is well-suited for studying the effect of environment on the corrosion of copper-nickel alloys in natural seawater.

DISCUSSION

Bianchi and Longhi[12] have published potential-pH diagrams for copper in seawater, in which a variety of oxides, hydroxides, and hydroxychlorides were considered as stable phases. One of their diagrams is reproduced in Figure 13. The corrosion potentials observed in the present work (-0.06 to -0.3 V vs SCE or 0.18 to -0.06 V vs SHE) lie within the stability region for Cu_2O, but are close to the equilibrium potentials for the $Cu_2(OH)_3Cl/Cu_2O$ couple. We have observed the formation of a green deposit on the downstream filter when the electrode potential is swept to high noble values. Furthermore, a thin green film is found on the freely corroding samples, particularly at high concentrations of oxygen. The films are too thin for identification by X-ray diffraction, but work is currently in progress to examine the films using Auger spectrometry. The green coloration is consistent with the existence of copper hydroxychlorides in the corrosion products on the metal surface. Cuprous oxide (Cu_2O) is also most likely present on the corroded specimen surfaces.

Both the variation of corrosion potential with oxygen concentration, and the small amplitude potential step experiments, indicate that for short times (< 330 hours), the corrosion of 90:10 CuNi and 70:30 Cu:Ni in oxygenated, flowing seawater is cathodically controlled, provided that

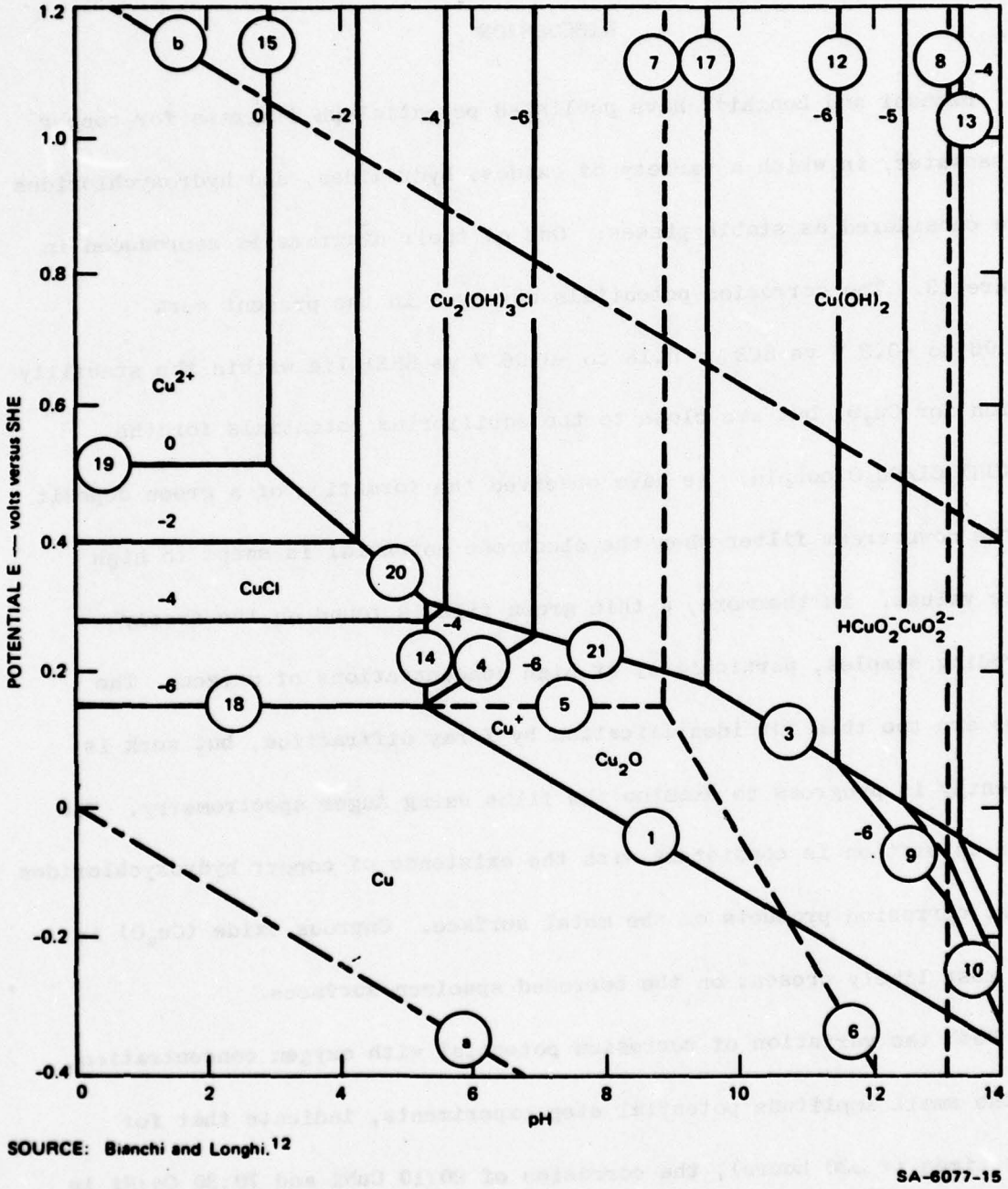

SOURCE: Bianchi and Longhi.[12]

SA-6077-15

Figure 13 Potential-pH Diagram for Copper in Seawater at 25 C (after Bianchi and Longhi (12))

$[O_2] \leq 0.85$ mg/l. Accordingly, the overall corrosion rate under these conditions is probably determined by transport of molecular oxygen to the surface or by electrochemical reduction. On the other hand, the corrosion potential data for high oxygen concentrations (≥ 6.60 mg/l) are consistent with anodic control, presumably determined by ionic or electronic transport through a surface film. It is possible that, given sufficient time, the cathodic control found at low oxygen concentrations will transform to anodic control once a film of sufficient thickness has been established on the surface.

The impedance spectra plotted in Figures 9 and 10 indicate that the corrosion of both alloys is characterized by at least two separate relaxation processes, each of which gives rise to a semicircle in $1/\omega C_s$ as a function of R_s. In the case of the 90:10 Cu:Ni alloy, the two semicircles are clearly resolved, with the high-frequency one centered on the real axis and the low-frequency semicircle centered well below the real axis (i.e., at point X, Figure 9). To a first approximation, the phenomena responsible for the semicircles can be represented by electrical equivalent circuits of the type shown in Figure 8(b). However, that circuit, which is characterized by a single definite relaxation time, will strictly yield a semicircle that is centered on the real axis only. Accordingly, we suggest that the charge transfer phenomenon responsible for the high-frequency semicircle is characterized by a single sharp relaxation time. Such

behavior is expected from a metal dissolution reaction, such as $Cu \rightarrow Cu^{+} + e$, or it is possibly because of the cathodic partial reaction $O_2 + 4H^{+} + 4e \rightarrow 2H_2O$. On the other hand, the low-frequency semicircle, with its center below the real axis, is characteristic of a charge transfer process that exhibits a distribution of relaxation times. If we assume that this semicircle arises from transport across a surface film, a distribution in the relaxation time ($= R_p C_p$, Figure 8(b)) is expected if a distribution in surface film thickness (and hence resistance and capacitance) is assumed to exist.

Possibly the most important finding of the present study is the effect of oxygen on the polarization *resistance* for various exposure times as plotted in Figure 14. Those data show that for $[O_2] \leq 6.60$ mg/l, the polarization resistance for the 70:30 Cu:Ni alloy is considerably greater than that for the 90:10 alloy, and that for both cases R_p increases with oxygen concentration. At the highest oxygen concentrations employed, however, the polarization resistance for the 70:30 Cu:Ni alloy drops sharply to a value that is comparable to that for the 90:10 alloy in the same system. Thus, the beneficial effect of high nickel, apparent at low oxygen concentrations, no longer exists in oxygen-saturated seawater, at least for the exposure times employed in this work.

A possible explanation for the sudden loss of the high corrosion resistance of the 70:30 Cu:Ni alloy in oxygen-saturated seawater is

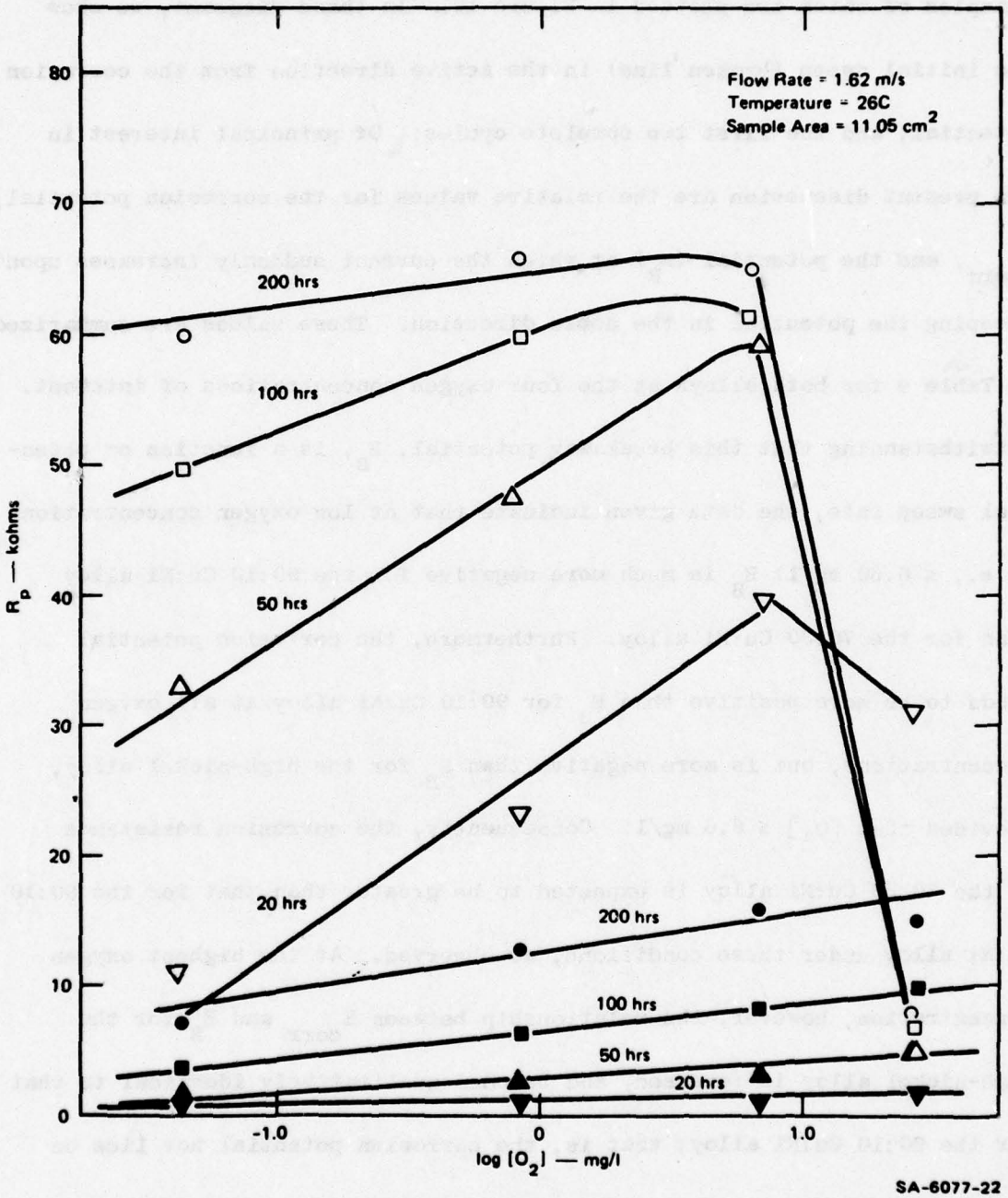

Figure 14 Variation of the Polarization Resistance (R_p) for 70:30 Cu:Ni (Open Points) and 90:10 Cu:Ni Alloy (Filled Points) in Flowing Seawater as a Function of Oxygen Concentration for Selected Exposure Periods

afforded by an examination of the cyclic voltammograms for the two alloys, examples of which are plotted in Figure 15. In these diagrams, we show the initial sweep (broken line) in the active direction from the corrosion potential, and the first two complete cycles. Of principal interest in the present discussion are the relative values for the corrosion potential, E_{corr}, and the potential (E_B) at which the current suddenly increases upon sweeping the potential in the noble direction. These values are summarized in Table 4 for both alloys at the four oxygen concentrations of interest. Notwithstanding that this breakaway potential, E_B, is a function of potential sweep rate, the data given indicate that at low oxygen concentrations (i.e., $\leq$ 6.60 mg/l) E_B is much more negative for the 90:10 Cu:Ni alloy than for the 70:30 Cu:Ni alloy. Furthermore, the corrosion potential tends to be more positive than E_B for 90:10 Cu:Ni alloy at all oxygen concentrations, but is more negative than E_B for the high-nickel alloy, provided that $[O_2] \leq 6.6$ mg/l. Consequently, the corrosion resistance of the 70:30 Cu:Ni alloy is expected to be greater than that for the 90:10 Cu:Ni alloy under these conditions, as observed. At the highest oxygen concentration, however, the relationship between E_{corr} and E_B for the high-nickel alloy is reversed, and becomes qualitatively identical to that for the 90:10 Cu:Ni alloy; that is, the corrosion potential now lies on the noble side of E_B. We believe that this reversal is caused both by changes in the rate of supply of oxygen to the surface and by the nature of the surface corrosion film.

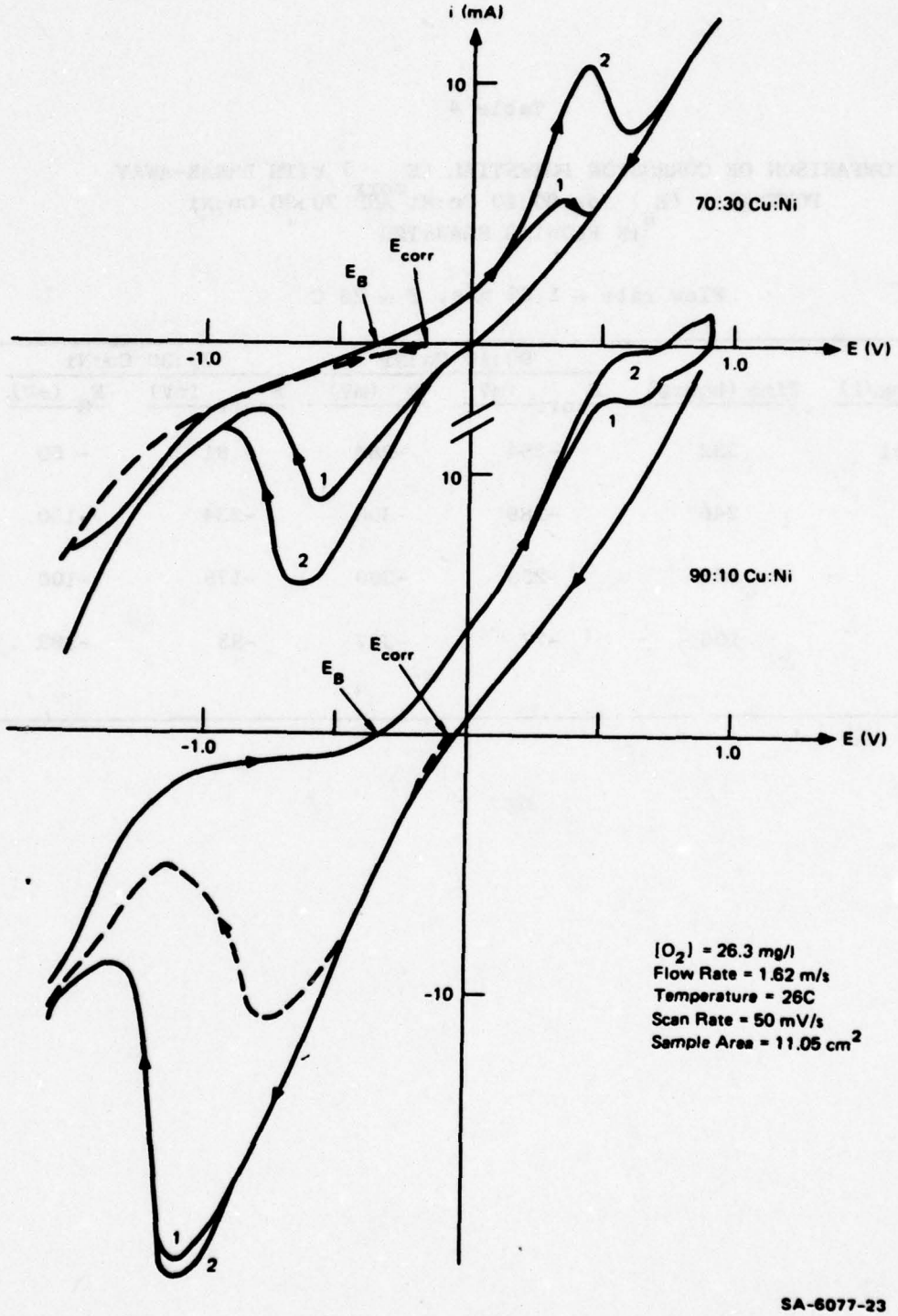

Figure 15 Cyclic Voltammograms for 90:10 Cu:Ni Alloy and 70:30 Cu:Ni Alloy in Flowing Seawater. The broken line shows the initial sweep in the active direction from the corrosion potential.

Table 4

COMPARISON OF CORROSION POTENTIAL (E_{corr}) WITH BREAK-AWAY POTENTIAL (E_B) for 90:10 Cu:Ni AND 70:30 Cu:Ni IN FLOWING SEAWATER

Flow rate = 1.62 m/s, T = 26 C

		90:10 Cu:Ni		70:30 Cu:Ni	
$[O_2]$ (mg/l)	Time (hours)	E_{corr} (mV)	E_B (mV)	E_{corr} (mV)	E_B (mV)
0.0451	332	-284	-284	- 81	- 50
0.85	246	-289	-300	-234	-150
6.60	189	-250	-300	-178	-100
26.3	196	-77	-327	-83	-383

SUMMARY AND CONCLUSIONS

An experimental flow loop has been constructed that permits detailed corrosion and electrochemical investigation of copper-nickel alloys in flowing seawater under closely controlled environmental and hydrodynamic conditions. Linear polarization, ac impedance, and potential step techniques have been used to evaluate the polarization resistance of 90:10 Cu:Ni and 70:30 Cu:Ni alloys in flowing seawater at oxygen concentrations of 0.0451, 0.85, 6.60, and 26.3 mg/l.

The principal findings made during the course of this study are now summarized.

(1) Satisfactory agreement has been obtained between the directly measured weight loss and that calculated from the variation of polarization resistance with time, thereby demonstrating the applicability of electrochemical methods for measuring the corrosion rates of copper-nickel alloys in natural oxygenated seawater.

(2) The 70:30 Cu:Ni alloy exhibits superior corrosion resistance to the 90:10 Cu:Ni alloy over the exposure times employed, provided that the oxygen concentration is maintained at or beneath the air-saturated value of 6.60 mg/l. At higher

oxygen concentration, a sharp breakdown in the corrosion resistance of the high nickel alloy is observed, to the extent that in the oxygen saturated system ($[O_2]$ = 26.3 mg/l) no difference between the high and low nickel alloys is apparent. It is believed that the loss in corrosion resistance of the 70:30 Cu:Ni alloy is due to a shift in the corrosion potential to a value that is more noble than the potential at which large anodic currents are observed when the potential is swept in the active to noble direction.

(3) Comparison of the corrosion potentials with the potential-pH diagrams for copper in seawater indicates that the corrosion product should be Cu_2O or a copper hydroxchloride. The green deposit observed to collect on the seawater filter is consistent with the latter suggestion but we believe Cu_2O is also present on the specimen surface.

(4) The variation of corrosion potential with oxygen concentration, and some potential step data indicate that, for the short exposure times considered here, the corrosion reaction is cathodically controlled at low oxygen concentrations, but is anodically controlled at high concentrations. Impedance spectra indicate the existence of two clearly separated

relaxation processes, one of which is consistent with transport through a surface film having a distribution in thickness

ACKNOWLEDGMENT

Financial support of this work by the Office of Naval Research (Contract No. N00014-77-C-0046) is gratefully acknowledged.

REFERENCES

1. H. H. Uhlig, Corrosion and Corrosion Control, 2nd. Edit., John Wiley and Sons, New York, 1971.

2. D. D. Macdonald, Transient Techniques in Electrochemistry, Plenum Publishing Co., New York, 1977.

3. Standard Methods for the Examination of Water and Wastewater Including Bottom Sediments and Sludges, 12th Edit., American Public Health Assoc., New York,

4. B. C. Syrett, Corrosion , Vol. 32, p. 242 (1976).

5. J. Czech, Oscilloscope Measuring Technique, Springer-Verlag, New York, 1965.

6. D. D. Macdonald, to be published.

7. I. Epelboin, M. Keddam, and H. Takenouti, J. Appl. Electrochem., Vol. 2, p. 71 (1972).

8. D. W. Bird, Corrosion Science, Vol. 13, p. 913 (1973).

9. B. C. Syrett, Corrosion, Vol. 33, p. 257 (1977).

10. L. M. Callow, J. A. Richardson, and J. L. Dawson, Br. Corros. J., Vol. 11, p. 123 (1976).

11. M. Stern and A. L. Geary, J. Electrochem. Soc., Vol. 104, p. 56 (1957).

12. G. Bianchi and P. Longhi, Corrosion Science, Vol. 13, p. 853 (1973).

Appendix II

AN IMPEDANCE INTERPRETATION OF SMALL AMPLITUDE CYCLIC VOLTAMMETRY -- I: THEORETICAL ANALYSIS FOR A RESISTIVE - CAPACITIVE SYSTEM

by

Digby D. Macdonald*

Materials Research Center
SRI International
Menlo Park, California 94025

ABSTRACT

The transient response of an equivalent circuit for an electrode/solution interface to a small-amplitude sawtooth potential excitation is derived by use of transform analysis. The response consists of both transient and steady-state contributions. The predicted steady-state response yields a hysteresis loop that is qualitatively similar to those exhibited by real systems under small-amplitude cyclic voltammetric (SACV) conditions. Numerical analysis illustrates the dependence of the response on the voltage sweep-rate, the magnitude of the potential excitation function, and the values for the resistances and capacitance in the equivalent circuit. Analytical functions are derived for the steady-state response, and the application of these expressions to the analysis of experimental data for corroding 90:10 Cu:Ni alloy in flowing seawater is described.

Small-amplitude cyclic voltammetry (SACV) (1), in which a sawtooth potential excitation function is imposed across an electrode/solution interface, has been used for both fundamental studies of the structure and capacitance of the double layer, and for evaluating the corrosion rates of metals in condensed systems. At high voltage sweep-rates, the capacitive components dominate the interfacial impedance, and the observed current response can be used to estimate the capacitance of the surface (1). Conversely, at low sweep-rates the capacitive current is frequently negligible compared with the faradaic contribution; thus, the SACV response is principally determined by the charge transfer (polarization) resistance of the interface.

The SACV technique is used extensively in corrosion research for estimating the polarization resistance of a metal-solution interface at the corrosion potential (2). Typically, a 10- to 20-mV peak-to-peak sawtooth excitation is imposed across a corroding interface by use of a potentiostat. The current response is then recorded over one or more cycles, and the polarization resistance is estimated from the gradient of the potential (E) versus current (I) plot at the corrosion potential. The E versus I plot is frequently nonlinear, but more important for the present analysis, the plot may exhibit considerable hysteresis. The nonlinear response has been discussed (2,3), and it appears that this phenomenon can be used to obtain information on the nature of the corrosion process. On the other hand, little attention has been focused on the origin of the hysteresis, even though this property plays a central role in the interpretation of data from the closely related ac impedance technique (1).

In this paper, the origin of the hysteresis in current versus potential as observed under SACV conditions is analyzed in terms of the impedance of an equivalent electrical circuit. It is shown that the degree of hysteresis is sensitive to the potential sweep rate, and that the observed current response can be used to estimate values for the resistances and capacitances at the interface.

Impedance Operators

Provided that the amplitude of the excitation voltage is sufficiently small, the components of the impedance at a metal/solution interface can be regarded as linear; that is, the impedances of the individual components are independent of voltage. Accordingly, the interface may be represented by an equivalent electrical circuit consisting of linear components only, and the response of the system to an excitation signal E(t) can be obtained by application of Eq. [1].

$$I(t) = E(t)/Z(p) \qquad [1]$$

where p is the impedance operator defined as

$$p = d/dt \qquad [2]$$

$$1/p = \int dt \qquad [3]$$

The impedance function Z(p) is chosen so that Z(p) x I(t) is equal to the voltage drop across the device in question. For instance, the drops in voltage across resistive, capacitive and inductive components are given by

$$\text{Resistive:} \quad E(t) = RI, \; Z(p) = R \qquad [4]$$

$$\text{Capacitive:} \quad E(t) = (1/C) \int I dt, \; Z(p) = 1/pC \qquad [5]$$

$$\text{Inductive:} \quad E(t) = L(dI/dt), \; Z(p) = Lp \qquad [6]$$

Furthermore, the total voltage drop across a series combination of components is given by

$$E(t) = \sum_i E_i(t) \qquad [7]$$

whereas the total current through a parallel network is

$$I(t) = \sum_i I_i(t) \qquad [8]$$

Accordingly, the impedance functions for series and parallel combinations of components are given by Eqs. [9] and [10], respectively

$$Z(p) = \sum_i Z_i(p) \qquad [9]$$

$$I/Z(p) = Y(p) = \sum_i [1/Z(p)] = \sum_i Y_i(p) \qquad [10]$$

The function Y(p) is commonly termed the admittance function for the circuit under consideration.

Inspection of Eqs. [1], [4], [5], [6], [9], and [10] shows that if the impedance (or admittance) operator of a complex circuit is known, then prediction of the current response to a specified excitation voltage function E(t) will involve solution of one or more integral/differential equations. One of the most effective methods for handling this type of problem is by use of Laplace (or Fourier) transforms. The application of these integral transforms for predicting the transient responses of electrical circuits is known as Transform Analysis. Although Pilla (4), and others (1,5,6), have used numerical transformation techniques in the analysis of the ac impedance characteristics and potentiostatic responses of electrochemical systems, transform analysis of either experimental data or equivalent electrical circuits does not appear to have been employed in the study of SACV.

Transform Analysis

It can be shown (7), that upon transformation of Eq. [1] into Laplace space, that is

$$\bar{I}(s) = \bar{E}(s)/Z(s) \qquad [11]$$

with

$$\mathcal{L}[f(t)] = \bar{f}(s) = \int_0^{\infty} f(t)e^{-st}dt, \qquad [12]$$

the impedance function Z(s) has the same analytical form as Z(p) with the impedance operator, p, replaced by the Laplace variable, s. This convenient property permits the straightforward derivation of an expression for the Laplace transform of the current in terms of the variable s. Inverse transformation (analytically or numerically) therefore yields the required current response in terms of real time.

By way of illustration, we consider a simple series RC circuit. The impedance operator for this circuit is obtained from Eq. [4] and [5] as

$$Z(p) = R + 1/pC \qquad [13]$$

The current response to a voltage step applied at t = 0 is therefore given in Laplace space as

$$\bar{I}(s) = ED/(1 + sRC) \qquad [14]$$

where the Laplace transform of E(t) is (8)

$$\mathcal{L}[E(t)] = E/s \qquad [15]$$

Inverse transformation of Eq. [14] is straightforward by use of standard tables (8) to yield the familiar exponential decay of current with time

$$I(t) = (E/R)e^{-t/RC} \qquad [16]$$

Simulated Metal/Solution Interface

The simplest general electrical equivalent circuit for a metal/solution interface is a parallel combination of a resistor (R_p) and a capacitor (C) in series with a second resistor (R_s) as shown in Fig. 1a. The resistance R_p may be identified with the charge-transfer (or polarization) resistance, whereas R_s is commonly associated with any pure resistance (e.g. from the solution, or low capacitive films) between the metal and the tip of the reference electrode probe. Although at first sight this equivalent circuit may appear to be unrealistically simple, it can frequently simulate the relaxation behavior of a real interface, particularly if a single relaxation process dominates the electrochemical behavior over a wide range of frequency. In the complex plane representation of the impedance, this behavior is characterized by a single first quadrant semicircle centered on the real axis. Although other relaxation processes may exist at other frequencies, their contributions to the overall impedance of a series combination of elements of the type shown in Fig. 1a will be small, provided that the relaxation times are sufficiently well-separated.

With these limitations in mind, the impedance of the interface under linear conditions is given by

$$Z(p) = R_s + \frac{R_p}{1 + pR_pC} \qquad [17]$$

The excitation voltage applied in the controlled potential mode across the interface is in the form of the sawtooth shown in Fig. 1b and is represented mathematically by Eq. [18]

$$E = \begin{cases} E_m\left[\frac{t}{\lambda} - 2n\right] & 2n\lambda < t < (2n+1)\lambda \text{ (forward sweep)} \\ E_m\left[2(n+1) - \frac{t}{\lambda}\right] & (2n+1)\lambda < t < (2n+2)\lambda \text{ (reverse sweep)} \end{cases} \qquad [18]$$

FIGURE 1

EQUIVALENT CIRCUIT AND VOLTAGE EXCITATION FUNCTION FOR THE MODEL CONSIDERED FOR THE METAL-SOLUTION INTERFACE

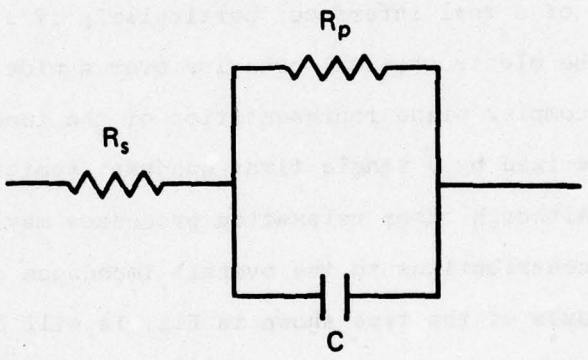

(a) EQUIVALENT CIRCUIT FOR THE METAL-SOLUTION

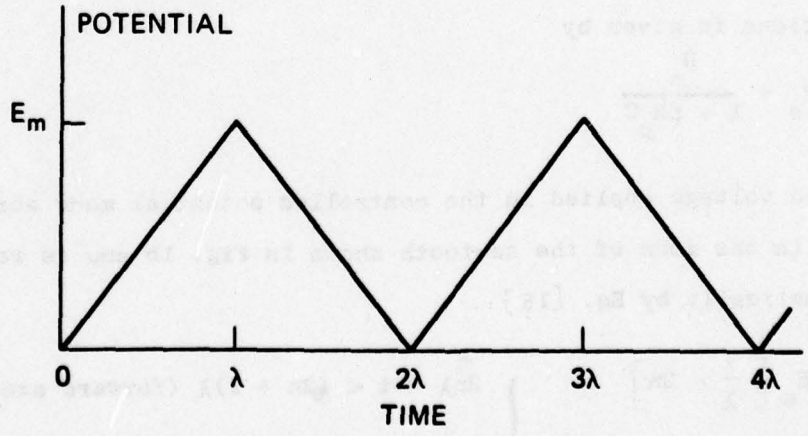

(b) SAW-TOOTH VOLTAGE EXCITATION FUNCTION

where E_m is the maximum value of the excitation voltage, λ is the time of reversal of the voltage scan, and n = 0, 1, 2.... is the cycle number. The Laplace transform of Eq. [18] is given in transform tables (8) as

$$\bar{E}(s) = E_m (1 - e^{-\lambda s})/\lambda s^2 (1 + e^{-\lambda s}) \qquad [19]$$

Substitution of Eq. [17] and [19] into Eq. [11] with p = s therefore yields the Laplace transform of the response current as

$$\bar{I}(s)/E_m = \left[(1 - e^{-\lambda s})/b\lambda s(1+ e^{-\lambda s})\right]\left[1/s\ (s + \frac{a}{b}) + R_p C/(s + \frac{a}{b})\right] \qquad [20]$$

where

$$a = R_s + R_p \qquad [21]$$

$$b = R_s R_p C \qquad [22]$$

Inverse transformation may be accomplished by use of the convolution theorm (7,8)

$$\mathcal{L}^{-1}\left[\bar{I}(s)/E_m\right] = \int_0^t F(x)\ G(t - x)\ dx \qquad [23]$$

where F(x) and G(t-x) are the inverse transformations of f(s) and g(s) given below

$$f(s) = (1-e^{-\lambda s})/s(1 + e^{-\lambda s}) \qquad [24]$$

$$F(x) = \begin{cases} +1 & 2n\lambda < x < (2n + 1)\lambda \\ -1 & (2n + 1)\lambda < x < (2n + 2)\lambda \end{cases} \qquad [25]$$

$$g(s) = 1/s(s + \frac{a}{b}) + R_p C/(s + \frac{a}{b}) \qquad [26]$$

$$G(t-x) = b/a + Ke^{\frac{ax}{b}} \qquad [27]$$

with

$$K = (R_p C - b/a)\, e^{-\frac{at}{b}} \qquad [28]$$

Substitution of Eqs. [25] and [27] into Eq. [23], followed by integration over successive forward and reverse sweeps, yields

$$I^f(t) = (E_m/a\lambda)\left\{ t - 2n\lambda - (R_p C - b/a)\left[2\sum_{m=0}^{2n} (-1)^m e^{-\frac{a(t-m\lambda)}{b}} - e^{-\frac{at}{b}} - 1 \right] \right\} \qquad [29]$$

for the current on the forward sweep with $2n\lambda < t < (2n+1)\lambda$, and

$$I^r(t) = (E_m/a\lambda)\left\{ 2(n+1)\lambda - t + (R_p C - b/a)\left[2e^{\frac{a\lambda}{b}} \sum_{m:0}^{2n} (-1)^m e^{\frac{-a(t-m\lambda)}{b}} - e^{\frac{-at}{b}} - 1 \right] \right\} \qquad [30]$$

for the reverse sweep with $(2n+1)\lambda < t < (2n+2)\lambda$. The summations contained in Eqs. [29] and [30] are geometric progressions. Summation over the indicated limits therefore yields

$$I^f(t) = (E_m/a\lambda)\left\{ t - 2n\lambda - (R_p C - b/a)\left[2e^{-at}\left(1 + e^{\frac{(2n+1)a\lambda}{b}}\right)/\left(1 + e^{\frac{a\lambda}{b}}\right) - e^{-\frac{at}{b}} - 1 \right] \right\} \qquad [31]$$

and

$$I^r(t) = (E_m/a\lambda)\left\{ 2(n+1)\lambda - t + (R_p C - b/a)\left[2e^{-\frac{(t-\lambda)a}{b}}\left(1 + e^{\frac{(2n+1)a\lambda}{b}}\right)/\left(1 + e^{\frac{a\lambda}{b}}\right) - e^{\frac{-at}{b}} - 1 \right] \right\} \qquad [32]$$

for the forward $[2n\lambda < t < (2n + 1)\lambda]$ and reverse $[(2n + 1)\lambda < t < (2n + 2)\lambda]$ sweeps respectively.

It is convenient to redefine the time scales so that zero time for the forward sweep coincides with $2n\lambda$ (i.e., with the start of the nth forward sweep) and with $(2n + 1)\lambda$ for the reverse sweep. This is accomplished by use of the following transformations

$$t' = t - 2n\lambda \qquad [33]$$

$$t'' = t - (2n + 1)\lambda \qquad [34]$$

Thus, substitution for t in Eqs. [31] and [32] using Eqs. [33] and [34], respectively, yields the following expressions for the current transients for the forward and reverse sweeps

$$I^f(t') = (E_m/a\lambda)\left\{ t' - e^{-\frac{at'}{b}} (R_pC - b/a)\left[2(e^{-\frac{2na\lambda}{b}} + e^{\frac{a\lambda}{b}})/ (1 + e^{\frac{a\lambda}{b}}) - e^{-\frac{2na\lambda}{b}}\right] + (R_pC - b/a)\right\} \qquad [35]$$

$$I^r(t'') = (E_m/a\lambda)\left\{ \lambda - t'' + e^{-\frac{at''}{b}} (R_pC - b/a)\, x \left[2(e^{-\frac{2na\lambda}{b}} + e^{\frac{a\lambda}{b}}) / (1 + e^{\frac{a\lambda}{b}}) - e^{-\frac{(2n+1)a\lambda}{b}}\right] - (R_pC - b/a)\right\} \qquad [36]$$

Equations [35] and [36] demonstrate that the current response contains both steady-state and transient components. Of principal interest in this work is the steady state that is established when $na\lambda/b \to \infty$. Under these conditions $e^{-2na\lambda/b}$ and $e^{-(2n + 1)a\lambda/b} \to 0$, so that Eq. [35] and [36] reduce to

$$I^{f}_{ss}(t') = (E_m/a\lambda)\left\{ t' - (R_pC - b/a)\left[2e^{\frac{a(\lambda-t')}{b}} / (1 + e^{\frac{a\lambda}{b}}) - 1\right]\right\} \quad [37]$$

$$I^{r}_{ss}(t'') = (E_m/a\lambda)\left\{ \lambda - t'' + (R_pC - b/a)\left[2e^{\frac{a(\lambda-t'')}{b}} / (1 + e^{\frac{a\lambda}{b}}) - 1\right]\right\} \quad [38]$$

Because SACV experiments are normally carried out with potential sweep rate as the independent variable, a further transformation of Eqs. [37] and [38] is necessary. Thus, substitution of $\lambda = E_m/v$, where v is the potential sweep-rate, into Eqs. [37] and [38] yields

$$I^{f}_{ss}(t') = (v/a)\left\{ t' - (R_pC - b/a)\left[2e^{\frac{a(E_m-vt')}{vb}} / (1 + e^{\frac{aE_m}{vb}}) - 1\right]\right\} \quad [39]$$

$$I^{r}_{ss}(t'') = (v/a)\left\{ E_m/v - t'' + (R_pC - b/a)\left[2e^{\frac{a(E_m-vt'')}{vb}} / (1 + e^{\frac{aEm}{vb}}) - 1\right]\right\} \quad [40]$$

Equations [39] and [40] therefore give the complete steady-state response of the equivalent circuit shown in Fig. 1a as a function of time and sweep-rate as the independent variables.

Numerical Analysis

Equations [39] and [40] show that the steady-state response of the equivalent circuit shown in Fig. 1a to a sawtooth voltage excitation is a complex function of the resistances and capacitances of the circuit elements, the maximum voltage, E_m, and the voltage sweep-rate, v. The relationships given are sufficiently complex that the dependence of the response on the independent variables is best illustrated by numerical analysis; that is, the current on the forward and reverse sweeps is calculated from Eqs. [39] and [40] for selected values for R_s, R_p, C, E_m, and v.

Typical steady-state current-voltage curves as a function of voltage sweep-rate are shown in Fig. 2. In general, the polarization curves exhibit hysteresis between the forward and reverse sweeps, with exponential-type decays at the start of both sweep directions. The curves plotted in Fig. 2 show that the degree of hysteresis is sensitive to the voltage sweep-rate, and only at the lowest sweep-rate considered is the degree of hysteresis negligible. These calculated voltammograms are similar in both form, and in response to the independent variable, v, as those frequently observed for real systems (see next section).

In practice, it is possible to obtain reasonably precise data for the gradient of the current/voltage curve at the end of both the forward and the reverse sweeps. Furthermore, the hysteresis current, ΔI, defined as

$$\Delta I = I_{ss}^{f}(t' = \lambda/2) - I_{ss}^{r}(t'' = \lambda/2) \qquad [41]$$

is also conveniently measured from the observed current response (see Fig. 2). Differentiation of Eqs. [39] and [40] with respect to t' and t'', and substitution of $t' = t'' = \lambda$, therefore yields

$$1/R_{app} = 1/(R_p + R_s) + 2R_p e^{-\frac{aE_m}{bv}} / R_s(R_p + R_s) \qquad [42]$$

where the apparent polarization resistance, R_{app}, is equal to $(\partial E/\partial I_{ss})$; that is, it is equal to the slope of the polarization curve at $t' = \lambda$ for the forward sweep and at $t'' = \lambda$ for the reverse sweep. Similarly, substitution of Eqs. [39] and [40] into Eq. [41] yields the following expression for the hysteresis current

$$\Delta I = \left[2R_p^2 C/(R_p + R_s)^2 - 4R_p^2 C e^{-\frac{aE_m}{2vb}} / (R_S + R_p)^2\right] v \qquad [43]$$

FIGURE 2

CYCLIC VOLTAMMAGRAMS FOR THE ELECTRICAL EQUIVALENT CIRCUIT SHOWN IN FIGURE 1(a) AS A FUNCTION OF VOLTAGE SWEEP RATE

R_s = 10 ohms, R_p = 1000 ohms, C = 1000 μF, E_m = 20 mV

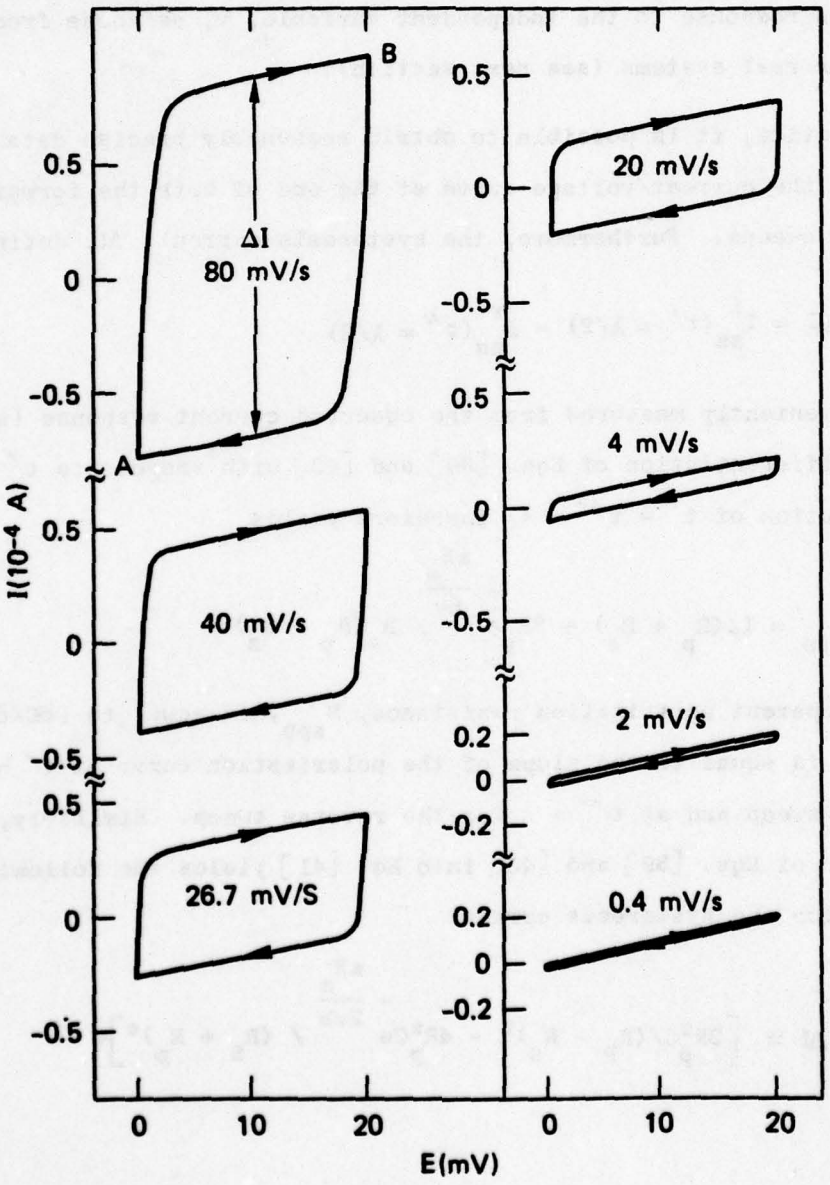

The variation of R_{app} and ΔI with the voltage sweep-rate, v, for the selected values for R_s, R_p, E_m, and C is shown in Fig. 3. The true dc resistance, $(R_s + R_p)$, is indicated for comparison. At low sweep-rates for the case considered, R_{app} is relatively insensitive to v, and the apparent resistance is found to be very close to the true value of $R_s + R_p$. At high sweep-rates, however, the apparent resistance decreases with increasing v as a consequence of the concomitant increase in conductance of the parallel capacitor. Mathematically, this corresponds to increasing significance of the second term in Eq. [42]. Although the decrease in R_{app} with sweep-rate is small for the case considered, it must be stressed that much larger dependencies of R_{app} on v can be observed for different values for R_s, R_p and C, as illustrated later by experimental data for corroding 90:10 Cu:Ni alloy in flowing seawater.

The hystersis current for the particular case under consideration is found to vary almost linearly with sweep-rate in accordance with Eq. [43]. At high sweep-rates, however, the slope of the ΔI vs v correlation is predicted to decrease as the second term in the square brackets becomes significantly larger than zero. In the limit of $v = 0$, the ΔI versus v plot extrapolates to zero because, under dc conditions, the impedance of the parallel capacitor is infinite.

The effect of varying the series resistance on the predicted SACV response is shown in Fig. 4. Although R_{app} increases as the series resistance is made larger, the difference between R_{app} and $(R_s + R_p)$ is negligible for the conditions chosen as shown by the data plotted at the top of Fig. 4. On the other hand, the hysteresis current is found to decrease as the series resistance is made larger. This is a consequence of the change in the character of the impedance from capacitive for low values of R_s to resistive for high R_s values.

FIGURE 3

DEPENDENCE OF THE APPARENT POLARIZATION RESISTANCE, R_{app}, AND HYSTERESIS CURRENT, ΔI, ON VOLTAGE SWEEP RATE

R_s = 10 ohms, R_p = 1000 ohms, C 1000 μF, E_m = 20 mV

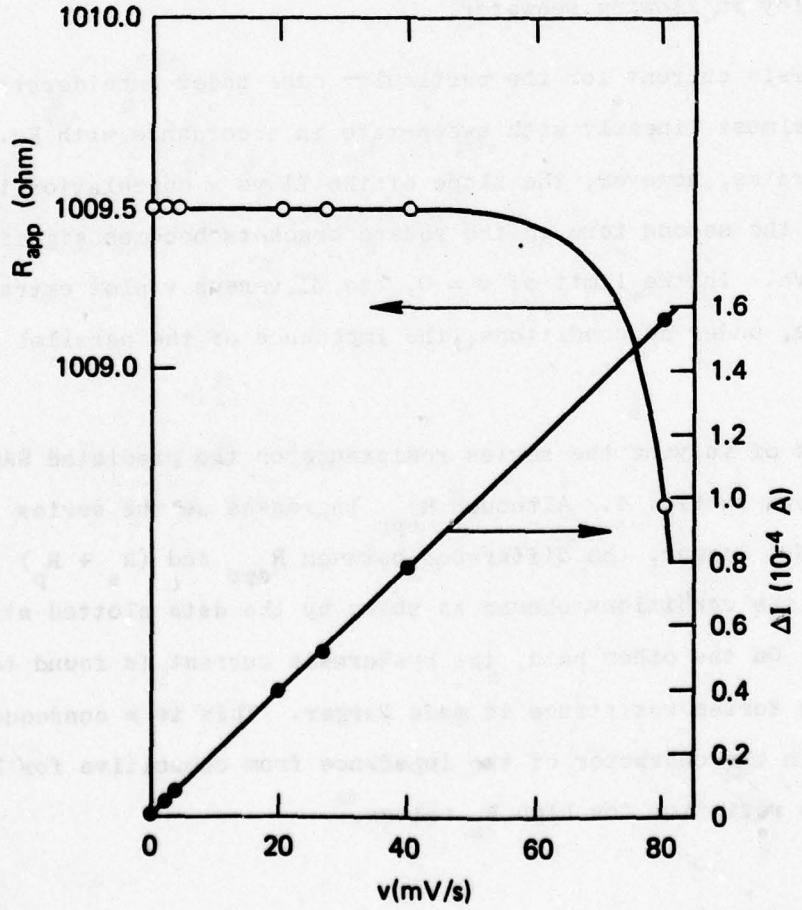

The parallel resistance also has a marked effect on the form of the SACV response, as shown by the data plotted in Fig. 5. Thus, the apparent resistance increases sharply with R_p, but, again, the difference between R_{app} and the resistive part of the impedance is negligible for the conditions chosen (upper curve, Fig. 5). For low values for R_p, the hysteresis current is predicted to be very small, and remains so over a wide range of R_p values. In this case, the parallel capacitor is effectively shorted-out, so that the response is almost totally resistive. At high R_p values, the impedance of the parallel RC combination is determined principally by the capacitance, so that the hysteresis response approaches that for the series circuit containing R_s and C.

SACV response data for varying capacitance are plotted in Fig. 6. The apparent resistance is found not to be highly dependent on the capacitance, C for the conditions chosen, although a dependence is expected for different values for the voltage sweep-rate, v. Conversely, a nearly linear ΔI vs C correlation (and hence log ΔI vs log C plot) is exhibited by the data in accordance with Eq. [43] for large values for the exponent $aE_m/2vb$.

Analysis of Experimental Data

From an experimental viewpoint, the theory developed in this work can be used in analyzing observed SACVs for real systems. Accordingly, it is desirable that mathematical functions and techniques be developed to decompose a generalized impedance into the resistive and capacitive components. Because the equivalent circuit considered is composed of three elements, it is necessary, from a mathematical viewpoint, to develop three independent relationships between the response and the experimentally independent variable, v. In principle, these relationships may then be solved simultaneously to yield the desired values for R_s, R_p, and C.

FIGURE 4

DEPENDENCE OF THE APPARENT POLARIZATION RESISTANCE, R_{app}, AND THE HYSTERESIS CURRENT, ΔI, ON THE SERIES RESISTANCE, R_s

R_p = 1000 ohms, C = 1000 μF, E_m = 20 mV, v = 2 mV/s

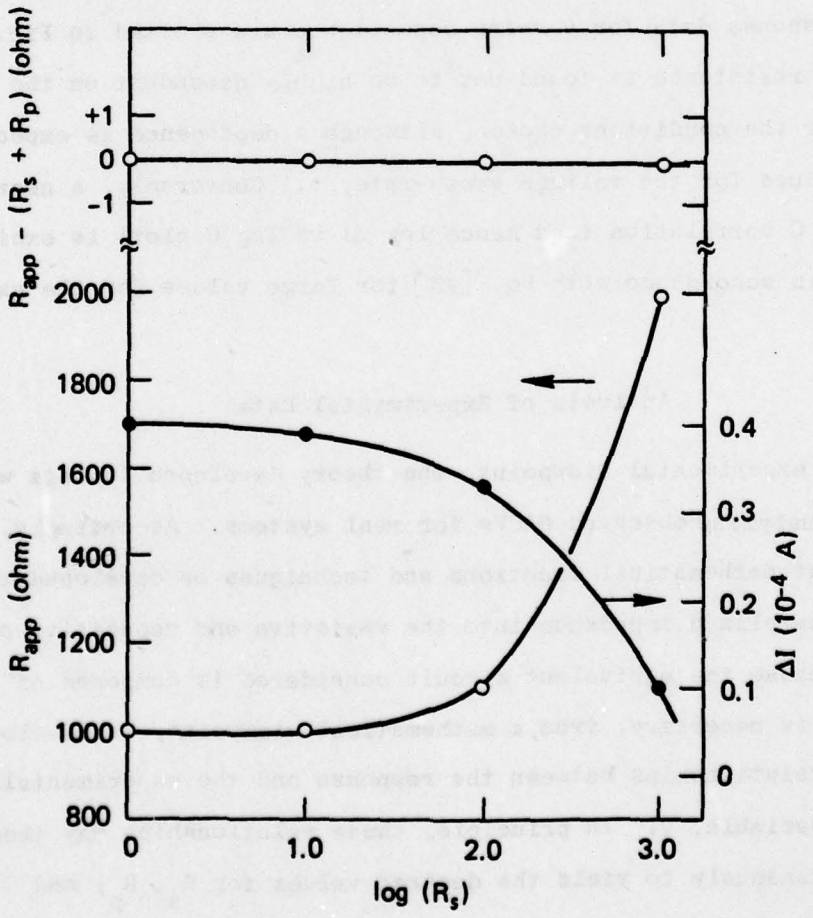

FIGURE 5
DEPENDENCE OF THE APPARENT POLARIZATION RESISTANCE, R_{app},
AND THE HYSTERESIS CURRENT, ΔI, ON THE PARALLEL RESISTANCE, R_p

R_s = 10 ohms, C = 1000 μF, E_m = 20 mV, v = 2 mV/s

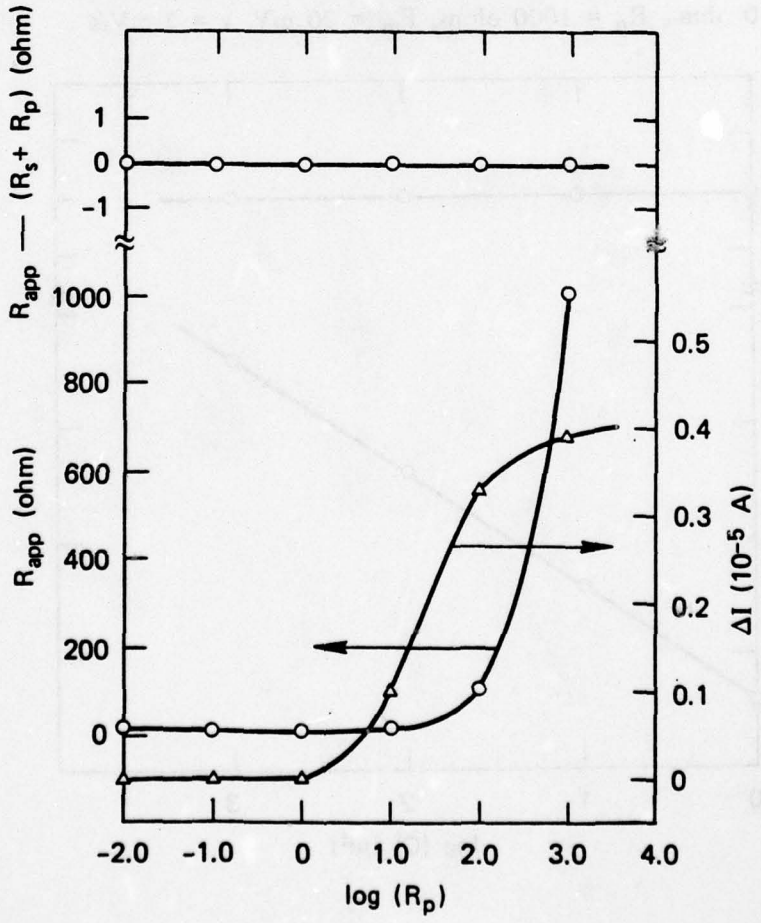

FIGURE 6

DEPENDENCE OF THE APPARENT POLARIZATION RESISTANCE, R_{app}, AND THE HYSTERESIS CURRENT, ΔI, ON THE CAPACITANCE, C

R_s = 10 ohms, R_p = 1000 ohms, E_m = 20 mV, v = 2 mV/s

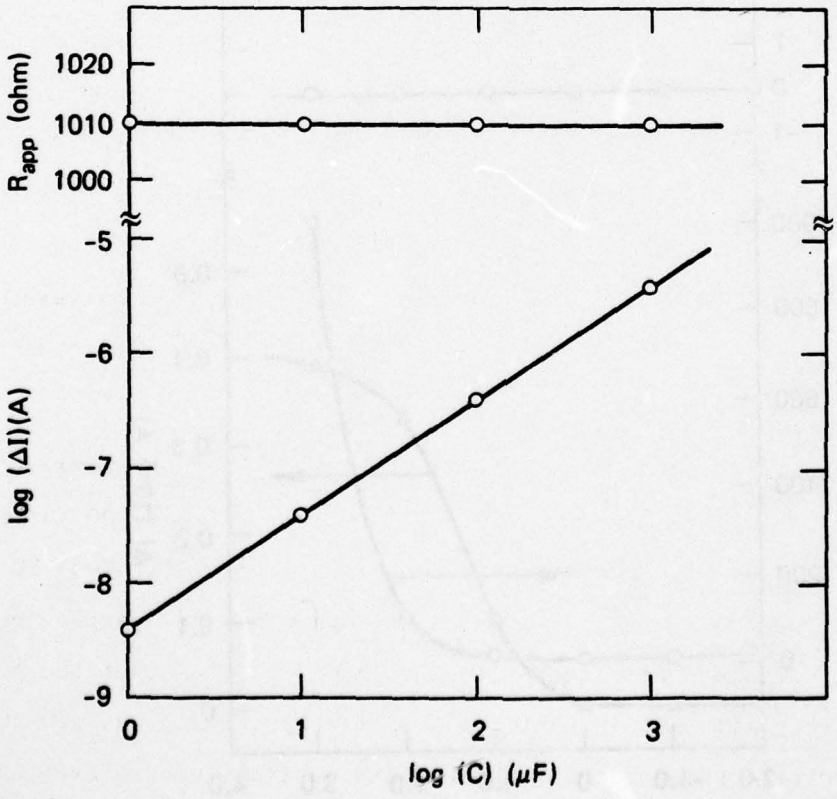

Two of the required relationships are given by Eqs. [42] and [43]. A third expression may be derived by noting that the diagonal resistance, R_d, is given by

$$1/R_d = \left[I^f_{ss}(t' = \lambda) - I^r_{ss}(t'' = \lambda) \right] / E_m \qquad [44]$$

This parameter is determined experimentally as the gradient of the line joining points A and B of the voltammogram shown in Fig. 2 for a sweep-rate of 80 mV/s. Substitution of Eqs. [39] and [40] into Eq. [44] therefore yields

$$1/R_d = 1/(R_s + R_p) + \left\{ 2R_p^2 C \left(e^{\frac{aE_m}{bv}} - 1\right)/E_m (R_p + R_s)^2 \left(e^{\frac{aE_m}{bv}} + 1\right) \right\} v \qquad [45]$$

This equation predicts that a plot of I/R_d versus v is non linear with a positive first derivative, $d\,(1/R_d)/dv$ that decreases with sweep-rate Furthermore, I/R_d is predicted to extrapolate to $1/(R_s + R_p)$ in the limit of zero sweep-rate (compare with Eq. [42]). Note, nowever, that the diagonal resistance depends more on the independent variable, v, than does the apparent resistance, R_{app} (Eq. [42]). Accordingly, if data are available for only a limited range of sweep-rate, it is probably more satisfactory to extrapolate $1/R_{app}$, rather than $1/R_d$, to zero sweep-rate to obtain an estimate of $(R_s + R_p)$.

The essential features of the procedure for analyzing experimental data are illustrated by reference to the SACVs for corroding 90:10 Cu:Ni alloy in flowing seawater shown in Fig. 7. The experimental details of this work will be published in a subsequent paper (9). Comparison of these curves with those calculated theoretically (Fig. 2) shows that the responses are qualitatively similar, in that both exhibit hysteresis between the forward and reverse sweeps, and both show exponential-type relaxation phenomena at the start of the scans in both direction.

FIGURE 7

SMALL-AMPLITUDE CYCLIC VOLTAMMOGRAMS FOR 90:10 Cu:Ni ALLOY IN FLOWING SEAWATER

Flow velocity = 1.62 m/s, $[O_2]$ = 0.045 mg/liter, specimen area = 11.05 cm^2, T = 26°C, exposure time = 50 hr

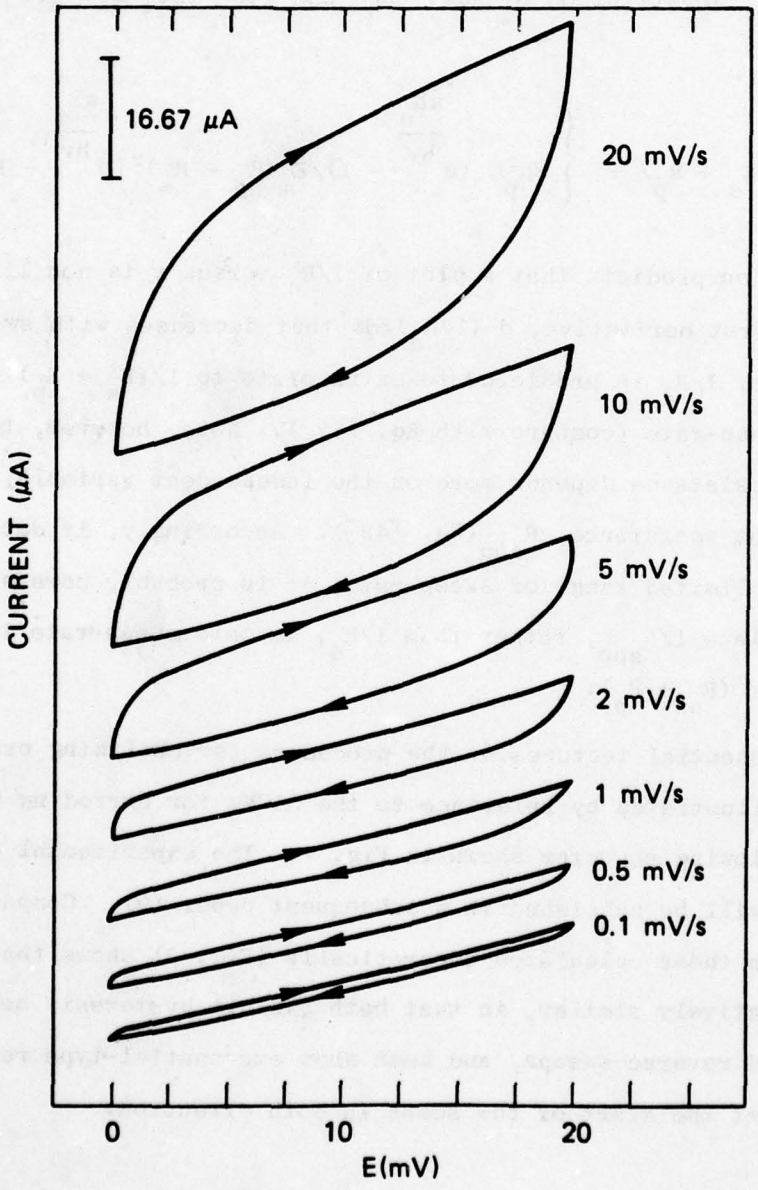

Plots of $1/R_{app}$ and $1/R_d$ against sweep-rate for 90:10 Cu:Ni alloy in flowing seawater are shown in Fig. 8. These curves confirm the theoretical prediction that the plots should be approximately parabolic (Eqs. [42] and [45]), and that $1/R_d$ is more dependent on sweep-rate than is $1/R_{app}$. In both cases, extrapolation to zero sweep rates yields the same value of 1316 ± 25 ohms for $R_s + R_p$. The dependence of the hysteresis current, ΔI, on sweep-rate, is shown in Fig. 9. Again, the theoretical prediction of an approximately parabolic function that extrapolates to $\Delta I = 0$ for vanishingly small sweep-rates is observed. The gradient of the ΔI against v plot at $v = 0$ is related to the values of the equivalent circuit components through Equ. [46].

$$(d\,\Delta I/dv)_{v\to 0} = 2R_p^2 C/(R_p + R_s)^2 \qquad [46]$$

Assuming that $R_p \gg R_s$ (see below), this expression yields an interfacial capacitance of 2500 ± 200 μF.

The validity of the values for R_p and C as determined by SACV can be assessed by comparison with data obtained by the more conventional ac impedance technique (1). Typical impedance diagrams for 90:10 Cu:Ni alloy in the same experiment at three different exposure times are shown in Fig. 10. These data were obtained by analysis of the Lissajous figures generated by simultaneously imposing the sinusoidal excitation voltage and response current across the X and Y axes, respectively, of an oscilloscope (frequency >1 Hz) or fast-response X-Y recorder (frequency <1 Hz) (1,9). For all three exposure times, the impedance plots take the form of a single semicircle, or combination of semicircles. At sufficiently low frequency, all the impedance diagrams exhibit single semicircular plots, as expected for dominance of the impedance by a single relaxation process having an equivalent circuit of the type adopted in this theoretical analysis (Fig. 1a). Other relaxation processes are evident at higher frequencies, as shown clearly by the impedance diagram for the longest exposure time. Thus,

FIGURE 8

PLOTS OF EQUATIONS [42] AND [45] FOR 90:10 Cu:Ni ALLOY IN FLOWING SEAWATER

Experimental conditions as listed in Figure 7

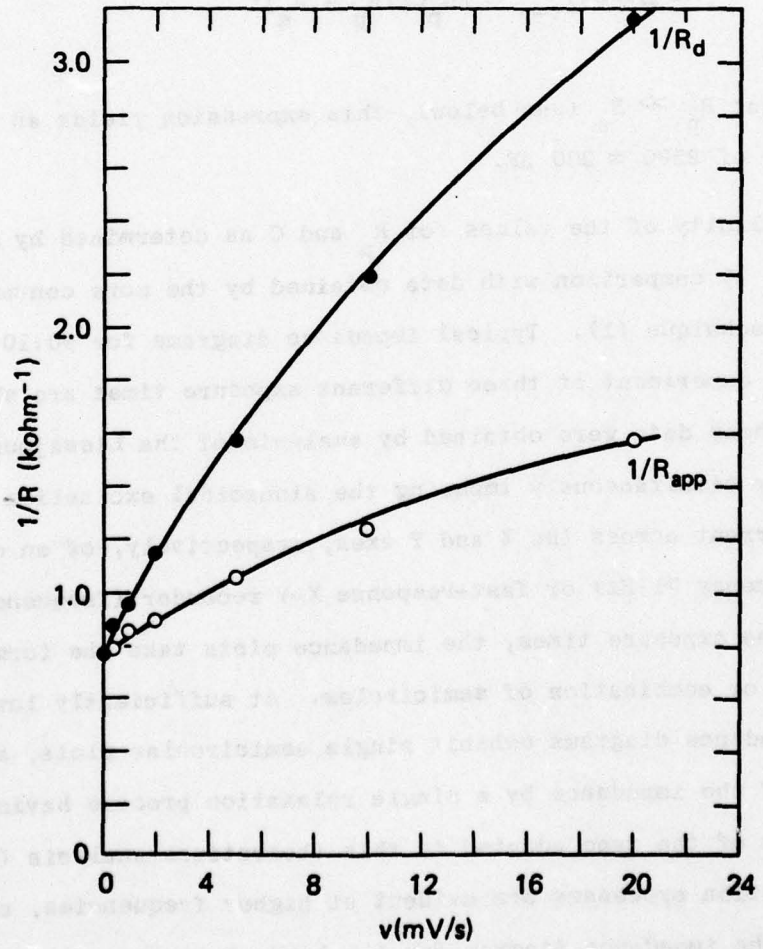

FIGURE 9
PLOT OF EQUATION [43] FOR 90:10 Cu:Ni ALLOY IN FLOWING SEAWATER
Experimental conditions as listed in Figure 7

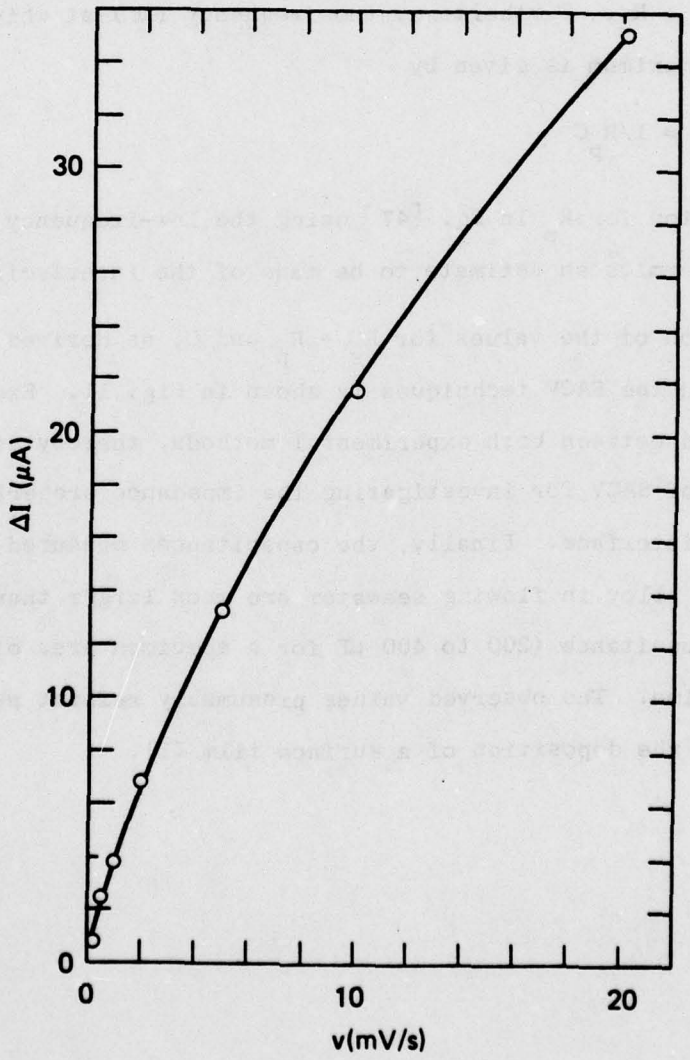

semicircles with maxima at ~ 0.025 Hz and ~ 60 Hz are evident, in addition to the low-frequency semicircle with its maximum at~0.0025 Hz. We have obtained extensive impedance data for both 90:10 Cu:Ni alloy and 70:30 Cu:Ni alloy in flowing seawater as a function of oxygen and sulfide concentrations. The analyses of these diagrams will be presented in a later publication (9).

In all three cases shown in Fig. 10, the impedance plots extrapolate at high frequency to very small values for the real component R', as expected for small values for the series resistance, R_s. The low-frequency intercept with the real axis is equal to the impedance of the dc path; that is, equal to $R_s + R_p$. Furthermore, the frequency (ω) at which the semicircle is at a maximum is given by

$$\omega = 1/R_p C \qquad [47]$$

Thus, substitution for R_p in Eq. [47] using the low-frequency intercept with the real axis permits an estimate to be made of the interfacial capacitance.

A comparison of the values for $R_s + R_p$ and C, as derived by use of the ac impedance and the SACV techniques is shown in Fig. 11. Excellent agreement is obtained between both experimental methods, thereby demonstrating the usefulness of SACV for investigating the impedance properties of a metal/solution interface. Finally, the capacitances measured in the work for 90:10 Cu:Ni alloy in flowing seawater are much larger than the expected double-layer capacitance (200 to 400 μF for a specimen area of 11 cm^2) and increase with time. The observed values presumably reflect pseudocapacitance associated with the deposition of a surface film (1).

FIGURE 10

COMPLEX PLANE IMPEDANCE DIAGRAMS FOR 90:10 Cu:Ni ALLOY IN FLOWING SEAWATER AS A FUNCTION OF EXPOSURE TIME

Experimental conditions as listed in Figure 7. Numbers next to each point refer to frequency in Hz

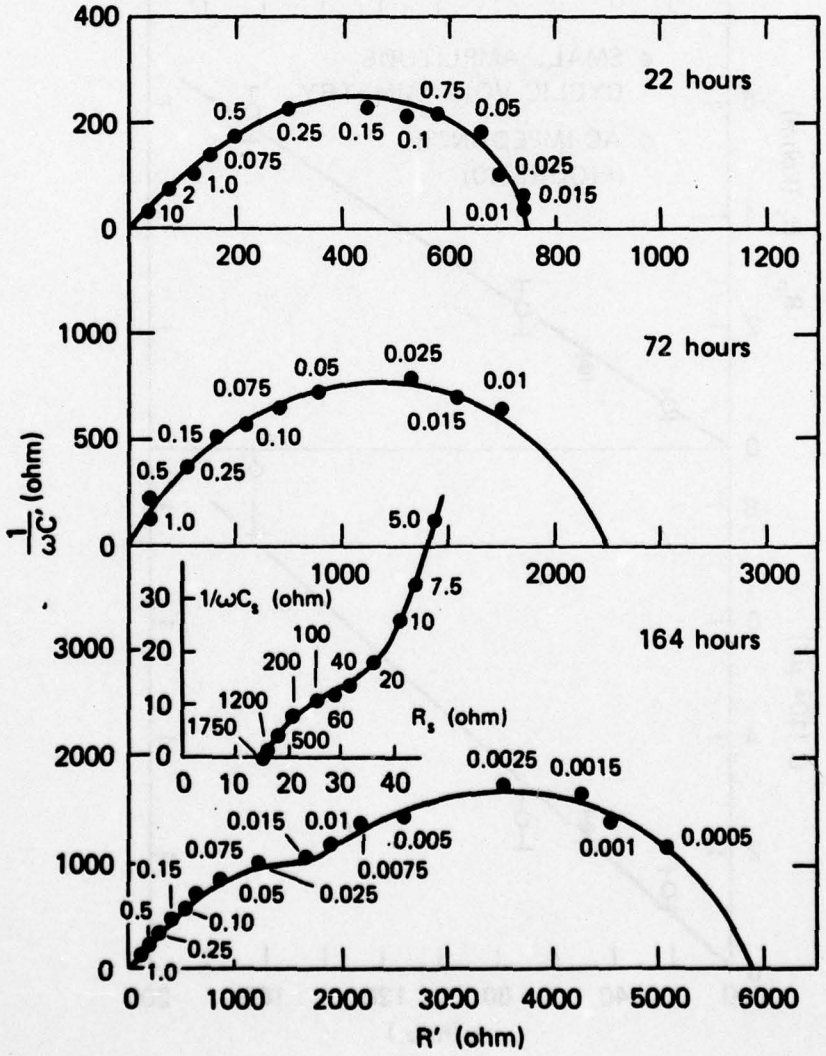

FIGURE 11

VARIATION OF $R_p + R_s$ (UPPER PLOT) AND C (LOWER PLOT) WITH EXPOSURE TIME FOR CORRODING 90:10 Cu:Ni ALLOY IN FLOWING SEAWATER

Experimental conditions as listed in Figure 7

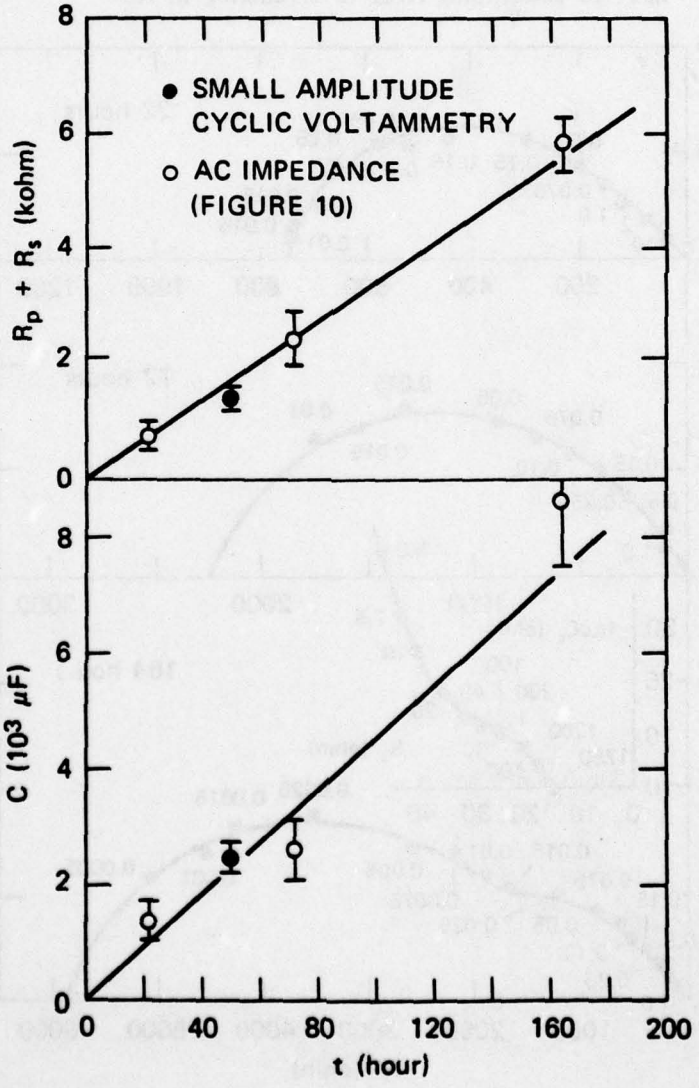

Acknowledgments

Financial support for this work by the Office of Naval Research (Contract No. N00014-77-C-0046, NR-036-116) is gratefully acknowledged. The author would like to thank Dr. C. M. Ablow for checking some of the derivations, and Drs. L. Nanis, R. L. Jones and B. C. Syrett for helpful discussions.

REFERENCES

1. D. D. Macdonald, "Transient Techniques in Electrochemistry", Plenum Press, New York (1977).

2. F. Mansfeld, Adv. Corr. Sci. Tech., 6, 163 (1976).

3. D. W. Bird, Corr. Sci., 13, 913 (1973).

4. A. A. Pilla, J. Electrochem. Soc., 117, 467 (1970).

5. M. D. Wijnen, Rec. Trav. Chim., 79, 1203 (1960).

6. E. Levart and E. Poirier D'Orsay, J. Electroanal. Chem., 12, 277 (1966).

7. S. Goldman, "Transformation Calculus and Electrical Transients," Prentice-Hall, Inc., New York (1950).

8. G. E. Roberts, and H. Kaufman, "Table of Laplace Transforms," Saunders, Philadelphia (1966).

9. D. D. Macdonald, B. C. Syrett, and S. S. Wing, to be published.

Appendix III

SURFACE ANALYSIS OF COPPER-NICKEL ALLOYS AFTER EXPOSURE TO FLOWING OXYGENATED SEAWATER

By

D. D. Macdonald, B. C. Syrett, and S. S. Wing

In Appendix I, we showed that the rate of corrosion of 90:10 Cu:Ni alloy and 70:30 Cu:Ni alloy in oxygenated flowing seawater was sensitive to the concentration of oxygen in the system. Thus, electrochemical evidence suggests that at high oxygen concentrations (e.g., at $[O_2]$ = 26.3 mg/liter) the decrease in corrosion resistance of 70:30 Cu:Ni alloy is due to a positive shift in the corrosion potential to a range in which the surface oxide film is no longer as protective. This breakdown in corrosion resistance renders the 70:30 Cu:Ni alloy as susceptible to corrosion in flowing seawater as is the 90:10 Cu:Ni alloy. At low oxygen concentrations ($\leq$ 6.60 mg/liter), however, it was found that the high nickel alloy is significantly more corrosion-resistant than the low nickel material. In this appendix, we report detailed surface analyses of the two alloys after exposure to high (26.3 mg/liter) and low (0.045 mg/liter) levels of dissolved oxygen in flowing seawater (flow velocity = 1.62 m/s). The analytical methods used include scanning electron microscopy (SEM), energy dispersive X-ray (EDX) analysis, and Auger electron spectrometry (AES) with argon ion sputtering.

SEM micrographs of the surfaces of 90:10 Cu:Ni alloy and 70:30 Cu:Ni alloy after exposure to 0.045 mg/liter and 26.3 mg/liter dissolved oxygen for 330 hours and 160 hours, respectively, are shown in Figures 1 to 4. In general, the surfaces appear to be rather featureless, with no evidence of two-layer film growth. High magnification examination indicates that the scales are porous to some extent (see Figures 1c, 2c, 3c, and 4c), but it is not possible to determine if the fissures penetrate the entire film. Furthermore, the micrographs indicate that the films formed after exposure to the highly oxygenated seawater are thicker than those formed on the alloys in the low oxygen system, despite the longer exposure time for the latter. This can be seen by comparing Figure 2b, which shows

(a) WIDTH OF PHOTOGRAPH = 0.19 cm

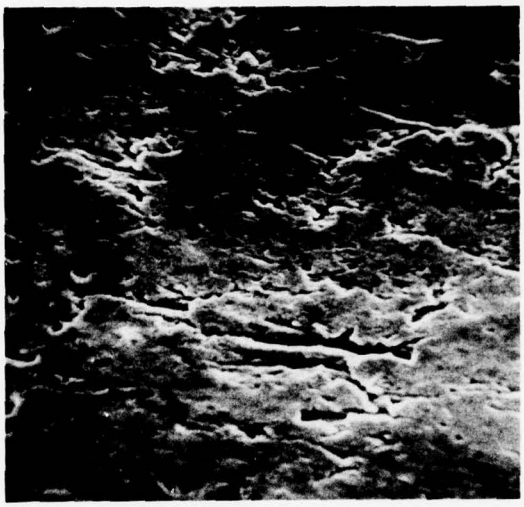

(b) WIDTH OF PHOTOGRAPH = 0.019 cm

(c) WIDTH OF PHOTOGRAPH = 0.0019 cm

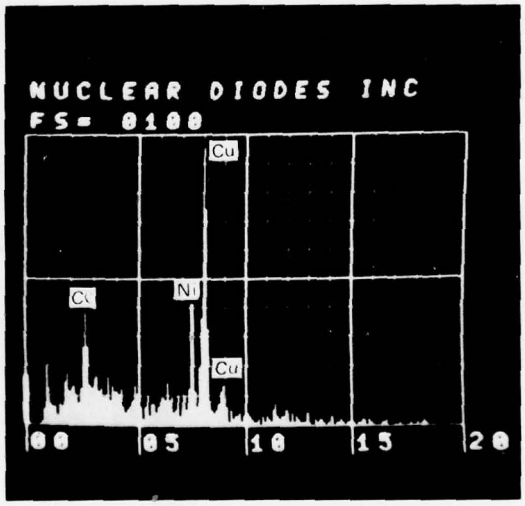

(d)

SA-6077-23

FIGURE 1 SEM MICROGRAPHS AND EDX ANALYSIS OF THE SURFACE OF 90:10 Cu:Ni ALLOY AFTER EXPOSURE FOR 275 HOURS TO FLOWING SEAWATER CONTAINING 0.045 mg/ml OF DISSOLVED OXYGEN

AD-A051 833 SRI INTERNATIONAL MENLO PARK CA F/G 11/6
A STUDY TO DETERMINE THE MECHANISMS OF CORROSION OF COPPER-NICK--ETC(U)
FEB 78 D D MACDONALD, B C SYRETT, S S WING N00014-77-C-0046
UNCLASSIFIED NL

2 OF 2
AD
A051833

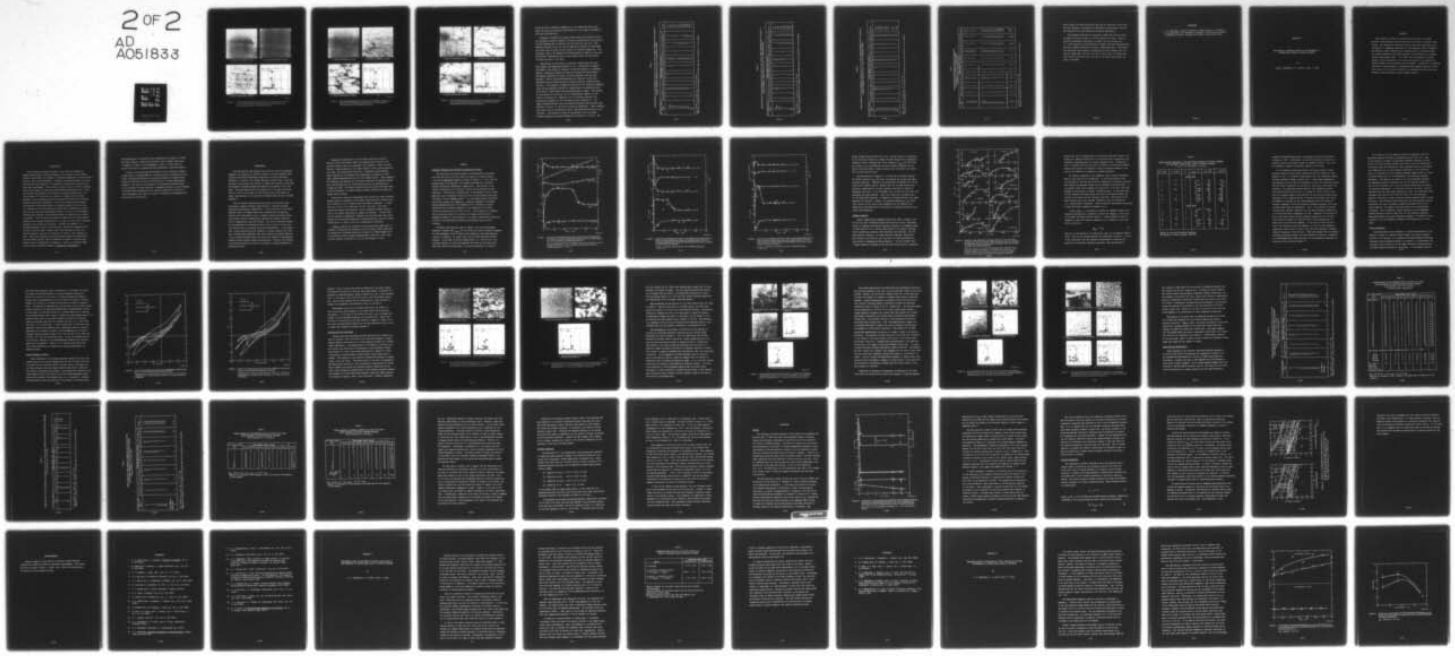

END
DATE
FILMED
4-78
DDC

(a) WIDTH OF PHOTOGRAPH = 0.19 cm

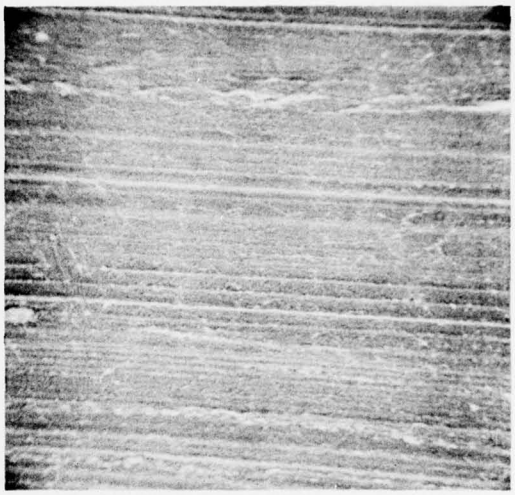

(b) WIDTH OF PHOTOGRAPH = 0.019 cm

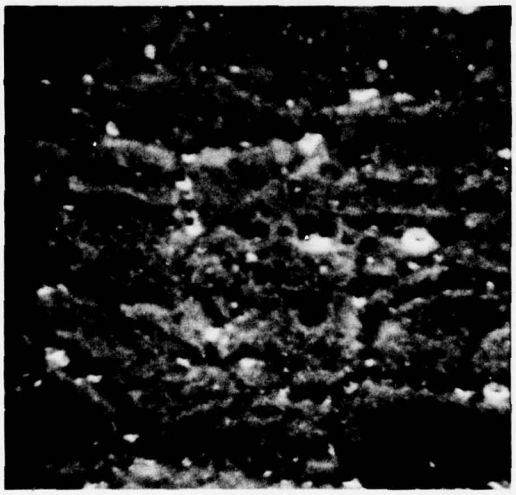

(c) WIDTH OF PHOTOGRAPH = 0.0019 cm

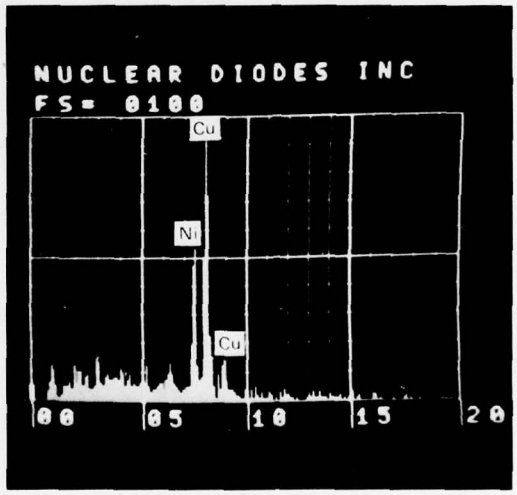

(d)

SA-6077-24

FIGURE 2 SEM MICROGRAPHS AND EDX ANALYSIS OF THE SURFACE OF 70:30 Cu:Ni ALLOY AFTER EXPOSURE FOR 275 HOURS TO FLOWING SEAWATER CONTAINING 0.045 mg/ml OF DISSOLVED OXYGEN

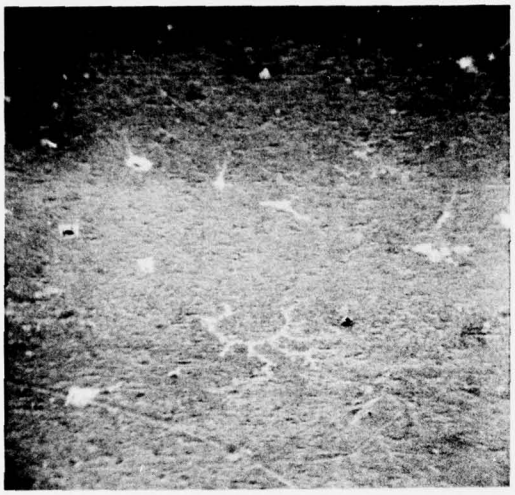

(a) WIDTH OF PHOTOGRAPH = 0.19 cm

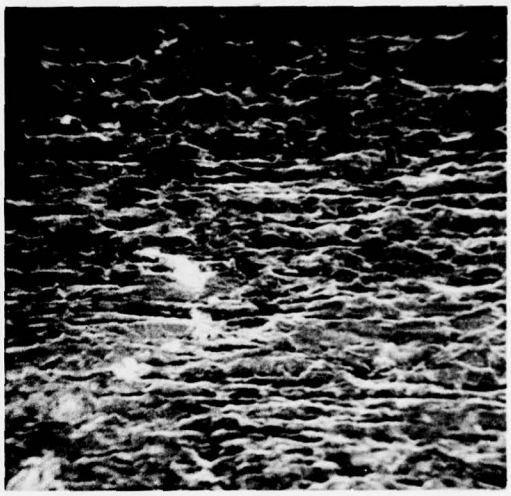

(b) WIDTH OF PHOTOGRAPH = 0.019 cm

(c) WIDTH OF PHOTOGRAPH = 0.0019 cm

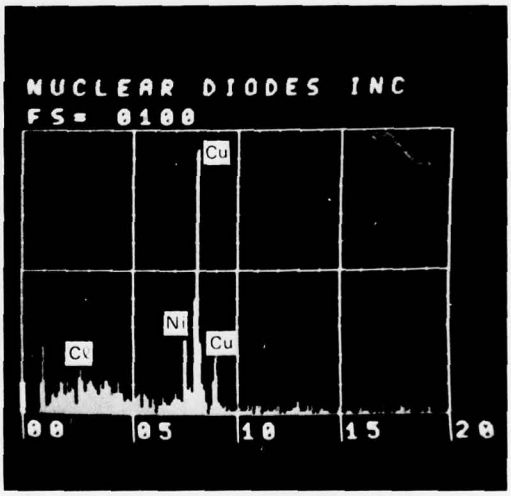

(d)

SA-6077-25

FIGURE 3 SEM MICROGRAPHS AND EDX ANALYSIS OF THE SURFACE OF 90:10 Cu:Ni ALLOY AFTER EXPOSURE FOR 160 HOURS TO FLOWING SEAWATER CONTAINING 26.3 mg/l OF DISSOLVED OXYGEN

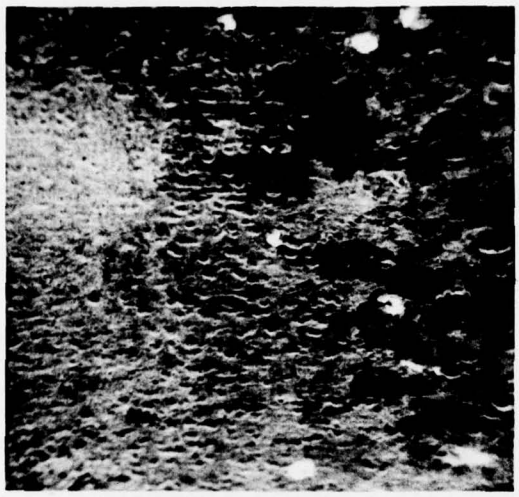

(a) WIDTH OF PHOTOGRAPH = 0.19 cm

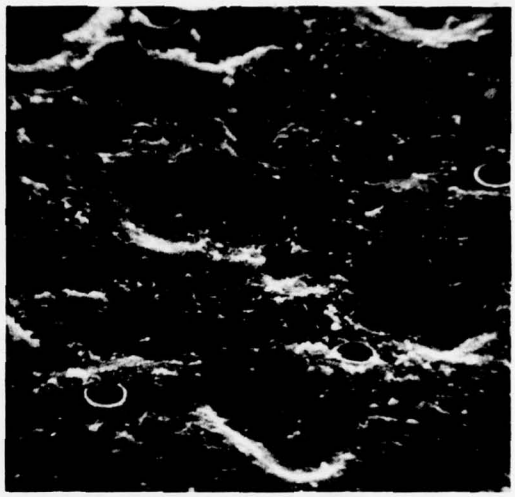

(b) WIDTH OF PHOTOGRAPH = 0.019 cm

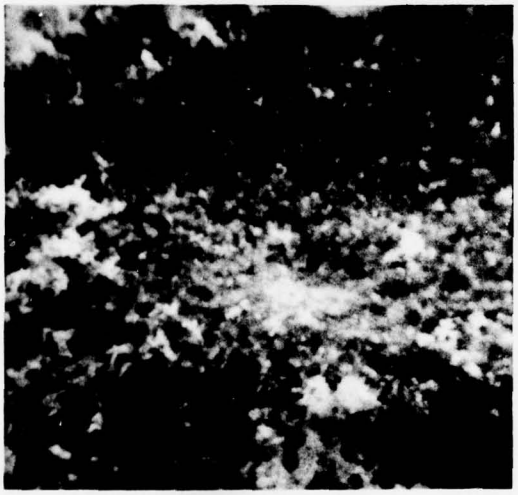

(c) WIDTH OF PHOTOGRAPH = 0.0019 cm

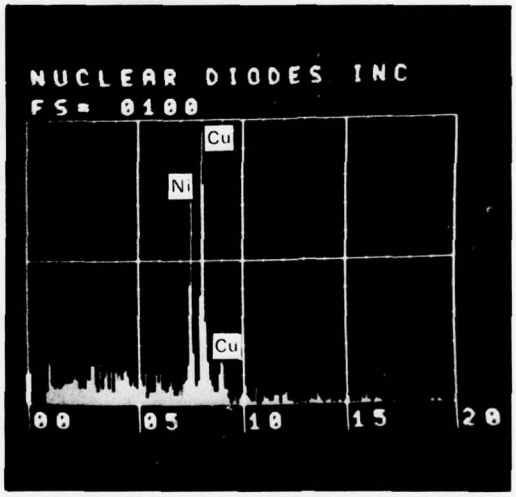

(d)

SA-6077-26

FIGURE 4 SEM MICROGRAPHS AND EDX ANALYSIS OF THE SURFACE OF 70:30 Cu:Ni ALLOY AFTER EXPOSURE FOR 160 HOURS TO FLOWING SEAWATER CONTAINING 26.3 mg/l OF DISSOLVED OXYGEN

striations due to elemental segregation in the underlying alloy, with Figure 4b, where any physical characteristics of the alloy are masked by the thick overlying film.

Attempts to identify the surface films using X-ray diffraction were not successful, possibly because of the poor crystallinity of the material, but more probably due to the fact that the films are very thin. EDX analysis (Figures 1d, 2d, 3d, and 4d) showed the presence of both copper and nickel, and, at least in one instance, of chlorine (Figure 1d). The instrument used is not capable of detecting oxygen or sodium, so that the EDX analyses reported here are of only marginal value for identifying the phases present in the films.

AES analyses of the films as a function of sputtering time (and hence depth) are summarized in Tables 1 to 4. The presence of copper and nickel in the films, as indicated by the EDX analyses, is confirmed. However, substantial amounts of oxygen and chlorine are also present, and smaller quantities of sulfur, calcium, potassium, and iron were detected. Sulfur, calcium and potassium are believed to arise from adsorption from the seawater and iron almost certainly originates from the alloy. The presence of oxygen and chlorine on the surface is expected, since the film probably consists of cuprous oxide (as indicated by previous work[1]), nickel oxide, and hydroxychlorides of copper. The presence of these phases is consistent with the thermodynamic behavior of the alloys as indicated by a comparison of the corrosion potential with potential-pH diagrams for the Cu-seawater system (Appendix I). The copper hydroxychlorides, which are characteristically green-colored, were observed to collect on the filter during the experiments. These compounds most likely form by precipitation from a super-saturated solution at the interface. Precipitation of some of the material onto the surface therefore explains the observed presence of chlorine in the film. The

Table 1

AUGER ANALYSIS OF THE CORROSION FILM ON 90:10 CU:Ni ALLOY AFTER EXPOSURE FOR 330 HOURS TO FLOWING SEAWATER CONTAINING 0.045 mg/l OF DISSOLVED OXYGEN

Ar^+ Etch Time* (min)	Peak Height (arb. units)									Cu/Ni
	$S_{(150)}$†	$Cl_{(180)}$	$K_{(250)}$	$C_{(270)}$	$Ca_{(295)}$	$O_{(510)}$	$Fe_{(595)}$	$Ni_{(716)}$	$CU_{(920)}$	
0	8	55	0	38	2	33	0	2	7	3.5
0.25	5	64	2	4	13	61	0	6	6	1.0
0.50	5	68	3	3	12	57	2	7	5	0.71
1.0	5	91	3	2	6	50	0	8	6	0.75
1.5	6	77	3	3	1	4	54	3	10	0.8
2.0	5	63	4	0	4	57	3	10	8	0.8
2.5	4	55	3	1	3	55	3	11	7	0.64
3.0	4	58	3	0	2	58	3	16	6	0.38
4.0	3	60	0	0	0	55	3	14	6	0.43
6.0	1	42	0	0	0	37	2	12	22	1.83
8.0	0	15	0	1	0	18	0	8	39	4.88
10	0	3	0	2	0	11	0	8	41	5.13
15	0	0	0	1	0	12	2	8	44	5.5

*I_E = 20 mA, E_t = 2 kV, p_{Ar} = 5 x 10^{-5} torr.
†Quantity in parenthesis in the voltage of the peak used for th analysis of the element.

Table 2

AUGER ANALYSIS OF THE CORROSION FILM ON 70:30 Cu:Ni Alloy AFTER EXPOSURE FOR 330 HOURS TO FLOWING SEAWATER CONTAINING 0.045 mg/l OF DISSOLVED OXYGEN

Ar^+ Etch Time* (min)	Peak Height (arb. units)									Cu/Ni
	$S_{(150)}$†	$Cl_{(120)}$	$K_{(250)}$	$C_{(270)}$	$Ca_{(295)}$	$O_{(510)}$	$Fe_{(595)}$	$Ni_{(216)}$	$Cu_{(920)}$	
0	9	32	0	54	2	23	0	1	4	4.0
0.25	4	45	2	4	12	61	0	6	6	1.0
0.5	4	62	2	2	4	56	1	8	11	1.38
1.0	3	41	2	2	2	44	2	12	18	1.5
2	0	3	0	1	0	13	2	14	31	2.21
3	0	0	0	2	0	10	0	12	32	2.67
4	0	0	0	1	0	9	0	14	32	2.28
5	0	0	0	1	0	8	0	13	33	2.54
10	0	0	0	0	0	6	0	15	33	2.20
15	0	0	0	0	0	6	0	13	33	2.54

*I_E = 20 mA, E_+ = 2 kV, p_{Ar} = 5 x 10^{-5} torr.

†Quantity in parenthesis is the voltage of the peak used for the analysis of the element.

Table 3

AUGER ANALYSIS OF THE CORROSION FILM ON 90:10 Cu:Ni ALLOY AFTER EXPOSURE FOR 160 HOURS TO FLOWING SEAWATER CONTAINING 26.3 mg/l OF DISSOLVED OXYGEN

Ar^+ Etch Time* (min)	Peak Height (arb. units)									Cu/Ni
	$S_{(150)}$†	$Cl_{(180)}$	$K_{(250)}$	$C_{(270)}$	$Ca_{(295)}$	$O_{(510)}$	$Fe_{(595)}$	$Ni_{(715)}$	$Cu_{(920)}$	
0	5	46	0	31	4	51	0	0	15	-
0.5	3	39	1	3	12	64	0	6	16	2.67
1.0	2	44	3	2	6	63	2	9	14	1.55
2.0	2	34	2	2	2	37	0	8	28	3.50
3.5	2	21	2	2	2	27	0	10	35	3.50
3.0	1	14	0	1	1	19	0	9	38	4.2
3.5	0	12	0	2	2	17	1	9	41	4.56
4.0	0	10	0	0	0	16	0	9	43	4.78
5.0	0	9	0	0	0	13	1	9	43	-
7.5	0	4	0	0	0	12	1	9	42	4.67
10.0	0	1	0	0	0	11	2	9	45	5.0
15.0	0	0	0	0	0	9	1	9	48	5.33

*I_E = 20 mA, E_+ = 2 kV, $p_{Ar} = 5 \times 10^{-5}$ torr.
†Quantity in parenthesis is the voltage of the peak used for the analysis of the element.

Table 4

AUGER ANALYSIS OF THE CORROSION FILM ON 70:30 Cu:Ni ALLOY
AFTER EXPOSURE FOR 160 HOURS TO FLOWING SEAWATER
CONTAINING 26.3 mg/l OF DISSOLVED OXYGEN

Ar^+ Etch Time* (min)	Peak Height (arb. units)									Cu/Ni
	$Fe_{(595)}$†	$S_{(150)}$	$Cl_{(180)}$	$K_{(250)}$	$C_{(270)}$	$Ca_{(290)}$	$O_{(510)}$	$Ni_{(715)}$	$Cu_{(920)}$	
0	0	2	20	4	10	2	45	4	8	2.0
0.5	1	2	12	4	6	2	48	5	8	1.1
1.0	0	2	10	4	5	3	50	4	7	1.7
2.0	2	1	9	4	4	2	50	4	7	-
3.0	3	1	9	4	3	3	52	5	7	1.4
5.0	3	3	10	4	3	3	48	5	7	-
10.0	3	3	13	4	3	5	55	7	9	1.3
Ar^+ etch beam intensity increased to E_+ = 1kV (80 $\mu a/cm^2$)										
11.0	3	3	12	4	2	7	58	7	8	1.11
13.0	2	5	18	6	2	7	52	6	8	1.3
15.0	1	3	15	5	1	7	48	7	11	1.5
17	3	4	12	5	1	7	43	8	13	1.6
19	3	3	10	4	1	6	34	7	16	2.3
22	2	2	7	3	2	5	30	9	17	1.8
27	3	2	5	2	2	4	25	11	22	2.0
32	3	1	13	3	3	4	23	12	22	1.8
37	5	2	8	2	3	4	19	10	20	2.0
42	2	0	6	1	3	3	17	12	20	1.67
47	2	1	5	2	3	4	15	11	24	2.18
52	2	0	3	1	3	2	13	12	25	2.08
57	3	0	2	0	3	2	13	13	25	1.92
67	2	0	2	0	3	0	10	12	27	2.25
Ar^+ Beam intensity increased to E_+ = (265 $\mu a/cm^2$)										
72	0	0	0	0	2	0	7	16	27	1.69
77	0	0	0	0	2	0	5	15	30	2.0
82	0	0	0	0	2	0	6	14	30	

*I_E = 20 mA, E_+ = 0.5 kV, $p_{Ar} = 5 \times 10^{-5}$ torr.
†Quantity in parenthesis is the voltage of the peak used for the analysis of the element.

small amounts of carbon detected in the film are believed to arise from posttest handling, and possibly by adsorption of plasticizers from the PVC surfaces of the loop during the corrosion experiments.

The elemental analyses as a function of depth show that the ratio of copper to nickel is lower in the film than in the alloy. This may indicate preferential dissolution of copper from the growing film, or a lower tendency for precipitation of copper oxide and hydroxychloride corrosion products compared with phases containing nickel. Furthermore, the sputtering times required to penetrate the films suggest that, for the low oxygen case, the film on the 90:10 Cu:Ni alloy is thicker than that on the 70:30 Cu:Ni alloy, but that in the high oxygen system the order is reversed.

REFERENCES

1. J. M. Popplewell, "Marine Corrosion of Copper Alloys: An Overview." To be presented at the Symposium on Effects of Pollution and Velocity on Seawater Corrosion, Corrosion 78, Houston, Texas, March 1978.

Appendix IV

THE EFFECT OF DISSOLVED SULFIDE ON THE CORROSION OF COPPER-NICKEL ALLOYS IN FLOWING SEAWATER

By

Digby D. Macdonald, B. C. Syrett, and S. S. Wing

ABSTRACT

The corrosion of 90:10 Cu:Ni and 70:30 Cu:Ni alloys in sulfide-polluted flowing seawater has been studied as a function of sulfide concentration. The experimental techniques used include small amplitude cyclic voltammetry, ac impedance measurements, large amplitude cyclic voltammetry, and extensive surface examination by scanning electron microscopy (SEM) with energy dispersive X-ray (EDX) analysis, X-ray diffraction, and Auger electron spectrometry (AES). It is shown that the presence of sulfide induces a loss in passivity of the alloy surface due to the formation of cuprous sulfide as the principal corrosion product. Furthermore, accelerated corrosion of these materials in sulfide-polluted seawater appears to arise from a shift in the corrosion potential to sufficiently active values that hydrogen evolution becomes a viable cathodic process.

INTRODUCTION

The influence of dissolved sulfide on the corrosion behavior of copper-nickel alloys in polluted seawater is the subject of much current interest, particularly with respect to materials performance in marine installations, such as heat exchangers. Although a considerable amount of work in this area has been reported,[1-9] no completely satisfactory corrosion mechanism has been proposed. This situation is partly due to a lack of reliable data on the variation of pertinent electrochemical parameters (e.g., corrosion current and potential) as a function of sulfide concentration, but, in many cases, it is also due to a failure to closely control system parameters such as oxygen concentration and pH when carrying out variable sulfide concentration experiments. This latter problem arises because the oxidation of dissolved sulfide by molecular oxygen not only results in a decrease in the concentration of oxygen that is available for corrosion, but also may cause considerable change in the pH of the environment. Available data indicate that dissolved sulfide is oxidized fairly rapidly in seawater. Thus, Ostlund and Alexander[10] showed that for air-saturated seawater with a sulfide concentration of 3.8 ppm, the half-life of hydrogen sulfide is of the order of 20 minutes. Avrahami and Golding,[11] in a detailed mechanistic study of this reaction, showed that elemental sulfur, as well as sulfite (SO_3^{2-}), sulfate (SO_4^{2-}), and thiosulfate ($S_2O_3^{2-}$) are reaction products, and that the oxidation of sulfur to the oxyanions is slow. This latter finding has been confirmed by Kemp, Hyne, and Rennie[12] who also found, however, that the oxidation of sulfur to sulfurous and sulfuric acid is catalyzed by UV radiation. Finally, the aerobic oxidation of sulfur in aqueous systems by <u>thiobacillus thiooxidans</u> is

well-documented,[13] and sulfuric acid concentrations as high as 1 mol/dm^3 have been observed. Because the corrosion rate of copper-nickel alloy in seawater is likely to be pH-dependent, there is a clear need for careful pH control in studying corrosion phenomena in polluted seawater.

As part of our continuing investigation of the corrosion of copper-nickel alloys in flowing seawater, we report here an investigation of the effect of dissolved sulfide on the corrosion behavior of copper-nickel alloys 706 (90:10 Cu:Ni) and 715 (70:30 Cu:Ni) in flowing deoxygenated seawater. This work is an extension of our previously reported study[14] on the corrosion of these materials in oxygenated systems, and was designed to provide basic information on the corrosion mechanism, as well as to yield information that would be of value in assessing the performance of the alloys in field service.

EXPERIMENTAL

The recirculating loop specimen test sections, and the associated apparatus for carrying out corrosion studies in flowing seawater under carefully controlled hydrodynamic conditions, have been described elsewhere.[14] Briefly, five tubular specimens (surface area = 11.05 cm^2/specimen) of each alloy were mounted in tandem test sections in the loop and exposed to sulfide-contaminated seawater for periods of up to 260 hours. The work reported here was carried out at the same fluid flow-rate of 1.62 m/s as was used in our previous study of the effect of oxygen concentration on the corrosion of copper-nickel alloys in natural seawater.[14]

Both the sulfide concentration and the pH of the solution were monitored at regular intervals using $Pb(ClO_4)_2$ titration and glass electrode potentiometry, respectively. It was found that at very short exposure times, the copper-nickel alloy specimens and the approach sections were sufficiently active to sharply reduce the sulfide levels below those initially established by sparging the seawater reservoir with the appropriate N_2/H_2S gas mixture. The loss in dissolved sulfide was counteracted by increasing the input level of H_2S in the gas for a brief period until the original level was reestablished. In one experiment, the H_2S concentration was allowed to increase linearly with time. This "sulfide sweep" experiment was used to define the general features of the corrosion process before the alloys were exposed to deoxygenated seawater having constant sulfide concentrations. The pH of the solution was controlled between 8.0 and 8.4 by injection of sodium hydroxide or hydrochloric acid.

Topographic examinations of the corroded surfaces were made by scanning electron microscopy (SEM), and compositional analyses of the corrosion product films were performed, where possible, using X-ray diffraction, energy dispersive X-ray (EDX) analysis, Auger electron spectrometry (AES), and galvanostatic reduction. Descaling of each specimen before exposure to the seawater was accomplished by immersion in HCl/H_2SO_4 (ASTM Recommended Practice G1-72 for copper alloys). After exposure, the specimnes were descaled by alternately immersing the exposed surfaces only into HCl/H_2SO_4 and 0.1 M NaCN solution until the specimens were stripped of scale. The sodium cyanide solution has been previously shown by Mor and Beccaria[4] to readily dissolve cuprous sulfide from copper and copper-nickel surfaces.

Polarization resistance measurements were carried out under potentiodynamic control by imposing a 20-mV peak-to-peak saw-tooth voltage across the interface by use of a potentiostat and function generator. A sweep rate of 0.1 mV/s, or in some cases 0.5 mV/s, was used. Very small hysteresis currents were observed, thereby indicating minimal contribution to the surface conductance by capacitive elements. A recent theoretical analysis by Macdonald[15] (Appendix II) has shown that under these conditions the electrode impedance, as measured directly from the current-voltage curve, is equal to the true dc polarization resistance.

Impedance spectra were measured using the previously described[14,16] technique of analyzing the dimensions of the Lissajous figures generated by imposing the sinusoidal excitation voltage (11 mV peak-to-peak) and the sinusoidal current response simultaneously across the X and Y axes of an XY recorder (0.0005 Hz to 1 Hz) or oscilloscope (> 1 Hz).

RESULTS

Corrosion Potential and Polarization Resistance Studies

The variation of corrosion potential and polarization resistance with time for 90:10 Cu:Ni and 70:30 Cu:Ni alloys in natural flowing (1.62 m/s) deoxygenated seawater is shown in Figures 1, 2, and 3 for the sulfide sweep (10-55 ppm H_2S), low sulfide (0.85 ppm H_2S), and high sulfide (16 ppm H_2S) experiments, respectively. Also plotted is the sulfide concentration as a function of time over the duration of each experiment. Polarization resistance data, as determined by use of small-amplitude cyclic voltammetry (SACV) and from the low-frequency real axis intercept of the ac impedance data[14,16] in the complex plane (see later), are plotted together for comparison. Excellent agreement is obtained, thereby demonstrating that the impedance of the interface is indeed dominated by the resistive component at the sweep-rate of the SACV excitation function used (0.1 and 0.5 mV/s). This finding is in keeping with our previous work on the corrosion of copper-nickel alloys in oxygenated seawater,[14] and conforms to the recently established theoretical criteria[15] for polarization resistance measurements using the SACV technique.

Corrosion potential data shown in Figure 1 for the sulfide-sweep experiment indicate that E_{corr} for the 70:30 Cu:Ni alloy initially increases, but then undergoes a shift to more active potentials after approximately 10 hours of exposure. At longer times, the corrosion potential becomes constant. In the case of the low nickel alloy (i.e., 90:10 Cu:Ni), the corrosion potential is much more negative than that for the high nickel alloy and, after an initial shift in the active direction, it tends to

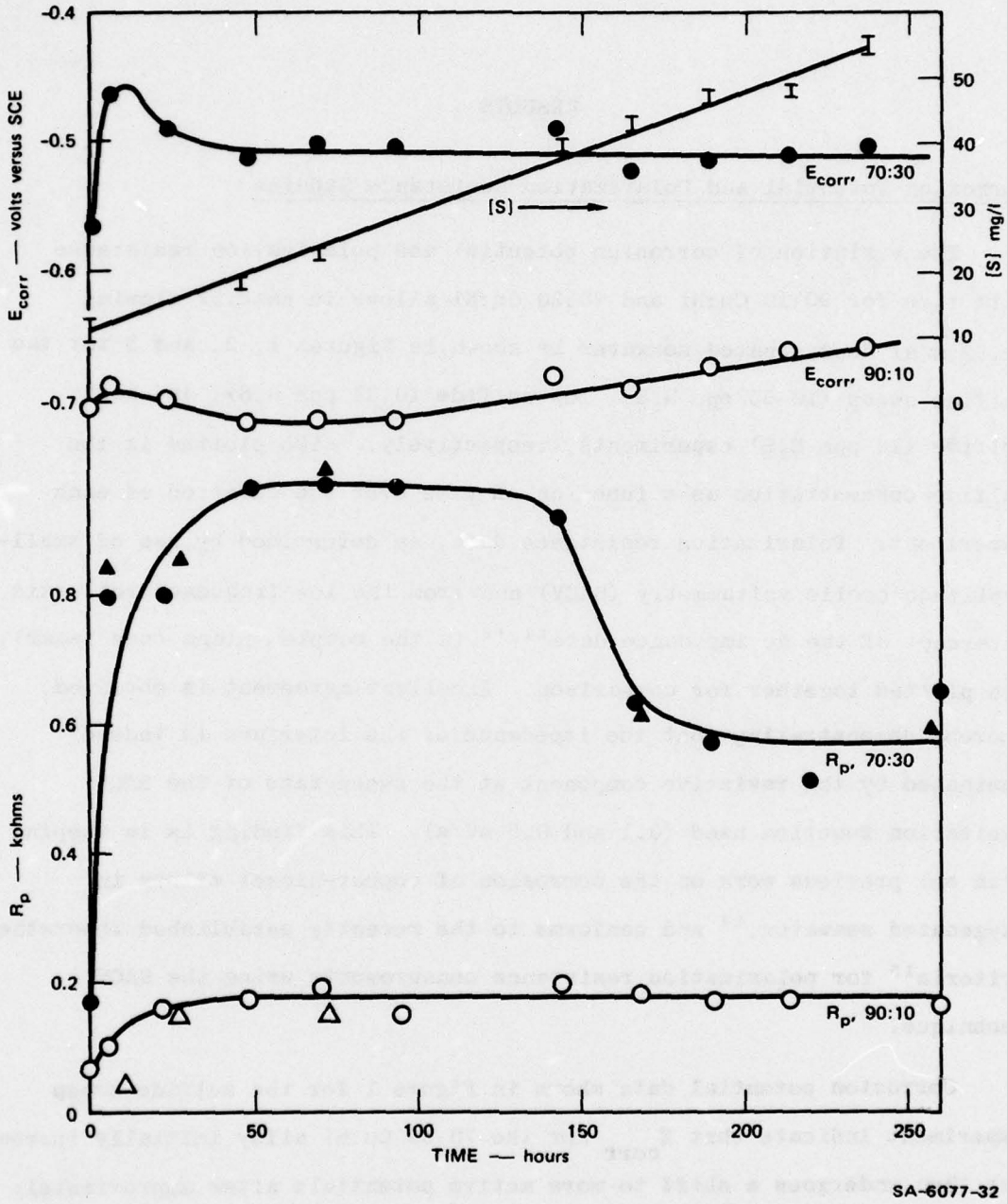

FIGURE 1 VARIATION OF CORROSION POTENTIAL AND POLANIZATION RESISTANCE WITH TIME OF 90:10 Cu:Ni (OPEN POINTS) AND 70:30 Cu:Ni (CLOSED POINTS) ALLOYS IN FLOWING DEOXYGENATED SEAWATER

The total sulfide concentration ([S]-calculated as sulfur) was varied linearly with time between 10 and 55 mg/l. △ and ▲ — polarization resistance data from the ac impedance experiments. T = 22 ± 2°C

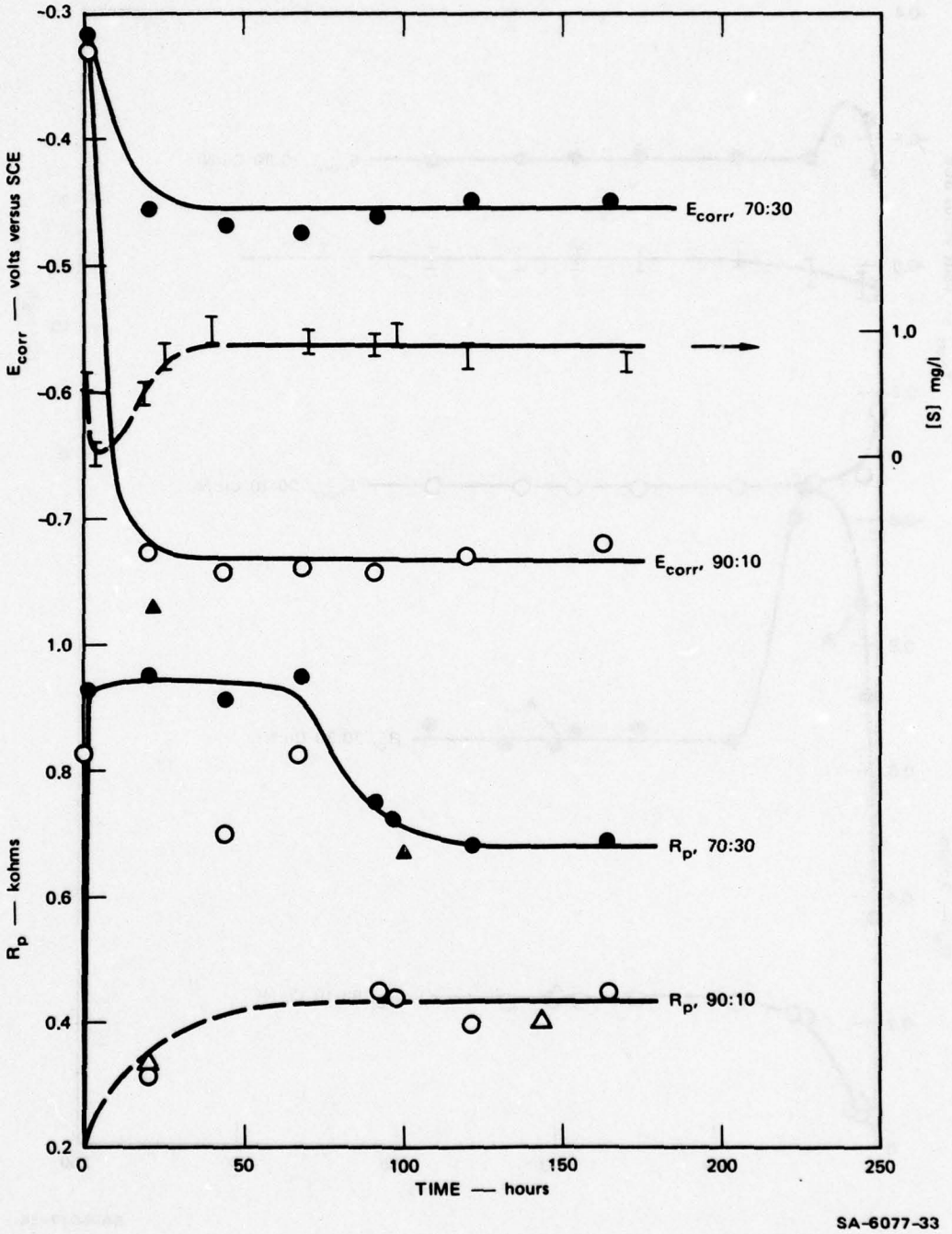

FIGURE 2 VARIATION OF CORROSION POTENTIAL AND POLARIZATION RESISTANCE OF 90:10 Cu:Ni (OPEN POINTS) AND 70:30 Cu:Ni (CLOSED POINTS) ALLOYS IN FLOWING DEOXYGENATED SEAWATER CONTAINING 0.85 mg/l TOTAL SULFIDE ([S]-CALCULATED AS SULFUR)

△ and ▲ – polarization resistance data from the ac impedance experiments.
T = 22 ± 2°C

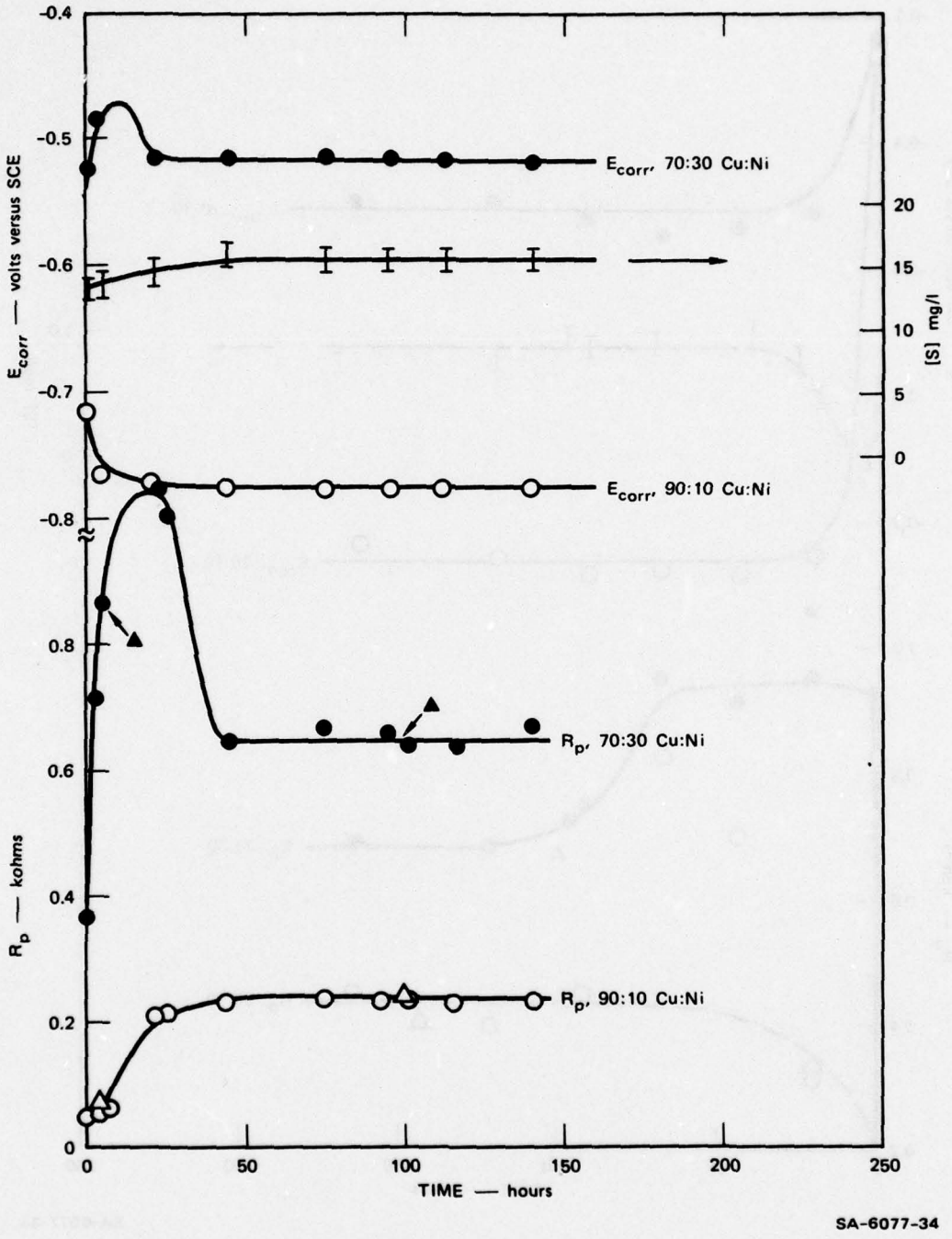

FIGURE 3 VARIATION OF CORROSION POTENTIAL AND POLARIZATION RESISTANCE OF 90:10 Cu:Ni (OPEN POINTS) AND 70:30 Cu:Ni (CLOSED POINTS) ALLOYS IN DEOXYGENATED FLOWING SEAWATER CONTAINING 16 mg/l TOTAL SULFIDE ([S] –CALCULATED AS SULFUR)

△ and ▲ – polarization resistance data from the ac impedance experiments.
T = 22 ± 2°C

become steadily more positive with time. Similar behavior is exhibited by the two alloys during the constant sulfide concentration experiments (Figures 2 and 3), although the initial maximum in E_{corr} for the 70:30 Cu:Ni alloy is not well-defined, and the corrosion potential for the 90:10 Cu:Ni alloy tends to remain constant with time after the initial shift to more active values.

The data plotted in Figures 1 to 3 show that both alloys exhibit an initial increase in R_p with time, as expected for systems that spontaneously passivate. Thereafter the polarization resistance for the low nickel alloy remains constant, whereas that for the high nickel alloy exhibits a sudden shift to a lower constant value after a period of invariance with time. To our knowledge, this is the first time that this phenomenon has been observed. Since this transition is observed only for the high nickel material, it appears to be associated with the nickel component of the alloy. However, the decrease observed in R_p is less than a factor of two, and is small compared with the change in the polarization resistance due to the presence of dissolved sulfide in the system (see Discussion).

Impedance Spectra

Typical complex plane impedance spectra are shown in Figure 4 for 90:10 Cu:Ni alloy (left-hand column) and 70:30 Cu:Ni alloy (right-hand column) in seawater containing 16 mg/liter sulfide at two exposure times (4 hours and 100 hours), and for these alloys in low oxygen (0.045 mg/liter) sulfide-free seawater under identical flow condtions. All the plots exhibit resolved, or at least partially resolved, semicircles with centers on or below the real (R_s) axis, as found previously for these alloys in oxygenated flowing seawater.[14] It can be show[16] that a simple semicircle centered on the real axis arises from an interfacial

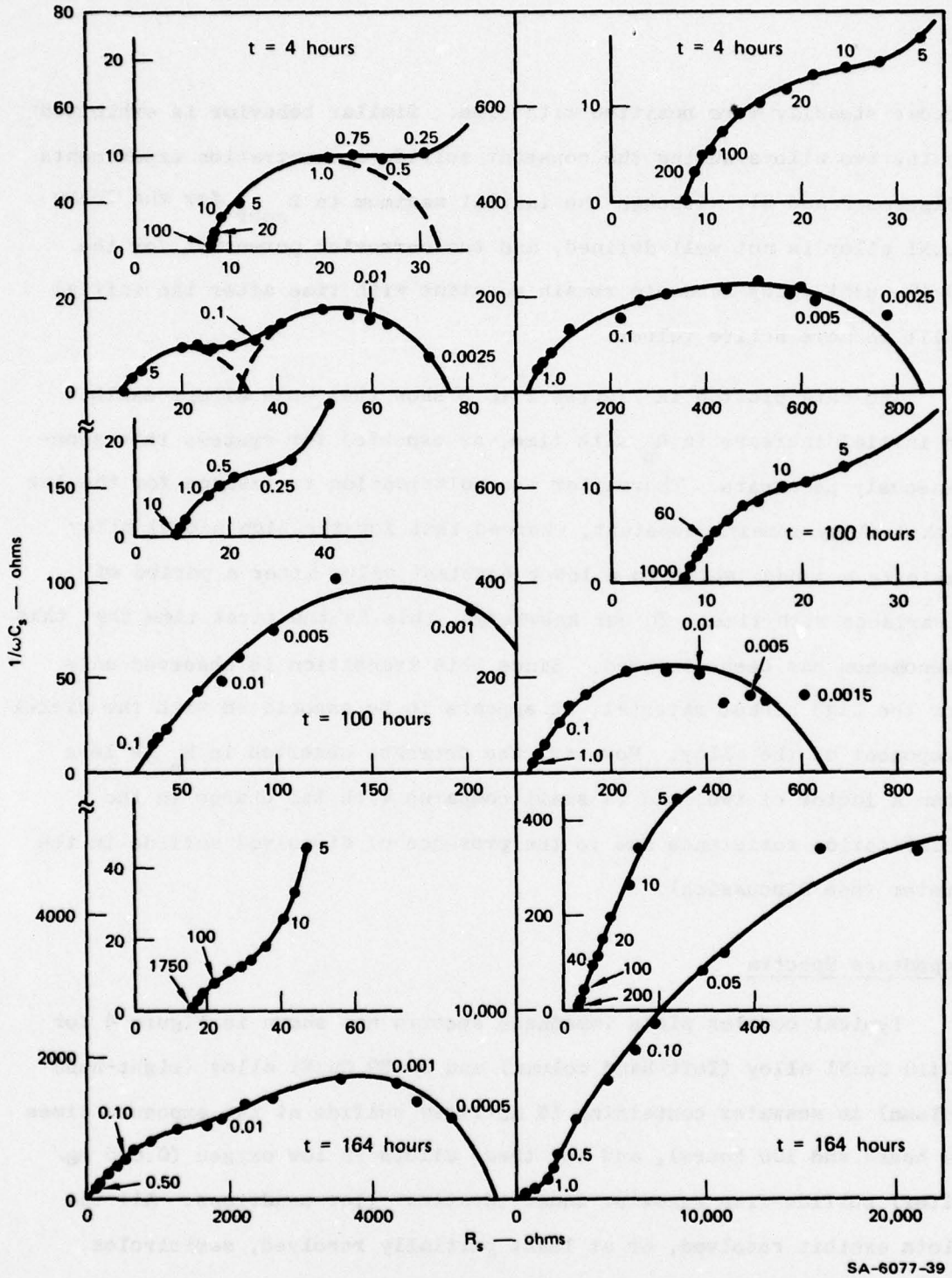

FIGURE 4 COMPLEX PLANE IMPEDANCE DIAGRAMS FOR 90:10 Cu:Ni (LEFT-HAND COLUMN) AND 70:30 Cu:Ni (RIGHT-HAND COLUMN) ALLOYS AS A FUNCTION OF EXPOSURE TIME IN SULFIDED (UPPER TWO ROWS) AND SULFIDE-FREE (BOTTOM ROW) FLOWING SEAWATER

Flow rate = 1.62 m/s, T = 22 ± 2°C. The dissolved oxygen concentration for the sulfide-free experiment was 0.045 mg/l. The number next to each point is the excitation frequency in Hz; for the sake of clarity, not all points are labeled. R_s and C_s *are the equivalent series resistance and capacitance, respectively*[16].

process that can be represented by an electrical equivalent circuit consisting of a parallel combination of a resistance and a capacitance, and therefore is characterized by a single relaxation time. A semicircle that is centered below the real axis is believed to arise from a process having a distribution of relaxation times, as commonly observed in the study of the dielectric relaxation of complex molecules.

The reactive component of the impedance vector becomes vanishingly small at both high and low frequencies. In the high frequency limit, the intercept on the real axis gives the impedance of any purely resistive path between the specimen surface and the reference electrode probe. In the present study, this intercept was found to be 7 to 10 ohms, which can probably be attributed to solution resistance alone. On the other hand, the low frequency intercept yields the total dc resistance between the interior of the metal and the reference electrode. Subtraction of the high frequency real-axis intercept therefore yields the interfacial (i.e., polarization) resistance. These interfacial resistances are plotted as open and closed triangles in Figures 1 to 3.

In many cases, it is possible to resolve the impedance spectra into component semicircles by inspection, as shown for example, in the plots in the upper left-hand corner of Figure 4. Theory predicts[16] that the frequency at which the reactive component is at a maximum in each semicircle is given by

$$\omega_{max} = 1/R_D C \qquad (1)$$

Where R_D is the diameter of the semicircle, and C is the parallel capacitance. Data for the resolved spectra are summarized in Table 1. In view of the uncertainty that was frequently experienced in resolving the spectra into individual relaxation processes, these data should be

Table 1

VALUES FOR THE COMPONENTS OF THE EQUIVALENT PARALLEL RC CIRCUIT ELEMENTS FOR CORRODING COPPER:NICKEL ALLOYS IN FLOWING SEAWATER
T = 22 ± 2 C, Flow-rate = 1.62 m/s

[S], mg/l	t, hours	N*	ω_{max}, Hz	R_D, ohms	C, $\mu f/cm^2$
		90:10 Cu:Ni			
0	22	2	0.17	725	120
			60	30	8.0
0	72	2	0.025	2400	240
			60	30	8.0
0	164	3	0.0025	4850	1200
			0.040	1750	210
			50	28	10
16	4	2	0.020	48	15000
			0.85	28	610
16	100	2	0.0020	216	34000
			0.35	30	1400
		70:30 Cu:Ni			
0	20	2	0.045	10200	31
			300	33	1.5
0	74	2	†	†	
			300	32	1.5
0	164	0	†	†	
16	4	2	0.025	800	720
			14.0	28	37
16	100	2	0.014	570	1700
			7.5	25	77

*Number of resolved relaxation phenomena.
†Unresolved at lowest frequency employed.

regarded as semiquantitative only, and probably contain uncertainties as large as ± 20%. Nevertheless, the data are sufficiently precise to establish useful relationships among the impedance behavior, time, and the presence or absence of dissolved sulfide in the system.

In the absence of dissolved sulfide, both alloys exhibit a high frequency semicircle with circuit parameters that are essentially independent of time. It therefore seems unlikely that this relaxation process involves transport through a surface film. A more likely explanation, particularly in view of the low resistance, is that this semicircle arises from the direct dissolution of the alloy to form ions in solution at the interface. The capacitance associated with this relaxation process (8-10 $\mu F/cm^2$ for 90:10 Cu:Ni and $\sim$ 1.5 $\mu F/cm^2$ for 70:30 Cu:Ni) is well below the expected range of 20-40 $\mu F/cm^2$ for the electrical double layer, especially as the roughness factor is probably much greater than unity. The addition of sulfide to the system apparently does not change the resistive component of the high frequency relaxation process, but it has a marked effect upon the capacitance. Thus, in the absence of sulfide, the equivalent parallel capacitance for the high frequency relaxation is 1.5 to 10 $\mu F/cm^2$, and is independent of time. Addition of 16 mg/liter of H_2S to the system causes the high frequency capacitance for the 90:10 Cu:Ni alloy to increase to 610 $\mu F/cm^2$ after 4 hours exposure and to 1400 $\mu F/cm^2$ after 100 hours exposure. In the case of the 70:30 Cu:Ni alloy, the increase is much less dramatic, in that the high frequency capacitance rises to only 77 $\mu F/cm^2$ after 100 hours exposure to flowing seawater containing 16 mg/liter H_2S. These data suggest that in seawater containing dissolved sulfide, the high capacitance observed is dominated by a pseudocapacitance associated with the electrochemical adsorption of sulfide ion onto the alloy surface.[16]

In the case of the low frequency relaxation processes, both the equivalent parallel resistance and capacitance vary with time. Thus, in the absence of sulfide, the equivalent parallel resistance for the 90:10 Cu:Ni alloy increases sharply with time, as does the capacitance. Insufficient data are available to fully establish trends in the equivalent capacitance for the low frequency relaxation for the 70:30 CuNi alloy, but examination of the impedance diagrams suggests that the trend to larger values with time is maintained by the equivalent parallel resistance. The addition of sulfide to the system markedly decreases the equivalent parallel resistance for the low frequency relaxation process for both alloys, but it has the reverse effect upon the equivalent parallel capacitance. In the case of 90:10 Cu:Ni alloy, both the resistance and the capacitance increase with time. The capacitance also increases with time for the 70:30 Cu:Ni alloy, but the equivalent parallel resistance is found to decrease between exposure times of 4 and 100 hours. The different trends noted above for the equivalent parallel resistances for the low frequency relaxation processes for the two alloys parallel the behavior noted previously for the polarization resistance. This is expected, because examination of the impedance spectra plotted in Figure 4 shows that the low frequency relaxation phenomena dominate the total interfacial impedance. The physical interpretation of the low frequency relaxation is discussed later in this paper.

Cyclic Voltammetry

Large amplitude cyclic voltammetry, in which the potential of the specimen is swept in a sawtooth manner between the limits of kinetic stability of the solvent, is a convenient and rapid method for defining the general electrochemical behavior of a system.[16] In particular, the technique yields information on the number and kinetic characteristics of charge transfer processes at the surface. In the present study we

have used large amplitude cyclic voltammetry to investigate the effect low levels of dissolved sulfide on the electrochemical behavior of 90:10 Cu:Ni and 70:30 Cu:Ni alloys in flowing deoxygenated seawater. Typical cyclic voltammograms for the two alloys of interest in flowing seawater as a function of sulfide concentration are shown in Figures 5 and 6. To simplify the presentation, we have shown only the fifth cycles; further cycling of the potential produced nearly superimpossible traces. In both cases, the principal effect of a sulfide addition is to destroy the so-called "double layer" region of copper and copper-based alloys,[17,18] thereby giving rise to large anodic faradaic currents at potentials slightly more noble than that for hydrogen evolution (i.e., more noble than about -1.0 V versus SCE). A high sulfide level (16 mg/liter) also apparently negates the formation of any significant amount of oxide or hydroxide at the surface, as shown by the disappearance of the oxide/hydroxide reduction peaks at about -0.6 V for the 90:10 Cu:Ni alloy and at about -1.0 V for the 70:30 Cu:Ni alloy. At the low sulfide level of 0.85 mg/liter, vestiges of the oxide/hydroxide formation and reduction peaks are still apparent. However, it is believed (see later) that under these conditions, the surface film consists predominantly of cuprous sulfide.

X-Ray Diffraction Studies

Visual inspection of the exposed specimen surfaces after they were removed from the test system revealed that for both the high (10-55 mg/liter H_2S) and low (0.85 mg/liter H_2S) sulfide levels, the majority of the black corrosion film was loosely adherent and tended to flake off the surface, particularly upon drying. X-ray diffraction analyses of the films formed on 90:10 Cu:Ni alloy in the low sulfide experiment demonstrated the existence of orthohombic Cu_2S (i.e., chalcocite). However, seven additional lines that could not be attributed to this phase were

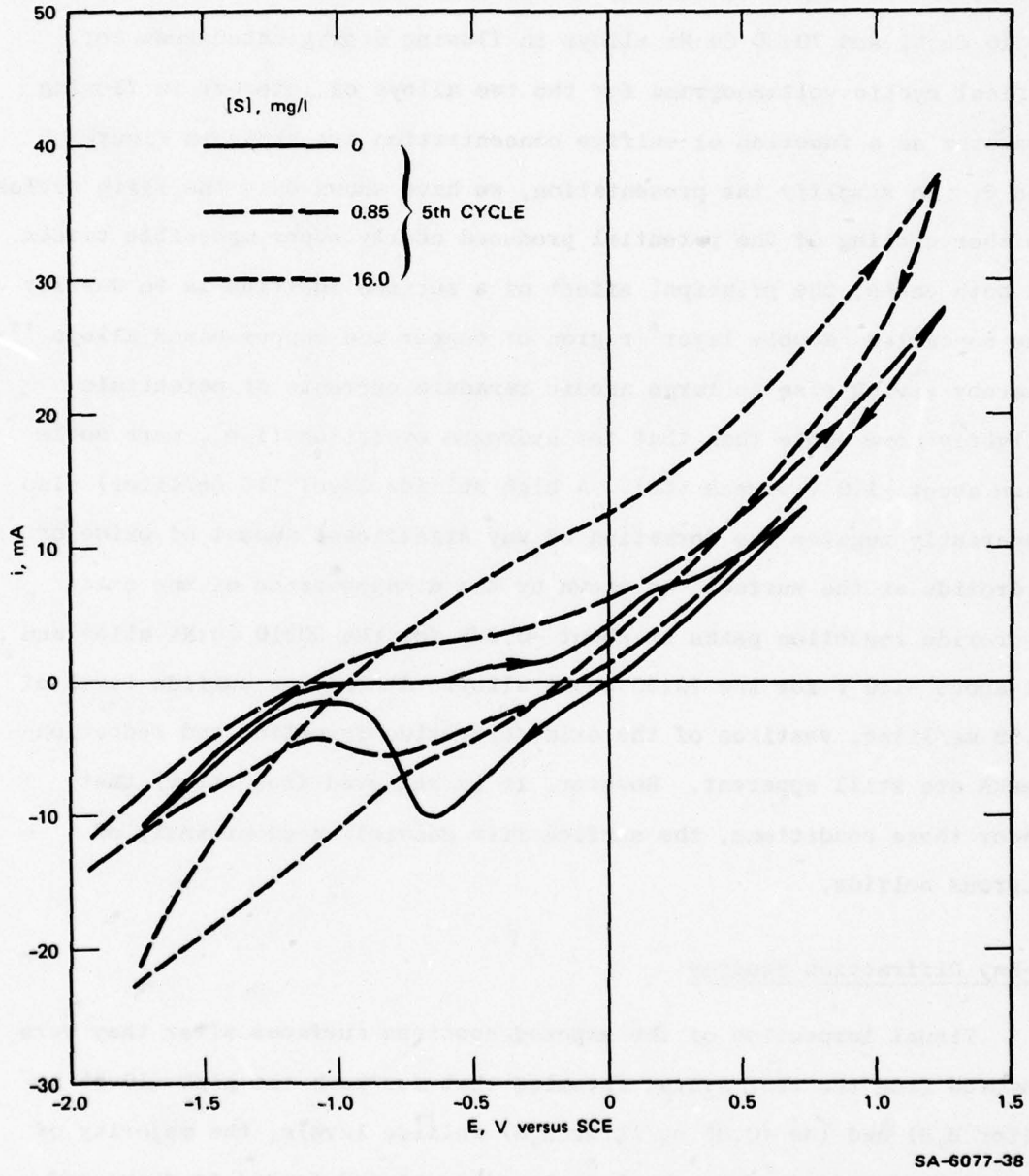

FIGURE 5 EFFECT OF SULFIDE ION ON THE CYCLIC VOLTAMMETRIC BEHAVIOR OF 90:10 Cu:Ni IN FLOWING DEOXYGENATED SEAWATER

Voltage sweep-rate = 50 mV/s; seawater flowrate = 1.62 m/s, T = 22 ± 2°C. The voltammogram for the sulfide-free case was obtained at an oxygen concentration of 0.045 mg/l.

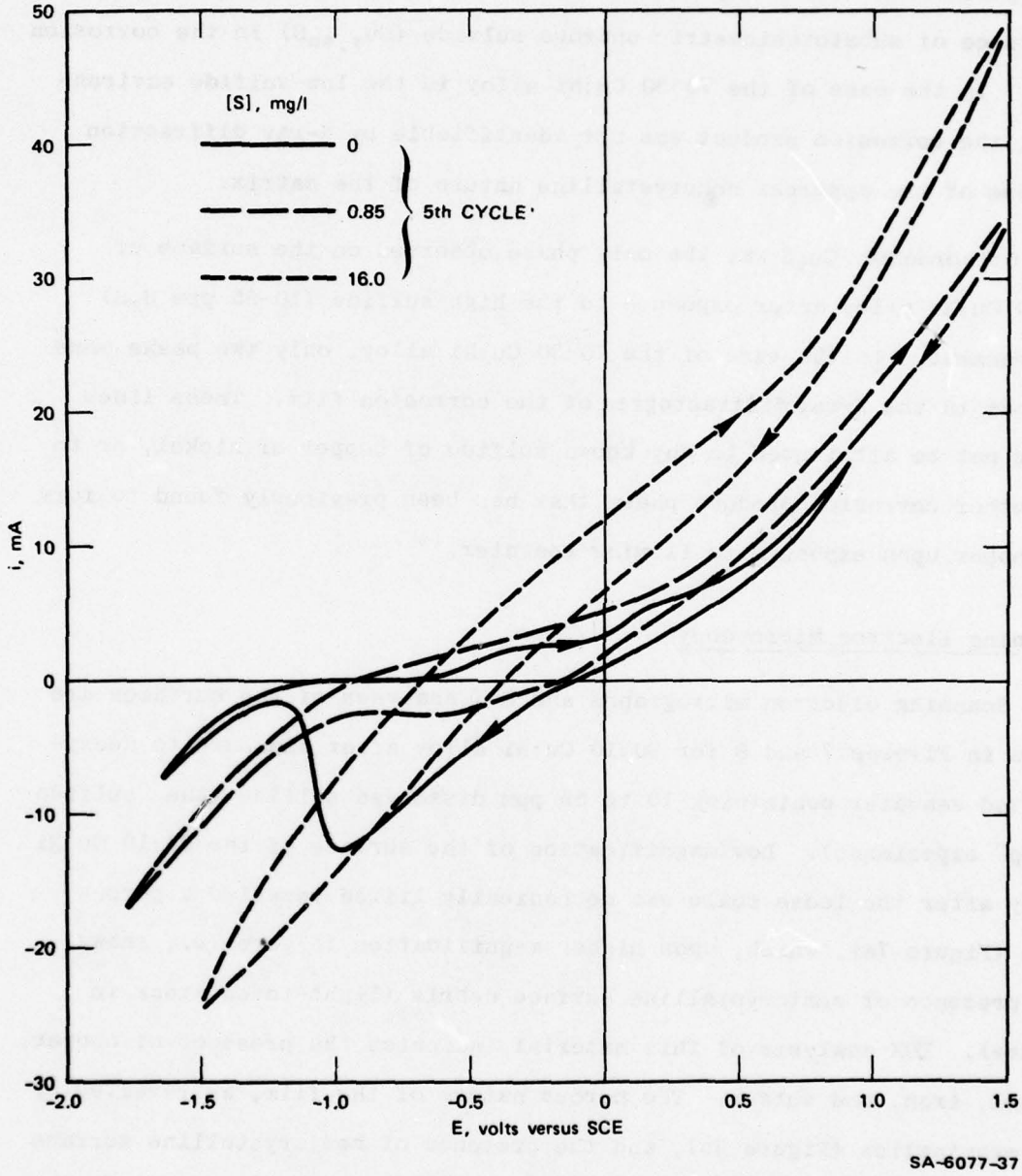

FIGURE 6 EFFECT OF SULFIDE ION ON THE CYCLIC VOLTAMMETRIC BEHAVIOR OF 70:30 Cu:Ni IN FLOWING DEOXYGENATED SEAWATER

Voltage sweep-rate = 50 mV/s, seawater flow-rate = 1.62 m/s, T = 22 ± 2°C. The voltammogram for the sulfide-free case was obtained at an oxygen concentration of 0.045 mg/l.

observed. Four of these lines could be indexed with the known diffraction pattern for cubic Cu_2S, and the other three appear to indicate the existence of substoichiometric cuprous sulfide ($Cu_{1.80}S$) in the corrosion film. In the case of the 70:30 Cu:Ni alloy in the low-sulfide environment, the corrosion product was not identifiable by X-ray diffraction because of the apparent noncrystalline nature of the matrix.

Orthorhombic Cu_2S was the only phase observed on the surface of 90:10 Cu:Ni alloy after exposure to the high sulfide (10-55 ppm H_2S) environment. In the case of the 70:30 Cu:Ni alloy, only two peaks were evident in the X-ray diffractogram of the corrosion film. These lines could not be attributed to any known sulfide of copper or nickel, or to any other corrosion product phase that has been previously found to form on copper upon exposure to flowing seawater.[19]

Scanning Electron Microscopy

Scanning electron micrographs and EDX analyses of the surfaces are shown in Figures 7 and 8 for 90:10 Cu:Ni alloy after exposure to deoxygenated seawater containing 10 to 55 ppm dissolved sulfide (the "sulfide sweep" experiment). Low magnification of the surface of the 90:10 Cu:Ni alloy after the loose scale was mechanically lifted revealed a porous film (Figure 7a), which, upon higher magnification (Figure 7b), shows the presence of semicrystalline surface debris (light-toned areas in figure). EDX analysis of this material indicates the presence of copper, nickel, iron, and sulfur. The porous nature of the film, as revealed by SEM examination (Figure 5b), and the presence of semicrystalline surface debris suggest that during the corrosion process, dissolution of the alloy occurs followed by precipitation of the insoluble corrosion product. EDX analysis of the base dark-toned material (Figure 7b) again revealed the presence of copper, nickel, iron, and sulfur. However, comparison

(a) WIDTH OF PHOTOGRAPH = 0.094 cm

(b) WIDTH OF PHOTOGRAPH = 0.0047 cm

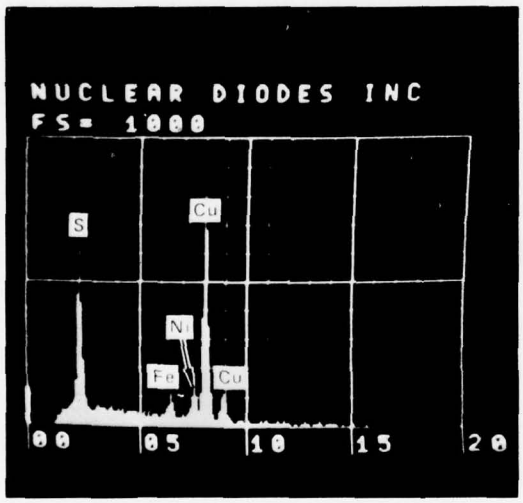

(c) EDX ANALYSIS OF LIGHT AREA CIRCLED IN (b)

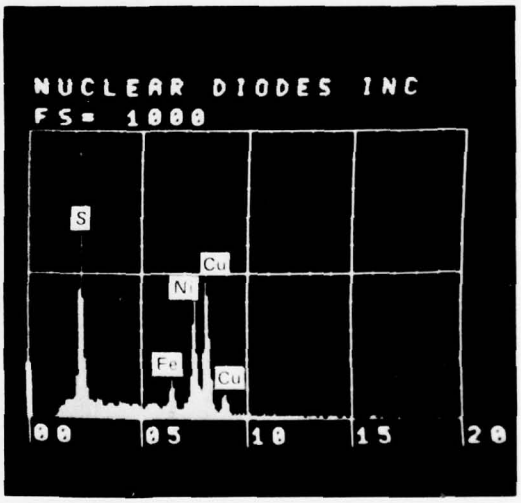

(d) EDX ANALYSIS OF DARK AREA CIRCLED IN (b)

SA-6077-27

FIGURE 7 SEM MICROGRAPHS AND EDX ANALYSES OF THE SUBSCALE SURFACE OF 90:10 Cu:Ni ALLOY AFTER EXPOSURE TO THE "SULFIDE-SWEEP" ENVIRONMENT (10-55 mg/l CALCULATED AS SULFUR)

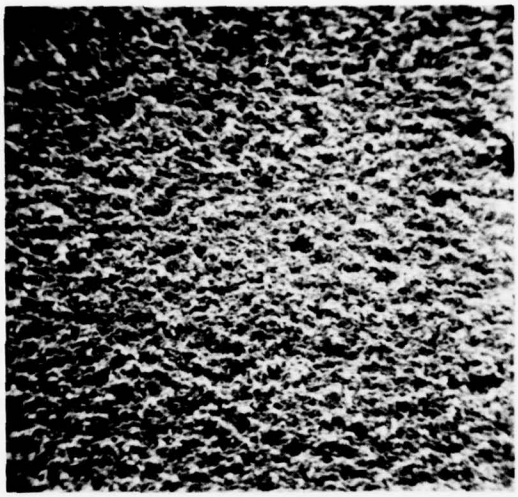

(a) WIDTH OF PHOTOGRAPH = 0.094 cm

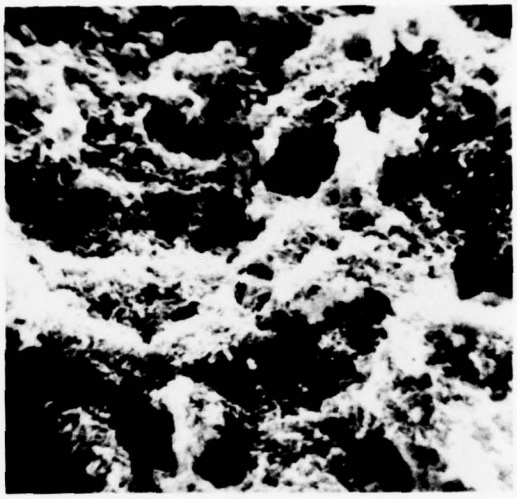

(b) WIDTH OF PHOTOGRAPH = 0.0047 cm

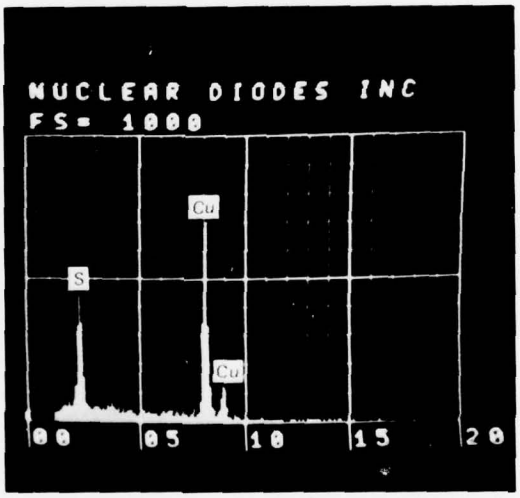

(c) EDX ANALYSIS AVERAGED OVER 25% OF THE SURFACE AREA SHOWN IN (b)

SA-6077-28

FIGURE 8 SEM MICROGRAPHS AND EDX ANALYSIS OF THE OUTER LOOSE SCALE LIFTED FROM 90:10 Cu:NI ALLOY AFTER EXPOSURE TO THE "SULFIDE-SWEEP" ENVIRONMENT ([S] = 10-55 mg/l CALCULATED AS SULFUR)

with the analysis of the light-toned surface debris shows that the base material is enriched in nickel. This may indicate preferential dissolution of copper from the matrix, or preferential dissolution of nickel from the surface debris, or it may mean that nickel-containing phases do not coprecipitate with the copper-containing phases.

SEM micrographs and EDX analyses of the loose surface scale are shown in Figure 8. The scale was found to be highly porous, and upon close examination appears to consist of microcrystalline material. EDX analyses (Figure 8c) averaged over 25% of the area shown in Figure 8b indicate the presence of copper and sulfur in the scale, but not nickel or iron as found for the more adherent scale (Figures 7c and 7d). This analysis is in agreement with the X-ray diffraction work discussed earlier, which indicated that the film consists essentially of polymorphs of Cu_2S.

SEM micrographs of the surface of 70:30 Cu:Ni after exposure of the alloy to 10-55 ppm dissolved sulfide during the "sulfide sweep" experiment are shown in Figure 9. Both the loose scale and the base material are clearly shown in Figure 9a. Higher magnifications of the scale and base material are shown in Figures 9b and 9c, respectively. EDX analysis of the scale (Figure 9d) indicates that this matrix is primarily copper and sulfur, and that it is severely depleted in nickel with respect to copper as compared with the material under the loose scale (Figure 9e). The micrograph of the base material shown in Figure 9c, and the EDX analysis given in Figure 9e, suggest that the surface is essentially free of sulfur and relatively clean. If so, the alloy clearly suffers severe etching in the presence of dissolved sulfide. The etch-lines exhibited in this micrograph indicate that the attack occurs principally at grain boundaries, although pitting attack is also evident. More convincing visual evidence of grain boundary attack in the case of 90:10 Cu:Ni is discussed below.

(a) SCALE SURFACE (WIDTH OF PHOTOGRAPH = 0.094 cm)

(b) SCALE SURFACE (WIDTH OF PHOTOGRAPH = 0.00047 cm)

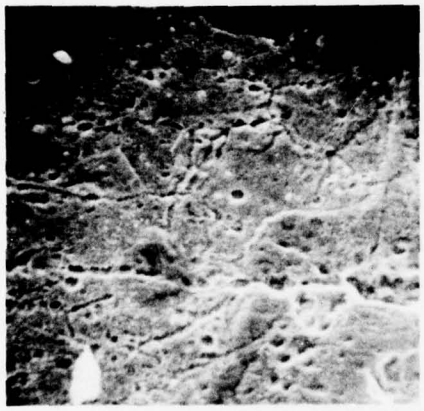

(c) SUBSCALE SURFACE (WIDTH OF PHOTOGRAPH = 0.0047 cm)

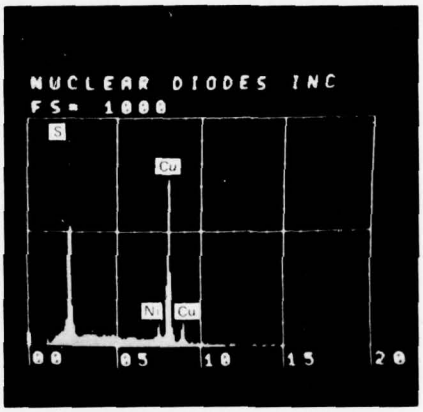

(d) ANALYSIS OF SCALE SURFACE

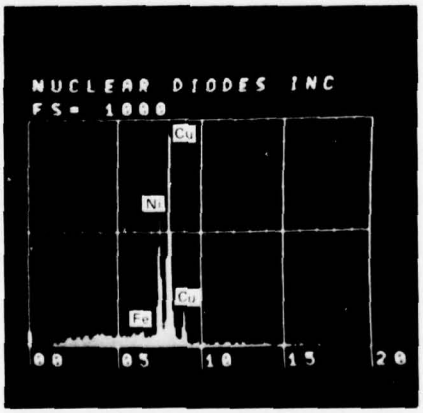

(e) ANALYSIS OF SUBSCALE SURFACE

SA-6077-29

FIGURE 9 SEM MICROGRAPHS AND EDX ANALYSES OF THE SCALE AND SUBSCALE SURFACES ON 70:30 Cu:Ni ALLOY AFTER EXPOSURE TO THE "SULFIDE-SWEEP" ENVIRONMENT ([S] = 10-55 mg/l CALCULATED AS SULFUR)

The surface examinations discussed above were performed on specimens that had been exposed to very high (up to 55 mg/liter) levels of dissolved sulfide. However, the low sulfide exposure tests are of more practical interest with respect to corrosion of copper-nickel alloys in polluted seawater. Surface examinations and analyses of 90:10 Cu:Ni and 70:30 Cu:Ni alloys in flowing seawater containing 0.85 mg/liter dissolved sulfide are shown in Figure 10 and 11, respectively. Low and high magnification examination of the 90:10 Cu:Ni alloy surface again reveals a loosely adherent corrosion film (Figure 10a) that consists of a highly particulate substructure with needle-like crystalline surface debris (Figure 10b). Of particular interest is the morphology of the film-free area shown in Figure 10a. Thus, high magnification (Figure 10c) of the base area shown in Figure 10a reveals extensive etching along what appear to be metal grain boundaries. EDX analysis of the scale (Figure 10d) demonstrates the presence of copper, nickel, iron (minor), and sulfur. The presence of nickel and iron in the scale is in contrast to that found for the scale formed on 90:10 Cu:Ni in the high sulfide environment (Figure 8c). Analyses were also performed in the middle of a grain and in the region of the grain boundary (Figure 10e). No compositional difference between these points could be detected. The analyses did show (Figure 10c), however, that compared with the scale (Figure 10d), the grains and grain boundaries (Figure 10e) appear to be deficient in nickel. This may reflect the spontaneous tendency of copper-nickel alloy surfaces toward enrichment in copper,[20] or more likely it may arise from the preferential dissolution of nickel from the surface matrix of the alloy because of corrosion.

Significant differences in morphology are exhibited by the 70:30 Cu:Ni alloy and the 90:10 Cu:Ni alloy after exposure to flowing seawater

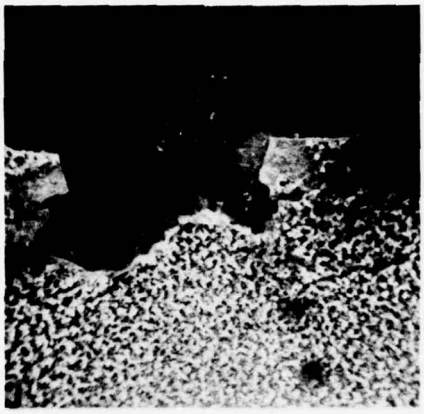

(a) SCALE SURFACE (WIDTH OF PHOTOGRAPH = 0.094 cm)

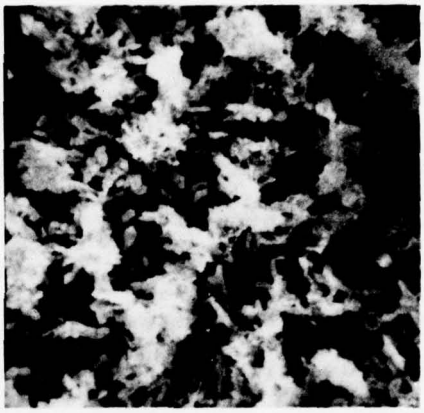

(b) SCALE SURFACE (WIDTH OF PHOTOGRAPH = 0.0047 cm)

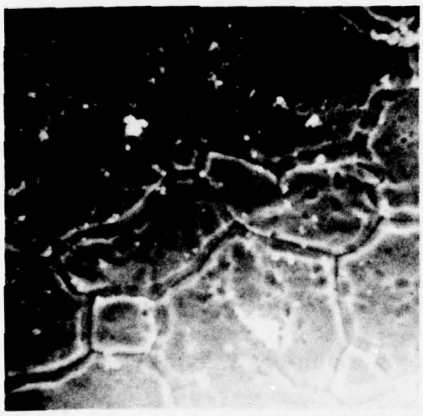

(c) SUBSCALE SURFACE (WIDTH OF PHOTOGRAPH = 0.0047 cm)

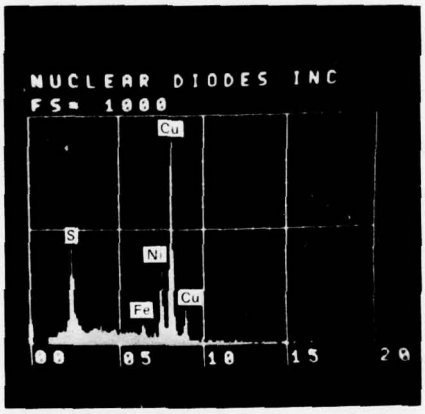

(d) ANALYSIS OF SCALE SURFACE

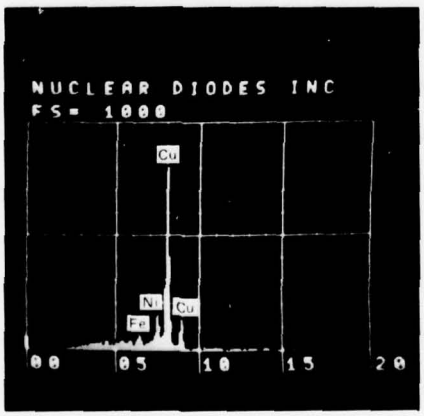

(e) ANALYSIS OF SUBSCALE SURFACE

SA-6077-30

FIGURE 10 SEM MICROGRAPHS AND EDX ANALYSES OF THE SCALE AND SUBSCALE SURFACES ON 90:10 Cu:Ni ALLOY AFTER EXPOSURE TO FLOWING SEAWATER CONTAINING 0.85 mg/l OF SULFIDE (CALCULATED AS SULFUR)

(a) SCALE SURFACE (WIDTH OF PHOTOGRAPH = 0.094 cm)

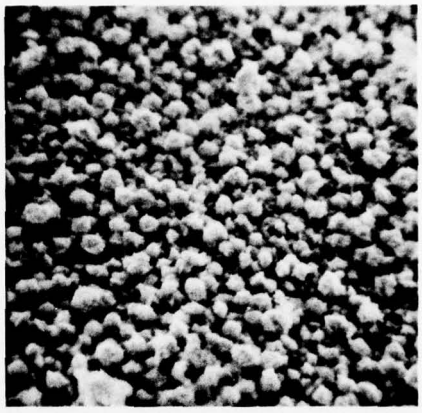

(b) SCALE SURFACE (WIDTH OF PHOTOGRAPH = 0.0047 cm)

(c) SUBSCALE SURFACE (WIDTH OF PHOTOGRAPH = 0.0047 cm)

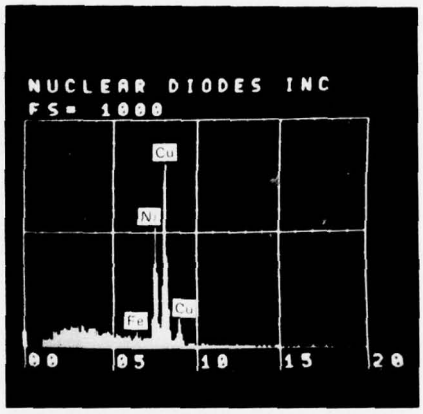

(d) ANALYSIS OF SUBSCALE SURFACE

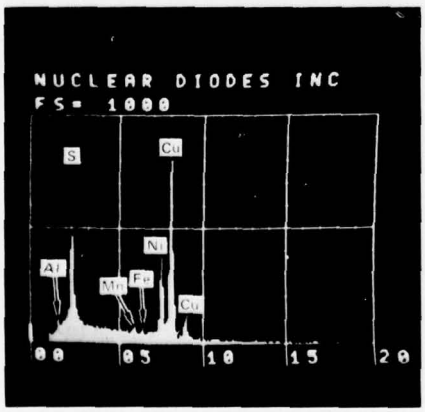

(e) ANALYSIS OF SCALE SURFACE

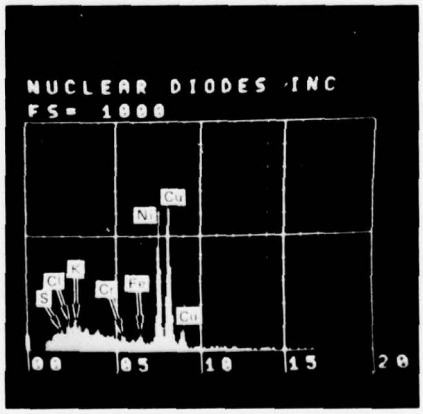

(f) ANALYSIS OF WHITE SPOTS SHOWN IN (c)

SA-6077-31

FIGURE 11 SEM MICROGRAPHS AND EDX ANALYSES OF THE SCALE AND SUBSCALE SURFACES ON 70:30 Cu:Ni ALLOY AFTER EXPOSURE TO FLOWING SEAWATER CONTAINING 0.85 mg/l (CALCULATED AS SULFUR)

that contains a small amount (0.85 mg/liter) of dissolved sulfide (compare Figures 11b and 10b, respectively). Although the films formed on both alloys contain closely-packed irregularly shaped crystallites, the film formed on the 90:10 Cu:Ni alloy (Figure 10b) contains a considerable amount of needle-like crystalline surface debris not found on the 70:30 Cu:Ni alloy. Furthermore, low magnification micrographs of the surfaces reveal the presence of striations on the film-free 90:30 Cu:Ni alloy surface (Figure 11a), whereas in the case of the 90:10 Cu:Ni alloy the attack appears to be concentrated at grain boundaries (Figure 10a).

EDX analyses of the scale and the underlying surface on the 70:30 Cu:Ni alloy after exposure to a low level of sulfide are shown in Figures 11e and 11d. Copper, nickel, and sulfur are present in the scale (Figure 11c), whereas analysis of the scale-free surface shows the presence of copper and nickel only (Figure 11d). This again suggests that the surface below the scale is essentially sulfur-free (c.f. Figure 10c) as far as is indicated by EDX analysis. Interestingly, analysis of the white spots shown in Figure 11c also revealed the presence of both copper and nickel and the absence of sulfur.

Auger Electron Spectrometry

Auger analyses of the corrosion scales and subscale surfaces of 90:10 Cu:Ni and 70:30 Cu:Ni specimens are summarized in Tables 2 to 7. The analyses were performed as a function of depth using argon ion sputtering. A freshly cut edge of each specimen was also analyzed to serve as an internal standard. All the scale analyses support the X-ray diffraction and EDX analysis results; that is, they show that the films consist predominantly of copper sulfide (Cu_2S and substoichiometric

Table 2

AUGER ANALYSIS OF THE CORROSION FILM ON 90:10 Cu:Ni ALLOY
AFTER EXPOSURE TO SULFIDE-POLLUTED FLOWING SEAWATER
Total Sulfide [S] = 10 to 55 mg/l
("Sulfide Sweep" Experiment)

Ar^+ Etch Time† (min)	Peak Height (arb. units)						Cu/Ni
	$S_{(150)}$†	$Cl_{(180)}$	$C_{(270)}$	$O_{(510)}$	$Ni_{(715)}$	$Cu_{(920)}$	
0	10	4	79	20	5	9	1.80
1	113	0	25	6	9	20	2.22
2	109	5	18	7	10	20	2.00
4	88	6	11	9	11	19	1.73
6	64	4	8	11	12	22	1.83
8	47	2	6	12	10	27	2.70
10	34	1	6	11	12	31	2.58
12	25	0	5	10	11	31	2.82
14	20	0	5	10	9	35	3.89
16	18	0	5	10	9	36	4.00
18	14	0	4	9	10	39	3.90
20	11	0	5	10	11	39	3.55
25	9	0	3	12	11	40	3.64
30	9	0	5	0	10	48	4.8
35	0	0	5	0	10	46	4.6
Cut edge of Specimen							
0	0	0	6	6	9	29	3.22

*I_E = 20 mA, E_+ = 1 kV, $p_{Ar} = 5 \times 10^{-5}$ torr.
†Quantity in brackets is the voltage of the peak used for the analysis of the element.

Table 3

AUGER ANALYSIS OF THE CORROSION FILM ON 70:30 Cu:Ni ALLOY
AFTER EXPOSURE TO SULFIDE-POLLUTED FLOWING SEAWATER
Total Sulfide [S] = 10 to 55 mg/l
("Sulfide Sweep" Experiment)

Ar^+ Etch Time† (min)	Peak Height (arb. units)						Cu/Ni
	$S_{(150)}$†	$Cl_{(180)}$	$C_{(270)}$	$O_{(510)}$	$Ni_{(715)}$	$Cu_{(920)}$	
Dark region							
0	61	8	42	4	2	10	5.0
0	40	33	35	37	8	17	2.13
1	89	13	11	20	10	22	2.20
2	80	13	8	17	12	22	1.83
3	77	13	8	15	10	23	2.30
4	69	13	8	16	11	23	2.10
5	66	13	5	16	12	24	2.00
6	62	12	5	14	11	22	2.00
7	55	10	6	14	13	23	1.77
8	67	8	7	12	13	24	1.85
10	45	7	7	13	13	22	1.69
12	43	5	6	12	12	24	2.00
14	40	7	6	14	12	24	2.00
16	39	4	6	12	11	27	2.45
18	36	6	6	13	11	25	2.27
20	37	4	7	12	12	28	2.33
22	43	3	7	9	12	28	2.33
27	26	3	6	7	13	30	2.31
32	23	16	6	5	13	30	2.31
37	20	6	4	8	14	28	2.00
42	18	2	4	7	13	32	2.46
52	15	2	5	9	13	33	2.56
Ion energy increased to 3kV (sputtering rate: ~ 5 x 1 kV rate)							
54(62)	15	2	4	8	14	30	2.14
56(72)	12	2	4	8	17	30	1.76
60(92)	10	2	4	8	14	33	2.36
70(142)	9	0	4	8	14	31	2.21
Cut Edge of Specimen (Ar^+ etch: 1 min at 1 kV)	30	10	7	11	11	29	2.63

*I_E = 20 mA, E_+ = 1 kV, p_{Ar} = 5 x 10^{-5} torr.
†Quantity in brackets is the voltage of the peak used for analysis of the element.

Table 4

AUGER ANALYSIS OF THE CORROSION SCALES ON 90:10 CU:Ni ALLOY AFTER EXPOSURE TO SULFIDE-POLLUTED SEAWATER
Total Sulfide [S] = 0.85 mg/l

Ar^+ Etch Time† (min)	Peak Height (arb. units)							Cu/Ni
	$S_{(150)}$†	$Cl_{(180)}$	$C_{(270)}$	$Ca_{(295)}$	$O_{(510)}$	$Ni_{(715)}$	$Cu_{(920)}$	
0	44	3	6	5	20	3†	5†	1.67
1	22	0	33	5	9	2†	4†	2.00
2	20	1	35	5	8	2†	3†	1.50
4	18	0	38	0	5	0	3†	-
10	22	0	35	0	3	0	4†	-
20	26	0	37	0	3	0	4†	-

*I_E = 20 mA, E_+ = 3 kV, $p_{Ar} = 5 \times 10^{-5}$ torr.
†Quantity in brackets is the voltage of the peak used for the analysis of the element.

Table 5

AUGER ANALYSIS OF THE SUBSCALE SURFACE ON 90:10 Cu:Ni ALLOY ALLOY AFTER EXPOSURE TO SULFIDE-POLLUTED SEAWATER
Total Sulfide [S] = 0.85 mg/l

Ar^+ Etch Time* (min)	Peak Heights (arb. units)							Cu/Ni
	$Fe_{(595)}$†	$S_{(150)}$	$Cl_{(180)}$	$C_{(270)}$	$O_{(510)}$	$Ni_{(715)}$	$Cu_{(920)}$	
0	6	28	15	19	51	12	21	1.75
1	6	12	14	3	53	12	27	2.25
2	5	9	10	0	47	11	29	2.64
4	5	8	7	2	35	11	37	3.36
6	6	7	5	2	27	9	38	4.22
8	4	3	3	2	20	9	42	4.67
10	4	3	2	0	12	10	48	4.80
12	3	3	2	2	9	7	53	7.57
15	4	0	0	2	8	9	50	5.56
20	4	0	0	3	4	9	51	5.67
25	4	0	0	2	3	8	55	6.88
(Cut Edge of Specimen)								
0	1	0	0	6	11	7	40	5.71

*I_E = 20 mA, E_+ = 1 kV, $p_{Ar} = 5 \times 10^{-5}$ torr

†Quantity in brackets is the voltage of the peak used for the analysis of the element.

Table 6

AUGER ANALYSIS OF THE CORROSION SCALE ON 70:30 Cu:Ni ALLOY
AFTER EXPOSURE TO SULFIDE-POLLUTED SEAWATER
Total Sulfide [S] = 0.85 mg/l

Ar^+ Etch Time* (min)	Peak Height (arb. units)						Cu/Ni
	$S_{(150)}$†	$Cl_{(180)}$	$C_{(270)}$	$O_{(510)}$	$Ni_{(715)}$	$Cu_{(920)}$	
0	51	4	35	14	3	7	2.33
1	33	2	59	9	2	5	2.5
2	39	2	51	11	3	6	2.0
4	39	1	51	10	2	5	2.5
9	39	0	56	10	4	8	2.0
14	36	0	65	3	2	8	4.0
20	38	0	62	3	3	7	2.33
25	45	0	69	5	3	8	2.66

*I_E = 20 mA, E_+ = 3 kV, p_{Ar} = 5 x 10^{-5} torr.
†Quantity in brackets is the voltage of the peak used for the analysis of the element.

Table 7

AUGER ANALYSIS OF SUBSCALE SURFACE ON 70:30 Cu:Ni ALLOY
AFTER EXPOSURE TO SULFIDE POLLUTED SEAWATER
Total Sulfide [S] = 0.85 mg/l

Ar^+ Etch Time* (min)	Peak Height (arb. units)						Cu/Ni
	$S_{(150)}$†	$Cl_{(180)}$	$C_{(270)}$	$O_{(510)}$	$Ni_{(715)}$	$Cu_{(920)}$	
0	7	41	40	44	7	10	1.43
1	9	27	7	48	11	22	2.0
2	4	15	5	35	11	29	2.63
3	2	11	4	27	11	33	3.0
4	2	9	4	24	10	36	3.6
5	2	8	3	20	11	37	3.36
6	2	7	2	19	11	37	3.36
8	2	7	2	17	13	34	2.62
10	0	5	3	15	13	36	2.77
17	0	2	3	7	13	37	2.85
20	0	0	4	7	15	36	2.40
25	0	0	4	6	14	38	2.71
(Cut edge of Specimen)							
0	0	0	13	11	13	35	2.69

*I_E = 20 mA, E_+ = 1 kV, $p_{Ar} = 5 \times 10^{-5}$ torr
†Quantity in brackets is the voltage of the peak used for the analysis of the element.

$Cu_{1.8}S$). Significant amounts of oxygen, chlorine, and carbon were also detected, particularly at short sputtering times. Likewise, oxygen and carbon were also observed on the cut metal surfaces. In this case, these elements presumably arise from contamination (e.g., adsorption of CO) during preparation. The large signal for carbon at short sputtering times for the corrosion scales is of interest in light of recent claims by Efird and Lee[21] that carbon plays a role in the accelerated corrosion of copper-nickel alloys in sulfide-polluted seawater. However, the present work was carried out in a recirculating loop constructed from PVC components. Accordingly, contamination of the growing corrosion scales with organic plasticizers is also a plausible explanation for the observed presence of carbon. The small amounts of oxygen and chlorine in the scales, and in the subscale surfaces, presumably reflect the presence of minor amounts of the oxides and hydroxychlorides of copper and possibly nickel.

The data given in Tables 2 and 3 suggest that the sputtering time used was sufficient to essentially penetrate the film, particularly in the case of the 90:10 Cu:Ni alloy, where the sulfur, chlorine, and oxygen peaks have decayed to zero at the longest sputtering time used. Even if the first two analyses are disregarded because of inherent uncertainty due to the presence of significant amounts of carbon on the surface, the results indicate that for both alloys the amount of nickel in the film remains essentially independent of depth. However, in the case of the low nickel alloy, the amount of copper increases as the film is sputtered away. Interestingly, comparison of the last two entries in Table 2 suggests that the metal/scale interface may be enriched with copper with respect to the bulk material. This phenomenon is not shown by the analysis for the 70:30 Cu:Ni alloy (Table 3).

Analyses of the subscale surface (Tables 5 and 7) for specimens that were exposed to a low level of dissolved sulfide (0.85 mg/liter) show that after sputtering, sulfur, chlorine, and oxygen are still present well below the original interface, in contrast to the results from EDX analysis (Figure 11d). Therefore the observed spalling of the sulfide scale from the surface is apparently not the result of lateral fracturing of the scale/alloy interface. Instead, the data suggest that a duplex film is formed, probably as a result of two distinct mechanisms for the formation of the solid corrosion product.

Cathodic Reduction

Previous work[8,22-25] has demonstrated that galvanostatic reduction of oxide and sulfide phases on copper is an effective method for estimating film thicknesses, through application of Faraday's law. These studies have shown that for a current density of about 100 $\mu A/cm^2$, the following plateaux potentials can be expected for mixed oxide/sulfide films on copper

(a) Reduction of Cu_2O: -0.56 to -0.65 V vs SCE

(b) Reduction of CuS: -0.77 to -0.83 V vs SCE

(c) Reduction of Cu_2S: -1.03 to -1.10 V vs SCE

(d) Reduction of H^+: about -1.27 V vs SCE

In the present work on copper-nickel alloys, it was found that the plateaux potentials were about 100 mV more noble than those listed above, presumably because of the presence of nickel in the alloy.

Two plateaux were observed during galvanostatic reduction of the scale on the 90:10 Cu:Ni alloy that had been exposed to the low level sulfide (0.85 mg/liter) environment: one for 66 seconds at about -0.7 V(SCE) and one for 840 seconds at -0.90 to -0.94 V(SCE). We believe that the more

active plateau is due to reduction of orthorhombic Cu_2S, in which case a film ~ 1200 Å thick is indicated. The first plateau at about -0.7 V (SCE) might be due to the reduction of cubic Cu_2S. If so, the charge passed corresponds to a film thickness of ~ 96 Å. Only one plateau, lasting for 1320 seconds, was observed for the 70:30 Cu:Ni alloy at a potential of -0.75 to -0.90 V (SCE). The corrosion product could not be identified by X-ray diffraction; however, if it is assumed that the film was composed of Cu_2S, a film thickness of ~ 1900 Å is calculated.

After exposure of the 90:10 Cu:Ni alloy to high sulfide levels (10 to 55 mg/liter) no distinct plateaux were evident, even though X-ray diffraction indicated the existence of orthorhombic Cu_2S. After exposure of the 70:30 Cu:Ni alloy, however, two plateaux were observed, one lasting 5220 seconds at -0.81 to -0.82 V (SCE) and the other lasting 1905 seconds at-0.92 to -0.98 V (SCE). The X-ray diffraction patterns for the surface were not sufficiently well-defined to permit identification of the components of the corrosion film. The more active plateau, however, probably arises from the reduction of chalcocite (orthorhombic Cu_2S), as in the low-sulfide experiment. If so, a film thickness of 2760 Å is calculated. The more noble plateau also occurs at a potential that was previously attributed to the reduction of cubic Cu_2S on the 70:30 Cu:Ni alloy in seawater containing low levels of dissolved sulfide.

In view of the tendency toward spalling, the film thickness values given above probably do not refer to the total film. Instead, it seems likely that only the subscale material was completely reduced by application of the cathodic current. This hypothesis is supported by visual examination of the surfaces after reduction, which showed the presence of loose unreduced scale. This presumably arises from poor electrical contact between the scale and subscale surfaces.

DISCUSSION

General

The corrosion rate data obtained in this study are in agreement with previous work,[1-9] which has shown that dissolved sulfide ion greatly reduces the corrosion resistances of both 90:10 Cu:Ni alloy and 70:30 Cu:Ni alloy in aqueous systems. The effect of sulfide ion on the corrosion resistances of the alloys in flowing deoxygenated seawater is well-illustrated by the data plotted in Figure 12 for the polarization resistance and corrosion potential after 170 hours of exposure. Data for the sulfide-free cases were taken from our previous study,[14] and were obtained under conditions that were identical to those used for this work. Thus, all specimens were cut from the same tube stock and the experiments were carried out at the same flow velocity (1.62 m/s) and temperature (22 ± 2°C). The data given for the sulfide-free case refer to an "oxygen-free" system; that is, where the oxygen concentration was less than 0.05 mg/liter.

The data plotted in Figure 12 show that only a very low sulfide concentration (≤ 0.85 mg/liter) is necessary to cause a dramatic decrease in the polarization resistance. In the case of the 90:10 Cu:Ni alloy, this sulfide concentration is sufficient to lower the polarization resistance by a factor of approximately 8, whereas for the 70:30 Cu:Ni alloy the polarization resistance is lowered by a factor of 70. Higher sulfide concentrations apparently have little effect on R_p, although the data for the 90:10 Cu:Ni alloy plotted on the expanded scale (bottom of Figure 12) indicate that the polarization resistance continues to decrease slowly as the sulfide concentration is increased. The

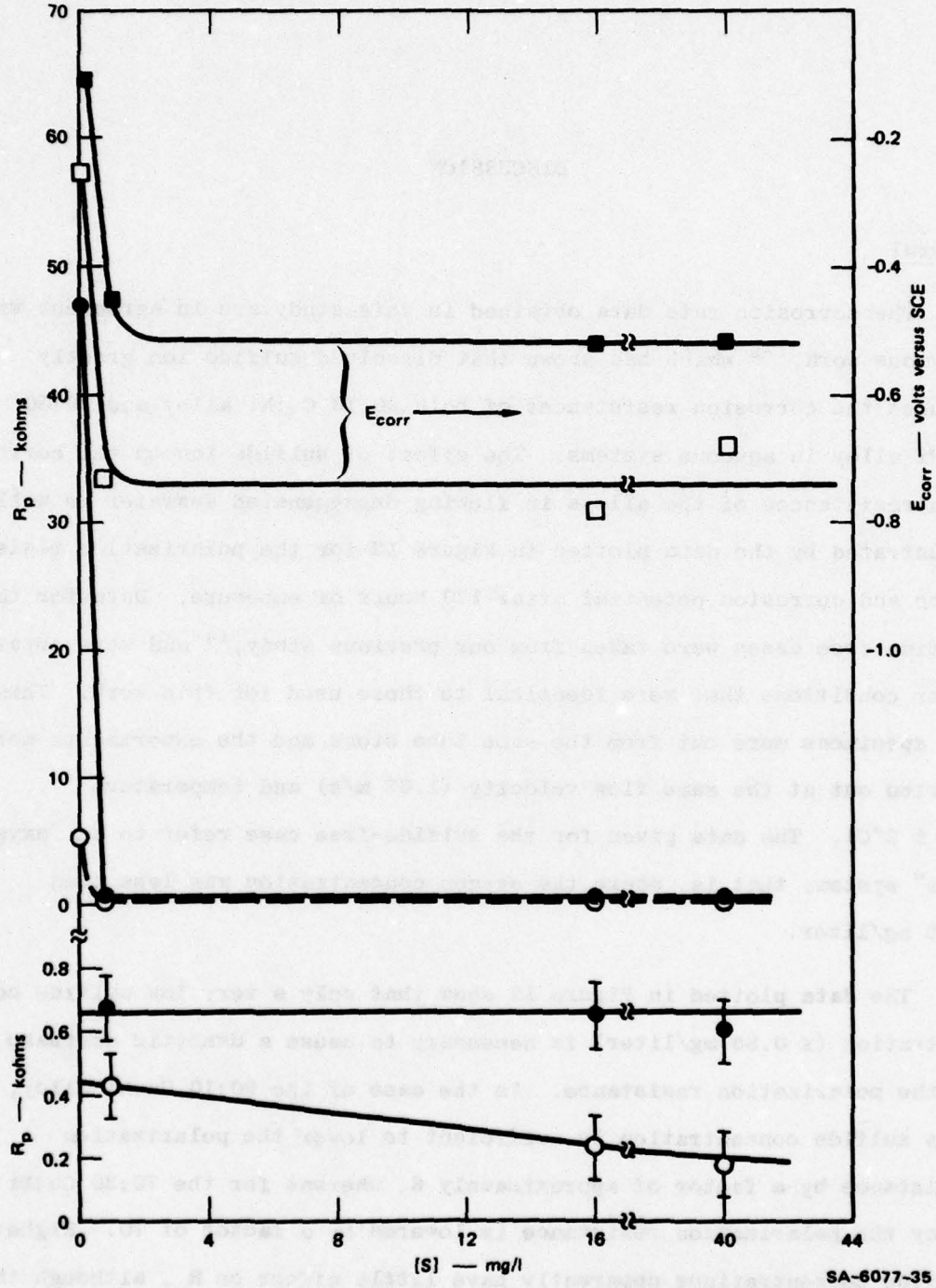

FIGURE 12 VARIATION OF THE POLARIZATION RESISTANCE AND CORROSION POTENTIAL WITH SULFIDE CONCENTRATION FOR 90:10 Cu:Ni ALLOY (OPEN POINTS) AND 70:30 Cu:Ni ALLOY (CLOSED POINTS) AFTER 170 HOURS EXPOSURE

Data for [S] = 0 were extrapolated from Reference 14. T = 22 ± 2°C. Flow rate = 1.62 m/s.

insensitivity of R_p to high sulfide concentration (> 0.85 mg/liter) observed in this work for the copper-nickel alloys parallels the finding for the effect of sulfide on the corrosion behavior of pure copper in deaerated water.[8]

The data plotted in Figure 12 show that the steady state corrosion potentials for the two alloys shift sharply to more active values upon the addition of a small amount (0.85 mg/liter) of sulfide to the system, and that further additions of sulfide have little effect. The corrosion potential behavior is consistent with sulfide-induced breakdown of passivity. This phenomenon is clearly illustrated by the cyclic voltammograms for the 90:10 Cu:Ni alloy and the 70:30 Cu:Ni alloy shown as a function of sulfide concentration in Figures 5 and 6, respectively. Thus, the addition of as little as 0.85 mg/liter of sulfide to the system causes a dramatic increase in the current in the "double layer" region between -0.5 V to -1.1 V. Furthermore, sulfide addition erases peaks that are commonly associated with the formation and reduction of surface oxide/hydroxide phases in the copper and copper-alloy systems.[17,18]

It seems reasonable, therefore, to attribute the loss in passivity to the conversion of the normally protective oxide film formed in the absence of dissolved sulfide to a nonprotective cuprous sulfide film that forms in the presence of sulfide. This hypothesis is supported by the X-ray diffraction, Auger spectrometry, and EDX analyses reported in this paper. Thus, polymorphs of cuprous sulfide were the only phases detected by X-ray diffraction on the alloy surfaces after exposure to dissolved sulfide. Although small amounts of other phases could be present, neither Auger analysis through the film nor surface EDX analysis indicated the predominance of phases containing chlorine or oxygen at the surface.

The loss of passivity due to the formation of cuprous sulfide rather than the oxide at the alloy surface is also well-illustrated by the electrochemical relaxation data generated by use of the ac impedance technique. Thus, if it is assumed that the low frequency relaxation process arises from charge transfer through a surface film, the drastic decrease in the associated parallel equivalent resistance upon the addition of sulfide is in keeping with the above hypothesis. Support for the assumption that the low frequency semicircle arises from charge transfer through a surface film is afforded by the observation (Figure 4) that the center of the semicircle generally lies well below the real axis. This is characteristic of systems that exhibit a distribution of relaxation times, as might be expected for charge transfer through a surface film having a distribution in thickness.

Corrosion Mechanism

The experimental evidence obtained in this work indicates that a primary effect of sulfide on the corrosion of 90:10 Cu:Ni alloy and 70:30 Cu:Ni alloy in flowing seawater is to induce a loss of anodic passivity, as shown by the sharp decrease in polarization resistance and the sudden shift of the corrosion potential in the active direction. However, the overall corrosion process involves both anodic and cathodic partial processes; for freely corroding systems, these processes satisfy the relationship

$$i_a + i_c = 0 \qquad (2)$$

where i_a and i_c are the anodic and cathodic partial currents, respectively. Furthermore, the corrosion potential must satisfy the relationship

$$E^\circ_c > E_{corr} > E^\circ_a \qquad (3)$$

where E_a° and E_c° are the equilibrium potentials for the anodic and cathodic partial reactions, respectively, under the prevailing conditions. Equation (3) provides the link between the kinetic behavior of the system and the thermodynamic properties as commonly expressed in terms of a potential-pH diagram.

Verink[26] has derived potential-pH diagrams for copper in sulfide-polluted seawater and in sulfide-free seawater under ambient conditions. Modified versions of these diagrams are plotted in Figure 13. In the absence of sulfide, E_{corr} for both alloys lies on the noble side of the equilibrium line for hydrogen evolution. Accordingly, the alloys cannot corrode via the reduction of H^+ (or water) as the cathodic partial reaction (see Equation 3). Instead, corrosion is possible only in the presence of dissolved oxygen. In the presence of sulfide, however, the corrosion potentials shift to more active values (Figure 11b). The corrosion potentials now satisfy Equation (3) with respect to hydrogen evolution as the cathodic partial process. In effect, therefore, sulfide ion converts the two copper/nickel alloys that are essentially noble in their behavior in sulfide-free and oxygen-free systems into active materials with respect to acid corrosion by hydrogen ion reduction. We believe that this phenomenon contributes greatly to the sulfide-induced accelerated corrosion of copper-nickel alloys in sulfide-polluted seawater.

The polarization resistance and ac impedance data demonstrate that sulfide ion sharply reduces the resistance of the surface film to the passage of charge. Furthermore, SEM examination indicates that at least two separate processes occur in the formation of the corrosion product; one that gives rise to the poorly adherent semicrystalline scale and another that forms the subscale film. This hypothesis is also

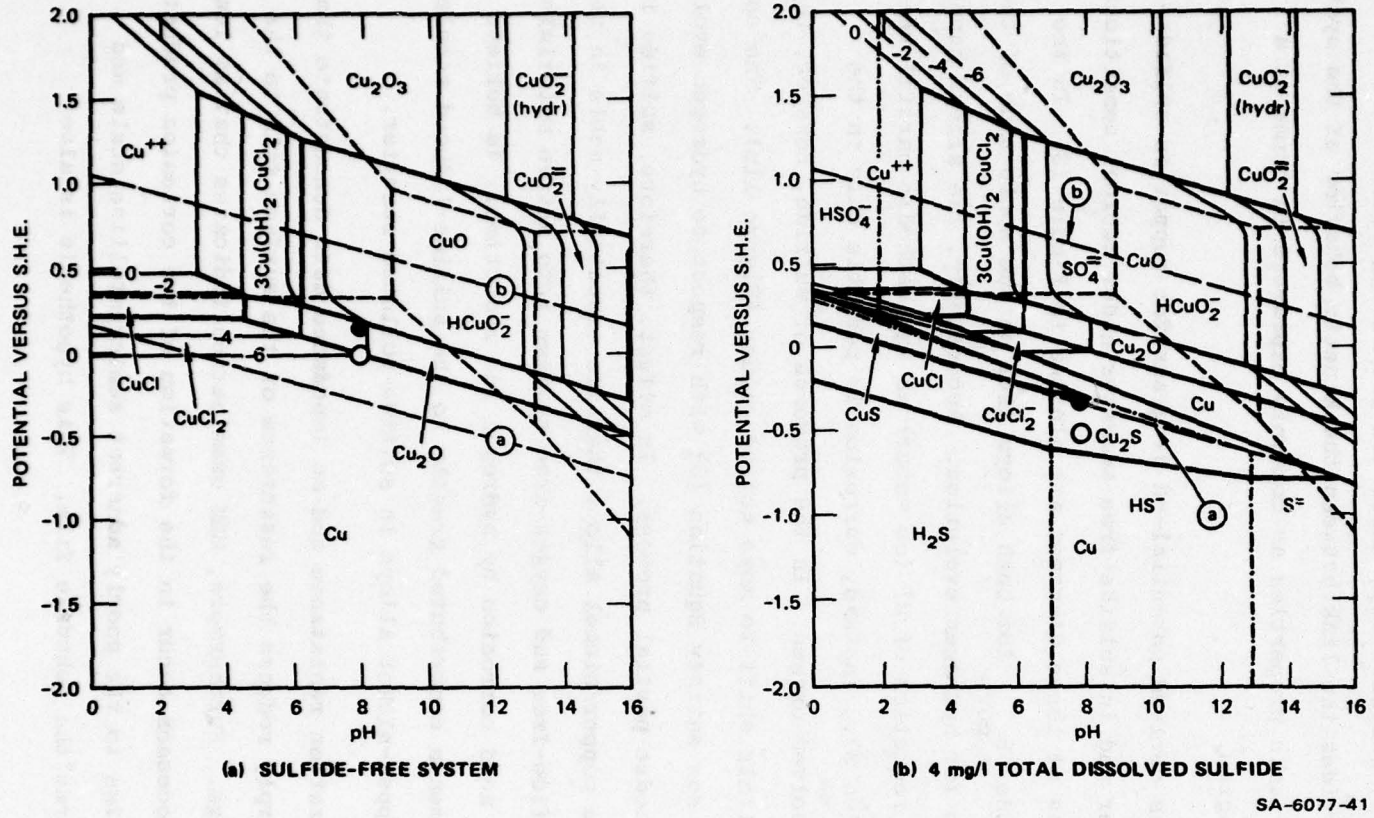

FIGURE 13 POTENTIAL pH DIAGRAMS[26] FOR COPPER IN SEAWATER AT 25°C

The equilibrium lines for hydrogen evolution (line (a)) and oxygen evolution (line (b)) have been drawn for gas partial pressures of 10^{-5} atm. O - E_{corr} for 90:10 Cu:Ni alloy. ● - E_{corr} for 70:30 Cu:Ni alloy.

consistent with the ac impedance data that exhibit multiple relaxation processes in the complex plane. It seems probable, therefore, that the subscale surface film develops by a solid-state mechanism that involves ionic and electronic diffusion through the crystal lattice. On the other hand, it is suggested that the loose scale forms by dissolution through the subscale film followed by precipitation of cuprous sulfide onto the alloy surface.

ACKNOWLEDGMENTS

Financial support of this work by the Office of Naval Research (Contract No. N00014-77-C-0046) is gratefully acknowledged. The authors also wish to thank E. Farley, J. Terry, and B. Wood for contributing to the analyses of the corroded surfaces.

REFERENCES

1. P. A. Akolzin and A. F. Bogachev, Protection of Metals, Vol. 5, p. 262 (1969).

2. H. Yamada and T. Nakamura, J. Japan Foundrymen's Soc., Vol. 36, p. 470 (1964).

3. J. C. Rowlands, J. Appl. Chem., Vol. 15, p. 57 (1965).

4. E. D. Mor and A. M. Beccaria, Corrosion, Vol. 30, p. 354 (1974).

5. J. F. Bates and J. M. Popplewell, Corrosion, Vol. 31, p. 269 (1975).

6. E. D. Mor and A. M. Beccaria, Br. Corr. J., Vol. 10, p. 33 (1975).

7. J. P. Lyndas and H. P. Hack, Corrosion 77, paper 93 (1977).

8. B. C. Syrett, Corrosion, Vol. 33, p. 257 (1977).

9. L. Giuliani and G. Bombara, Br. Corr. J., Vol. 8, p. 20 (1973).

10. H. G. Ostlund and J. Alexander, J. Geophys, Res., Vol. 68, p. 3995 (1963).

11. M. Avrahami and R. M. Golding, J. Chem. Soc. (A), p. 647 (1968).

12. E. Kemp, J. B. Hyne, and W. J. Rennie, Int. J. Sulfur Chem., A, Vol. 1, p. 69 (1971).

13. R. L. Starkey, Soil Sci., Vol. 101, p. 297 (1966).

14. D. D. Macdonald, B. C. Syrett, and S. S. Wing, Submitted to Corrosion (1977).

15. D. D. Macdonald. Submitted to J. Electrochem. Soc. (1977).

16. D. D. Macdonald, Transient Techniques in Electrochemistry (Plenum Press, New York 1977).

17. D. D. Macdonald and D. Owen, J. Electrochem. Soc., Vol. 121, p. 651 (1974).

18. D. D. Macdonald, Electrochim. Acta., Vol. 21, p. 169 (1976).

19. J. M. Popplewell, "Marin Corrosion of Copper Alloys: An Overview," to be presented at the Symposium on Effects of Pollution and Velocity on Seawater Corrosion," Corrosion 78, Houston, Texas, March 1978.

20. F. J. Kuijers and V. Ponec, Surface Sci., Vol. 68, p. 294 (1977).

21. K. D. Efird and T. S. Lee, "The Carbon Mechanism for Aqueous Sulfide Corrosion of Copper Base Alloys." To be presented at the Symposium on Effects of Pollution and Velocity on Seawater Corrosion, Corrosion 78, Houston, Texas, (March 1978).

22. W. E. Campbell and V. B. Thomas, "Tarnish Studies," Bell Telephone System Technical Publications, Chemistry Monograph B-1170 (1939).

23. T. P. Hoar and C. D. Stockbridge, Electrochim. Acta., Vol. 3, p. 94 (1960).

24. J. B. Dyes and H. A. Miley, Am. Inst. of Mining and Met. Eng. Trans., Vol. 133, p. 239 (1939).

25. L. E. Price and G. J. Thomas, Am. Electrochem. Soc. Trans., Vol. 76, p. 329 (1936).

26. E. D. Verink, in Electrochemical Techniques for Corrosion, Ed. by R. Baboian, NACE, Houston, Texas (1977).

Appendix V

PRELIMINARY STUDY OF THE EFFECT OF OXYGEN AND SULFIDE ON THE CORROSION OF COPPER-NICKEL ALLOYS IN FLOWING SEAWATER

By

D. D. Macdonald, B. C. Syrett, and S. S. Wing

Previous studies of the copresence of oxygen and hydrogen sulfide in aqueous systems, including seawater, have shown that oxidation of the various sulfide anions, and H_2S itself, takes place rapidly.[1-3] Thus, Ostlund and Alexander[1] found that for natural air-saturated seawater with an initial sulfide concentration of 3.8 mg/liter, the half-life of H_2S is of the order of 20 minutes. The oxidation products include elemental (colloidal) sulfur, and sulfur oxyanions, such as SO_3^{2-}, $S_2O_3^{2-}$, and SO_4^{2-} as found by Avrahami and Golding.[2] Kemp, Hyne, and Rennie[3] subsequently found that the oxidation of elemental sulfur itself in aqueous systems is catalyzed by UV radiation. The complex chemistry of the sulfur-water system appears to have been neglected in previous studies of metallic corrosion in sulfide-polluted seawater.

Some of the oxidation products of dissolved sulfide have also been found to be highly corrosion. For instance, Macdonald, Roberts, and Hyne[4,5] have shown that wet elemental sulfur is extremely corrosive towards carbon steel, and that the reaction is autocatalytic. In this case, the corrosion product (Mackinawite) catalyzes the overall reaction. Accordingly, the corrosion rate increases with time, rather than exhibiting the normally observed decrease as the reaction proceeds. Furthermore, the corrosion reaction was found to be greatly accelerated by chloride ion at concentrations much lower than that found in natural seawater.[6]

In view of the highly corrosive nature of elemental sulfur in some aqueous systems, we felt that as a first step in our study of the corrosion of copper-nickel alloys in seawater containing both dissolved oxygen and sulfide, we should determine if colloidal sulfur is corrosive toward the two alloys of interest. Accordingly, two specimens (1-5/16 inch x 1-5/16 inch x 1/4 inch) of each alloy were exposed to aqueous

systems containing 1 g atom/liter of colloidal sulfur that was produced by acidifying 500 ml of a 1 M solution of $Na_2S_2O_3$ to pH 2.5. After the colloidal sulfur had formed, the pH of the system was adjusted back to 8.1 with NaOH. The solutions were aerated, so that the SO_3^{2-} ions also produced by the thiosulfate decomposition would be oxidized rapidly to sulfate ions. (Note that sulfite ions are frequently used as oxygen scavangers.) Previous work[4-6] has shown that physical contact between the colloidal sulfur and the metal surface is necessary for rapid corrosion to occur, at least in the case of carbon steel. Accordingly, two additional specimens of each alloy were exposed to the solution containing sulfur, except that filter paper was used to protect the metal surfaces from direct contact with the colloidal sulfur. Two specimens of each alloy were also exposed to 1M Na_2SO_4 solutions (pH = 8.1) to serve as controls. The solutions were agitated vigorously to maintain the colloidal sulfur in suspension, and the experiments were carried out at the room temperature of 22 ± 2°C.

When the experiments were completed (68 hours), the specimens were descaled using H_2SO_4/HCl and 0.1 M NaCN (see Appendix III) and then weighed. The weight losses were used to calculate average corrosion rates for the alloys over the exposure period used. The corrosion rates are summarized in Table 1. Each value is the average for duplicate specimens that were exposed simultaneously to the environment of interest.

In addition to being corrosive to carbon steel,[4,5] elemental (colloidal) sulfur was found to be highly corrosive to the copper-nickel alloys under investigation. Thus, the presence of 1 g atom/liter of sulfur was found to increase the corrosion rates of 90:10 Cu:Ni alloy and 70:30 Cu:Ni alloy by factors of 61 and 4.15, respectively. Also in parallel with the results for carbon steel,[4,5] contact between the alloy and the colloidal sulfur appears to be necessary for very rapid corrosion

Table 1

CORROSION RATES FOR 90:10 Cu:Ni AND 70:30 Cu:Ni
ALLOY IN COLLOIDAL SULFUR CONTAINING SYSTEMS

System	Corrosion Rate, mpy‡	
	90:10 Cu:Ni	70:30 Cu:Ni
1.0 M Na_2SO_4	1.77 ± 0.35	0.84 ± 0.30
1.0 gm atom/l colloidal sulfur + 1.0 M Na_2SO_4 - contact*	108.0 ± 4.0	7.63 ± 0.28
1.0 gm atm /l colloidal sulfur + 1.0 M Na_2SO_4 - no contact†	7.41 ± 0.60	2.96 ± 0.04

*Contact between the colloidal sulfur and the alloy surface was unimpeded.

†Contact between the colloidal sulfur and the alloy surface was prevented by filter paper

‡Average corrosion rate for the 2.83 day exposure time in thousandths of 1 inch (mils) per year.

to occur, although compared with the control experiments, significantly higher corrosion rates were observed for both alloys when contact with sulfur was prevented. In this case, the corrodents were presumably dissolved species such as polysulfide ions.

It could be argued that the sulfur concentration used in this preliminary study was much higher than that found in the field. However, we are not aware of any quantitative measurements of the colloidal sulfur content of polluted seawater, particularly since analytical methods for the estimation of sulfide do not detect the zero-valent state. Accordingly, it is possible that because of the rapid oxidation of H_2S, the concentration of elemental sulfur in seawater could be much greater than is indicated by conventional analyses. Furthermore, colloidal sulfur could collect in "dead-legs" in a heat-exchanger, so that very high local concentrations might develop. Although the present work has not demonstrated that elemental sulfur attack occurs in service, it has shown that colloidal sulfur is highly corrosive toward marine copper-nickel alloys, particularly the 90:10 Cu:Ni material. This fact should therefore be considered during future interpretation of corrosion data for copper-nickel alloys in aerated seawater that contains dissolved sulfide.

REFERENCES

1. H. G. Ostlund and J. Alexander, J. Geophys, Res., 68, 2995 (1963).

2. M. Avrahami and R. M. Golding, J. Chem. Soc., A, 647 (1968).

3. E. Kemp, J. B. Hyne, and W. J. Rennie, Int. J. Sulfur Chem., A, 1, 69 (1971).

4. D. D. Macdonald, B. Roberts, and J. B. Hyne, "The Corrosion of Carbon Steel by Wet Elemental Sulfur," Corrosion Sci., in press (1978).

5. D. D. Macdonald, B. Roberts, and J. B. Hyne, "Corrosion of Carbon Steel During Cyclical Exposure to Wet Elemental Sulfur and the Atmosphere," Corrosion Sci., in press (1978).

6. D. D. Macdonald and J.B. Hyne, "A Study of Corrosion Phenomena in the Bulk Sulfur Carrier T. Akasaka," Report to Cansulex Ltd., Calgary, Alberta, 1976

Appendix VI

PRELIMINARY STUDY OF THE EFFECT OF FLUID VELOCITY ON THE RATE OF CORROSION OF COPPER-NICKEL ALLOYS IN SEAWATER

By

D. D. Macdonald, B. C. Syrett, and S. S. Wing

In a recent review, Syrett[1] has analyzed previous work concerning the effect of fluid velocity on the corrosion of copper-nickel alloys in seawater. The available data suggest that a critical velocity exists, above which rapid corrosion occurs of some of the alloys used in marine service. However, the effect of velocity is frequently obscured by poorly controlled experimental conditions and by the difficulties that are inherent in comparing data obtained using different experimental techniques. In this appendix, we report preliminary data on the effect of fluid velocity on the corrosion of 90:10 Cu:Ni alloy and 70:30 Cu:Ni alloy in aerated seawater. (See Task 5 in INTRODUCTION AND OBJECTIVES of the main body of this report.) Attempts have been made to eliminate the shortcomings of previous studies of this phenomenon. Thus, the data reported here for all fluid velocities were measured using the same test section geometry, oxygen concentration (6.60 mg/liter), and temperature (23 ± 2°C).

The experimental apparatus used for this work is described in Appendix I. Fluid velocity control was accomplished by diverting part of the recirculating stream around the test section; fluid velocities in the range 0.45 m/s to 3.67 m/s could be attained and controlled to within ±5 percent of the stated values. All the experiments performed so far have used sulfide-free, air-saturated seawater ($[O_2]$ = 6.60 mg/liter). Variable velocity experiments in seawater containing sulfide will be performed in the second year of this program.

Figure 1 shows polarization resistance (R_p) as a function of time for the two alloys in seawater at fluid velocities of 0.45 m/s and 3.67 m/s. Since the corrosion rate is inversely proportional to R_p, the data for the low fluid velocity indicate that the corrosion rate for

both alloys decreases continuously over the time of exposure used. Furthermore, the 70:30 Cu:Ni alloy is substantially more resistant to corrosion than is the 90:10 Cu:Ni alloy. On the other hand, at the highest fluid velocity used (3.67 m/s), no difference exists between the polarization resistances for the two materials, and the corrosion rate does not vary with time (Figure 1, lower plots).

The polarization resistances (and hence inverse of the corrosion rate) of the two alloys after 100 hours of exposure to aerated seawater at three fluid velocities (0.45 m/s, 1.62 m/s, and 3.67 m/s) are plotted in Figure 2. The data for the intermediate velocity (1.62 m/s) were taken from Appendix I. The alloy specimens used for the entire first year of study were taken from a common stock, so that direct comparison between the earlier work described in Appendix I and the work described here is possible. The data plotted for the two lower velocities after the alloys were exposed for 100 hours do not correspond to the steady-state behavior, since R_p is observed to increase continuously over the exposure times used. Accordingly, the steady-state values for R_p are probably greater than those plotted, as indicated by the arrows. We believe, however, that the data for the intermediate velocity are closer to the steady-state than are those of the lowest fluid velocity. Therefore, probably little difference exists between the steady-state corrosion rates for a given alloy at the two lowest velocities used. With this in mind, it is evident that both alloys suffer a sharp breakdown in corrosion resistance when the fluid velocity is increased from 1.62 m/s to 3.67 m/s. In the case of the 90:10 Cu:Ni alloy, the corrosion rate increases by at least a factor of 80, whereas for the 70:30 Cu:Ni alloy a substantially larger increase by a factor of about 500 is indicated. This velocity-induced breakdown in corrosion resistance of the high nickel alloy agrees with earlier reports,[1] but to our knowledge

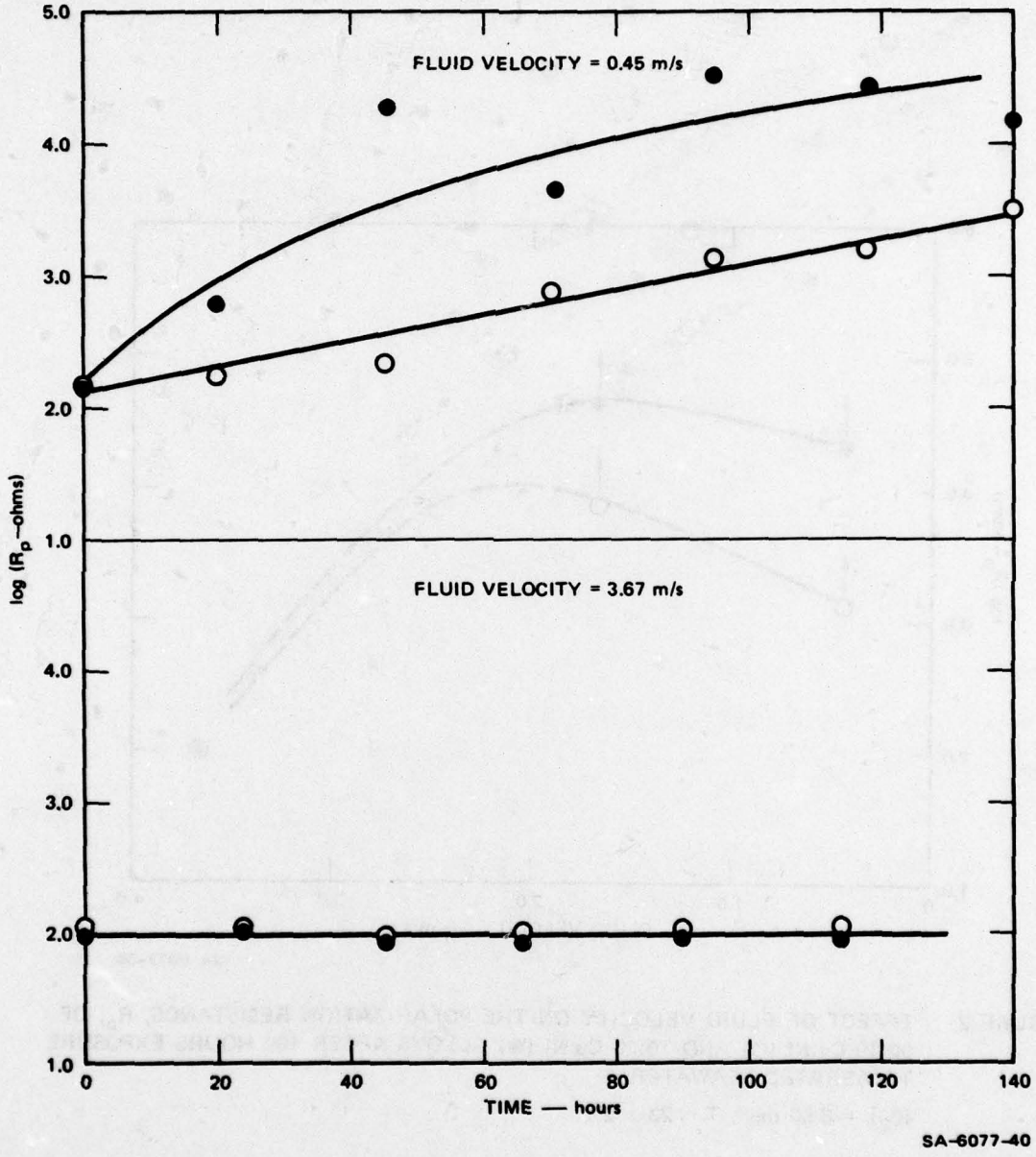

FIGURE 1 VARIATION OF POLARIZATION RESISTANCE, R_p, WITH TIME FOR 90:10 Cu:Ni (○) and 70:30 Cu:Ni (●) ALLOYS IN AERATED SEAWATER AT FLUID VELOCITIES OF 0.45 m/s AND 3.67 m/s

$[O_2]$ = 6.60 mg/l, T = 23 ± 2°C

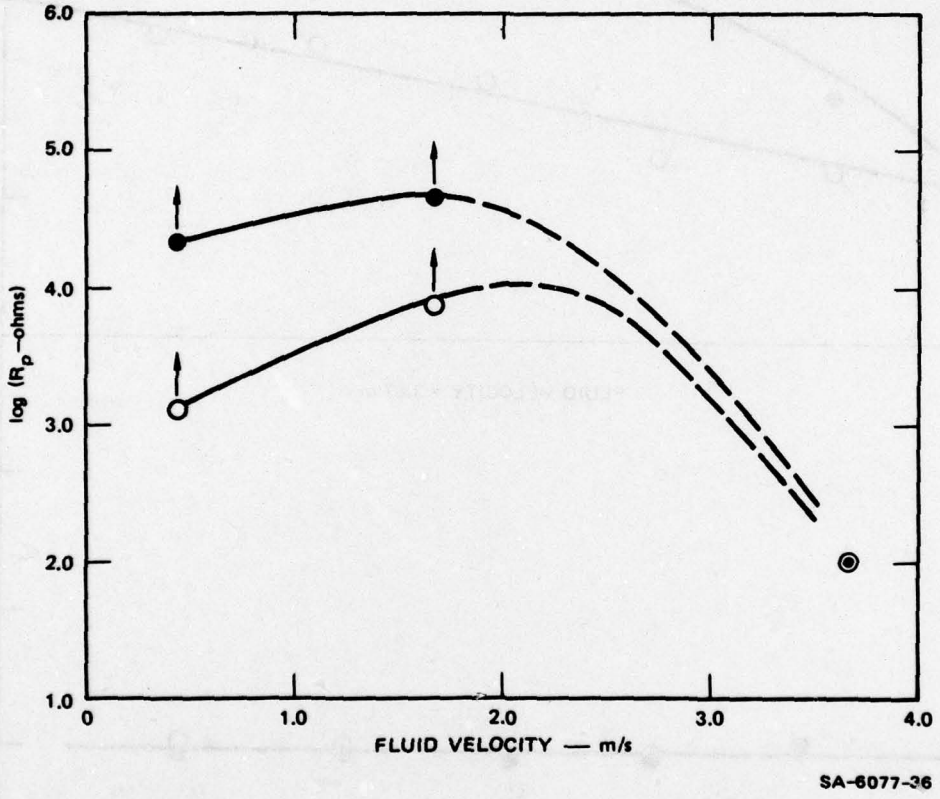

FIGURE 2 EFFECT OF FLUID VELOCITY ON THE POLARIZATION RESISTANCE, R_p, OF 90:10 Cu:Ni (○) AND 70:30 Cu:Ni (●) ALLOYS AFTER 100 HOURS EXPOSURE TO AERATED SEAWATER

$[O_2]$ = 6.60 mg/l, T = 23 ± 2°C

this phenomenon has not been observed previously for the 90:10 Cu:Ni alloy. We emphasize, however, that the data reported here are preliminary and are subject to confirmation during the second year of this program when the effect of velocity of the 90:10 Cu:Ni and 70:30 Cu:Ni alloys will be investigated in greater detail.

REFERENCES

1. B. C. Syrett, Corrosion, 32, 242 (1976).